PHOTOELECTRON SPECTROSCOPY OF MOLECULAR GASES

by

Vijay Kumar, M.Sc. (Panjab)

Department of Physics

A thesis

presented for the degree of

Doctor of Philosophy

in the

University of Adelaide

April, 1969.

CONTENTS

SUMMARY

The photoelectron energy spectra observed for different molecular gases at wavelengths from 584Å to the threshold energy of the electronic ground states of different molecular ions have been described in this thesis. The measurement of photoelectron spectra has been made at 5Å intervals. The branching ratios and hence the partial photoionization cross-sections for different competing processes have also been computed for these gases, viz. carbon dioxide, carbon monoxide, nitric oxide, nitrous oxide and ammonia.

The photoelectron spectrometer used for recording the energy spectra of the photoelectrons was of the retarding potential type, consisting of two concentric spherical grids and a plane grid; an earthed grid, an analysing grid to which a retarding potential of a step-function type was applied, and an anode. An incident photon beam produced by a helium capillary spark discharge lamp was dispersed by a one-metre near normal incidence monochromator with a slit width corresponding toa resolution of 8Å. The photoelectrons were produced in a small target area at the centre of the spherical grid system and, after being energetically analysed, were detected by a channel electron multiplier. The

best resolution obtained by the spectrometer was 3 Å.

The photoelectron spectra for these gases were obtained at different incident wavelengths and the relative areas associated with each peak in the spectra were measured. This information was combined with total photoionization cross-sections to produce partial cross-sections.

In the spectra of carbon dioxide, the four bands corresponding to $^2\Pi_g$, $^2\Pi_u$, $^2\Sigma_u^+$, $^2\Sigma_g^+$, electronic states of the ion wherever energetically possible, were clearly resolved. In carbon monoxide, nitric oxide and nitrous oxide, a low energy anomalous peak which did not vary in position with incident photon wavelength was observed in addition to peaks corresponding to direct ionization to the different excited states of the respective ions. This anomalous peak in carbon monoxide has been explained on the basis of Franck-Condon principle but in nitric oxide and nitrous oxide, the explanation of fluorescent autoionization is put forward. The photoelectron spectra of ammonia showed peaks corresponding to ground states of NH_3^+, NH_2^+ and NH^+ and also some other unknown peaks which may correspond to the other excited states of NH_3^+. In addition, a low energy anomalous peak was also observed which was explained on the basis of fluorescent

autoionization.

Photoelectron spectra have also been measured with beam resolution of 1·6Å at wavelengths corresponding to several autoionized resonance states of O_2 in the region above 775Å, and also at neighbouring off-resonance wavelengths. The off-resonance spectra showed a single broad maximum in the strength of the O_2^+ vibrational structure. However, the resonance spectra had additional features which are characteristic of the vibrational quantum number of the autoionized resonance. The form of these spectra were reproduced theoretically by the calculated Franck-Condon factors for the autoionizing transitions, using equilibrium inter-nuclear distance for the autoionized state as an adjustable parameter.

DECLARATION

This thesis contains no material which has been accepted for the award of any other degree or diploma in any University. To the best of the author's knowledge and belief it contains no material previously published or written by another person, except when due reference is made in the text.

Vijay Kumar,
30th April, 1969.

ACKNOWLEDGEMENTS

The experiments discussed in this thesis were performed in association with Mr. J. L. Bahr and Dr. A. J. Blake. The author would like to thank them for their healthy co-operation during the course of this work.

Thanks are due to the workshop staff of the Physics Department for their assistance in building the apparatus used in this work.

The author would like to thank most sincerely Dr. B. M. Horton for reading the manuscript, Dr. L. W. Torop and Mr. M. Tuckwell for healthy discussions and Mr. J. L. Gardner for his assistance in electronics.

Finally, the author would like to thank his supervisor, Professor J. H. Carver, for his enthusiasm, help and encouragement during the course of this work.

CHAPTER I

REVIEW OF PHENOMENA OF PHOTOELECTRON SPECTROSCOPY

I.1 Introduction

The interaction of monochromatic ultra-violet radiation with atoms and molecules and the measurement of emitted photoelectrons has led, in recent years, to a new kind of spectroscopy of ionic states, generally known as photoelectron spectroscopy. This type of interaction can sometimes result in dissociative ionization, giving free atoms or positive ions and electrons as the products. Thus photoelectron spectroscopy can provide information which can assist in problems such as the determination of energy thresholds for different photoionization processes, the variation of transition probability with the photon energy above the threshold and the identification of the products of photoionization. These problems have been investigated experimentally for some gases and are discussed in chapter III of this thesis.

I.2 Early Investigations

Several early attempts to observe photoionization of air by ultra-violet radiation made by Wilson (1899)

and Lenard (1900) were unsuccessful. Hughes (1910) using fluorite optics, observed positive ions produced by the interaction of photons with air. His results were confirmed by Lenard and Ramsauer (1910,11) in a similar experiment. The fact that the fluorite window has a cut-off at 1250Å ruled out the possibility of direct photoionisation as reported by Hughes and others. Weissler (1956) suggested that dissociative ionisation of air might explain these results.

Mohler et al. (1926,29) observed direct photoionization for Cs and Rb vapours in the region from the series limit towards shorter wavelength, using quartz optics. Kuns and Williams (1920,23) also detected photoionization in caesium vapour over a continuous range of wavelengths up to the threshold at 3180Å. Trumpy (1928) extended his investigations on both sides of the series limit, between 2300 and 2700Å.

Measurement of the number of ions produced per photon absorbed as a function of photon energy, is a useful tool for acquiring information about the energy states of the atoms and molecules and the nature of transitions between these states. Early attempts include the absorption coefficients of air measured by Schneider

(1940) between 380 and 1600Å. In the case of molecular oxygen, the absolute absorption was determined between 1300 and 1750Å (Ladenberg et al. 1933; Schneider, 1937). The absorption spectrum for molecular hydrogen was studied qualitatively by Hopfield (1930,33).

In recent years, measurements of the absolute photoionization cross-sections of many competing processes such as direct ionization, autoionization, dissociative ionization etc. have been made in great detail using improved techniques. These are reviewed in sections I.3a.3, I.3b.2 and I.6 of this chapter.

I.3 Photoionization Cross-Sections

Photoionization cross-sections of a large range of gases, atoms and molecules, are extremely difficult to determine experimentally. Because of this, computation of expected cross-sections, by different theoretical methods, is desirable. In atomic and molecular systems, the computations require approximations of one form or another. In the case of atomic systems, which are less complicated, cross-sections may be calculated readily and compared with experimental measurements. In this way, the reliability of the computational processes can be assessed.

I.3a Atomic Systems

I.3a.1 One-Electron System

Kramers (1923), using classical electrodynamics, considered a system consisting of a single electron moving around a nucleus of charge Z, and obtained the continuous absorption cross-section for X-rays, in the form

$$\sigma_\nu(n) = \frac{64\pi^4 e^{10} m z^4}{3\sqrt{3} c h^6 \nu^3 g_n n^3} \qquad (1.1)$$

where n is the initial Bohr state of the atom. But this approach neglected the effects of other electrons in the system.

The quantum mechanical treatment for hydrogen-like atoms was carried out by Suguira (1927,29), Gaunt (1930) and, more completely, by Menzel and Pekeris (1935). The total absorption cross-section given was of the form

$$\sigma_\nu(n) = G \cdot \frac{64\pi^4 e^{10} m z^4}{3\sqrt{3} c h^6 \nu^3 g_n n^3} \qquad (1.2)$$

where G is the Gaunt factor and g_n is the statistical weight. The Gaunt factor does not differ from unity by more than 20% and tends to unity as $n \to \infty$ in which case equation 1.2 reduces to equation 1.1.

The dipole approximation theory, based on quantum electrodynamics, provided an explicit formulation of the problem of photoionization in terms of wavefunctions of the initial state and the final state which lies in the continuum. The photoionization cross-section associated with a particular frequency ν, under these approximations, resulted in the expression

$$\sigma_\nu = \frac{8\Pi^3 e^2 \nu}{3Cg_i h\nu'} \sum_i \sum_f |M_{if}|^2 \qquad (1.3)$$

where $h\nu'$ is the photon energy in excess of the ionization threshold. M_{if} is the matrix element containing continuous wavefunctions and is defined by

$$|M_{if}|^2 = \left|\int \psi_f^* \sum_u \vec{r}_u \psi_i \, dv\right|^2 \qquad (1.4)$$

where $\vec{r}_u$ is the position vector of the u^{th} electron. The summation is carried out over the degenerate states in the initial and final energy levels.

I.3a.2 Many Electron Atoms

The application of equation 1.3 to non-hydrogenic atomic systems requires the use of approximate wavefunctions for the initial and final states. In the central field approximation, wavefunctions were taken

to be products of one-electron wavefunctions (Condon and Shortley, 1935), denoted by $U(n,\ell,m_\ell,m_s)$ with n,ℓ,m_ℓ and m_s as principal, azimuthal, orbital magnetic and spin quantum numbers. Configuration interaction in this case, was neglected. Only those transitions were considered in which one active electron was removed to the contuum while the distribution of other passive electrons between the shells remained unchanged. Under these conditions, the cross-section (Bates, 1946) is given as

$$\sigma_\nu(n) = AC'' \sum_{\ell'=\ell\pm1} C'_\ell \left| \int_0^\infty R_i(n\ell|r) R_f(k^2\ell''|r) r^3 dr \right|^2 \quad (1.5)$$

where R_i and R_f are the initial and final state radial wavefunctions of the active electron; r is the distance from the nucleus; k^2, the kinetic energy of the free electron at $r = \infty$; A is a function of ν and k^2 and C'_ℓ are the numerical coefficients tabulated by Bates. The coefficient C'' is a correcting factor to allow for the slight difference in $U(n,\ell,m_\ell,m_s)$ for the initial and final states.

The chief difficulty in this method is the evaluation of the overlap integrals given in equation 1.5.

The wavefunctions used above do not make allowance for electron exchange. For this, to start with, Hartree equations are obtained by setting up the wavefunctions as a product of one-electron orbitals (U) of the various electrons and finding the average value of the Hamiltonian for this function. The U's then varied in order to minimize the energy. The wavefunction so obtained from the product of U's is made to conform to the Pauli exclusion principle by writing it in the form of a Slater determinant. These can be obtained by Hartree-Fock method (Hartree, 1957) which varies the orbitals to minimize the energy for the determinantal functions. This makes allowance for electron exchange, since it is not specified which electron is in each of the single electron states.

Hartree or Hartree-Fock methods give inaccurate wavefunctions of the active electron because they do not include the effects of core polarisation. To improve the accuracy of the methods, Bates and Massey (1943) suggested that a term $V_p(r)$ should be added to the self-consistent potential energy. $V_p(r)$, which is a function of p, the polarisability of the core, r, the distance from the nucleus and r_c, the mean radius of the core,

represents the attraction between the active electron and the dipole moment induced by the active electron on the residual system.

The variational method used to compute the wavefunctions yields a good approximation only in a region which gives the main contribution to the energy integral (Chandraskhar, 1945). A critical study of the dipole length, velocity and acceleration formulations has been suggested to overcome the above difficulty. The three dipole forms of matrix elements are identical but in practice, they differ because of their dependence on different parts of the radial wavefunctions. Chandraskhar found the dipole velocity approximation as the most suitable for H^-.

Cooper (1962) and McGuire (1965) made additional simplifying assumptions for the state of the core in evaluating the final wavefunctions. In the unrelaxed core approximation, it was assumed that, apart from the removal of the active electron, the atom remained unchanged and the effect of the free electron on others was ignored. The matrix element then involved only the spatial distribution of one electron, before and after ionization. Seaton (1951) gave the final state wave-

functions as the antisymmetrized product of the active electron wavefunction and the electron wavefunctions of the ionic core. In this relaxed core approximation, the effect of the outgoing electron on the ionic field, was ignored. Cooper pointed out that the best effective central field for photoionization calculations would be somewhere between the two extreme cases. The unrelaxed core approximation was found better for high energy calculations but for regions near the ionization threshold, the relaxed core approximation gave better results.

I.3a.3 Comparison Between Experimental and Theoretical Cross-Section

The experimental determination of photoionization cross-sections in some cases have been followed by theoretical calculations of the cross-sections. A comparison of experiment with theory allows an evaluation of the various computational processes.

In the case of atomic hydrogen, the experimental verification of the calculated absorption cross-sections is incomplete. The observations by Chalonge (1934) and Page (1938) of emission spectra of atomic hydrogen were found to be in fair agreement with theoretical predictions of Kramers (1923). The only direct absorption

measurements were made by Beynon and Cairns (1965) at a photon wavelength of 850·6Å. The measurement yielded a value of 5·15 ± 0·18 Mbns, in reasonable agreement with theory.

Sodium was the first of the alkali metals to be investigated experimentally. Using spectroscopic techniques with the inert gas buffer between the active metal vapour and the end windows of the cell, Ditchburn et al. (1953) reported absorption cross-sections to 1600Å which were extended to 1100Å by hudson (1964), using photoelectric methods. Calculations, using the dipole length approximation (Seaton, 1951), showed a fair agreement with the experimental measurements but a poor agreement was obtained with the dipole velocity form. Unrelaxed ionic core method (Cooper, 1962) gave low values near the series limit. For higher energies, poor agreement was observed.

Each member of the rare gas group has been investigated by several experimental techniques, e.g. ion current methods (Samson and Kelly, 1964) and photographic techniques (Ditchburn, 1960). Helium has been most studied followed by neon and other gases. Experimental observations of these gases (Lee and Weissler, 1955),

using photographic techniques were extended to shorter wavelengths by Axelrod and Givens (1959). Using two ionization chambers in tandem, Samson and Kelly reported reliable results which seemed to fit well with the latest theoretical predictions (Stewart and Webb, 1963) based on the dipole length formulation.

Cross-sections for atomic oxygen are almost entirely based on theoretical predictions. The variation of cross-sections with the energy of the ejected electron was attempted by Bates and Seaton (1949) and Dalgarno and Parkinson (1960). The recent revision of theoretical computations by dipole length and dipole velocity formulations has been reported (Dalgarno, Henry and Stewart, 1964). The only experimental cross-sectional values from 500 to 900Å were obtained by Cairns and Samson (1965). The discrepancy observed between the two results may, possibly, be due to the presence of autoionization lines.

I.3b Molecules

Continuous absorption spectra, more frequently observed for polyatomic molecules than diatomic molecules, correspond to ionization or dissociation processes. The complexity of the spectrum is a result of the vast number of molecular energy states.

The total energy of the molecule consists of the potential and kinetic energies of the electrons and the nuclei. The electronic energy varies with the change in position of the nuclei. These nuclei carry out their vibrations under the influence of the electronic energy and the coulomb potential of the nuclei, the sum of which in general is called potential energy.

In the case of linear molecules, in which all the N nuclei lie in a straight line, (3N-5) relative co-ordinates describe their motion. Thus the potential in which the nuclei move in a given electronic state, can be represented by a (3N-5) dimensional hyper-surface in a (3N-4) dimensional space. Every electronic state of a polyatomic molecule is characterised by such a potential surface. Shapes of these surfaces are different for different electronic states. The existence of at least one minimum in the potential surface shows that the electronic state is stable. Such hyper-surfaces are difficult to visualize and to represent graphically.

In the case of a linear triatomic molecule such as CO_2, a particular electronic state can be represented by a four dimensional hyper-surface in a five dimensional space. In order to visualize, it is assumed that the two

bending co-ordinates are equal to zero. This simplifies the representation to a two-dimensional hyper-surface in a three dimensional space. This is done by means of contour lines. Figure I.1a shows the potential surface of the lowest singlet state of CO_2 as a function of the two C-O distances r_1 and r_2. In Figure I.1b is shown the potential surface for the lowest triplet state of CO_2 arising from $CO(^1\Sigma) + O(^3P)$. In fact, the two potential surfaces should be visualized, one above the other and intersecting each other.

In a given electronic state, a polyatomic molecule may be excited to any of the possible vibrational states. Each of these levels, in general called a vibronic state, has different combinations of electronic and vibrational quantum numbers. The normal or fundamental vibrations in the case of the linear molecule, CO_2, are shown in Figure I.2. In Figure I.2a are shown two different sets of symmetry axes for this molecule. There is an infinite number of 2-fold axes (C_2) passing through the carbon atom. The other is an infinity fold axis (C_∞) passing through the bond axis itself. Figures (b) and (c) show symmetric and antisymmetric stretches. In Figure (d) is shown the bending mode which consists of two vibrations, perpendicular to the infinity fold symmetry axis - one in

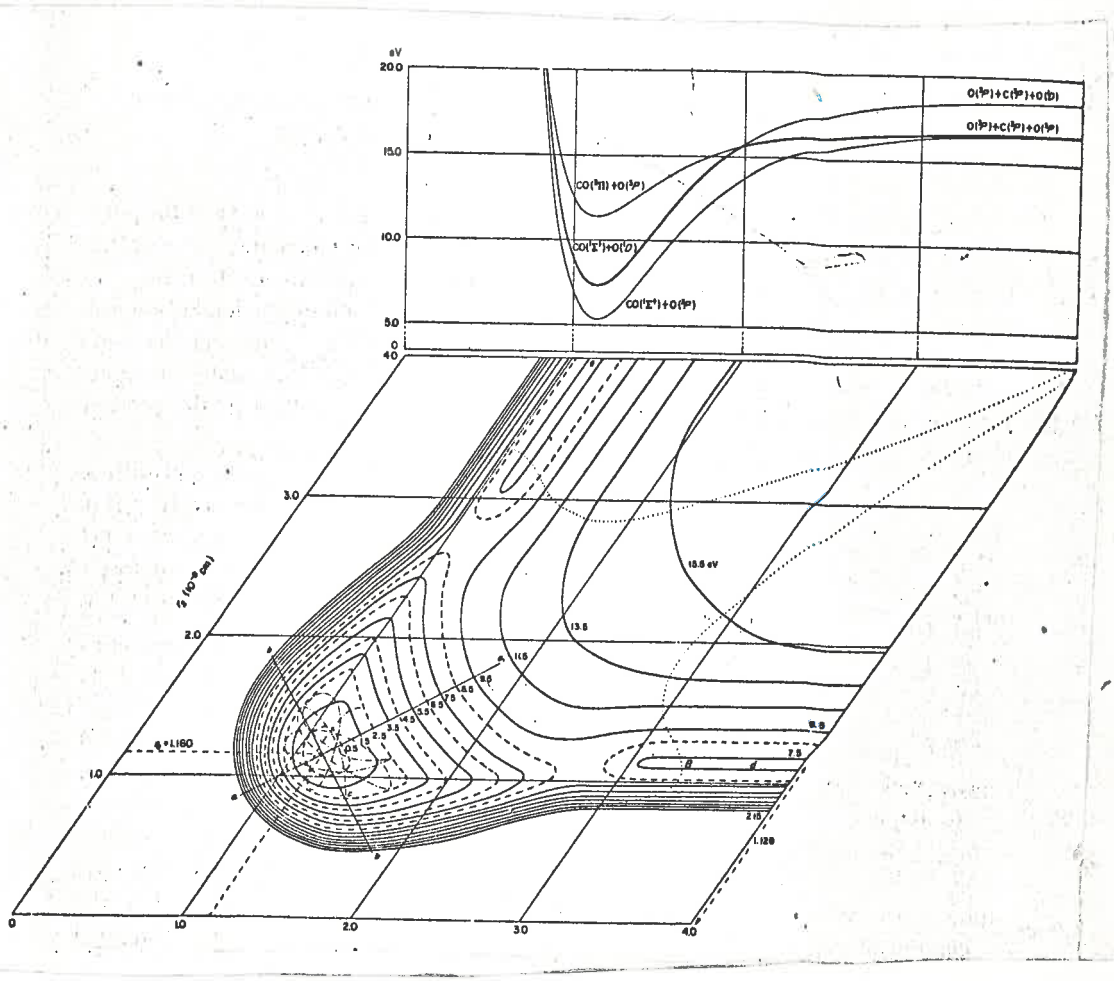

Fig. I.1a. Potential surface of the lowest singlet state of CO_2 as a function of the two C–O distances r_1 and r_2. (Herzberg, 1966).

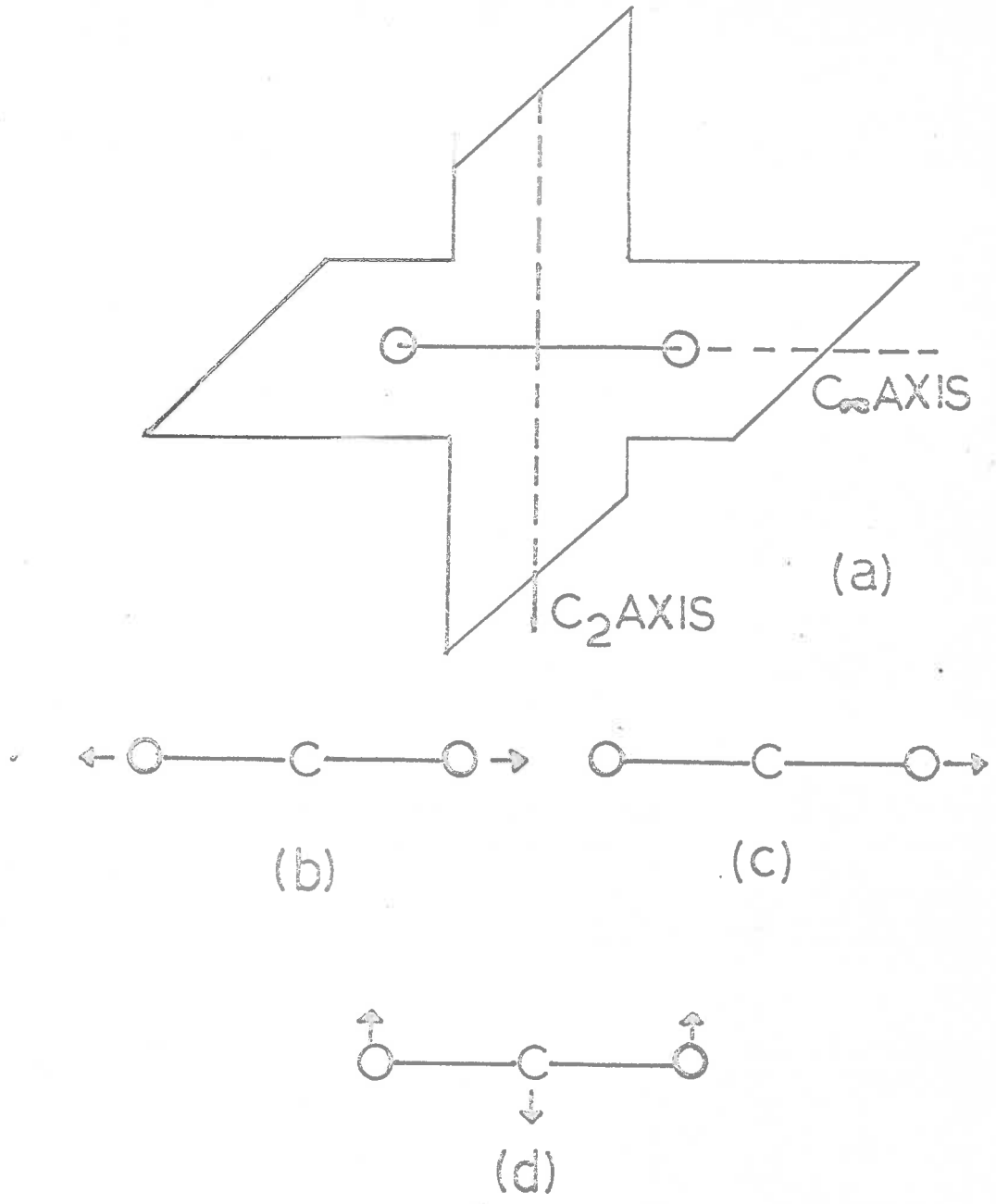

Fig. I.2 . Symmetry and fundamental vibrations of the carbon dioxde molecule .

the plane of the paper and the other out of the plane.

In comparison, electronic states of a diatomic molecule can be represented by potential energy curves (one-dimensional) in a two dimensional space. A potential energy curve for a hypothetical state of a diatomic molecule is shown in Figure I.3. The curve shows the equilibrium internuclear distance r_e and the vibrational levels for the state.

Various types of electronic states and their associated vibrational levels exist in polyatomic molecules but it is difficult to visualize them. For this reason, a diatomic molecule has been considered and in Figure I.4 are shown the potential energy curves of the electronic ground state of NO and a few states of the NO^+ ion as reviewed by Gilmore (1965). Allowed electronic transitions between the electronic ground state of NO and states of NO^+ give rise to intense ionization spectra.

In diatomic molecules, if a transition occurs between the lowest vibrational level of one electronic state to that of another, the equilibrium internuclear distances being different for the two states, then the relative positions or momenta of the nuclei must change during the transition. According to the Franck-Condon principle, such

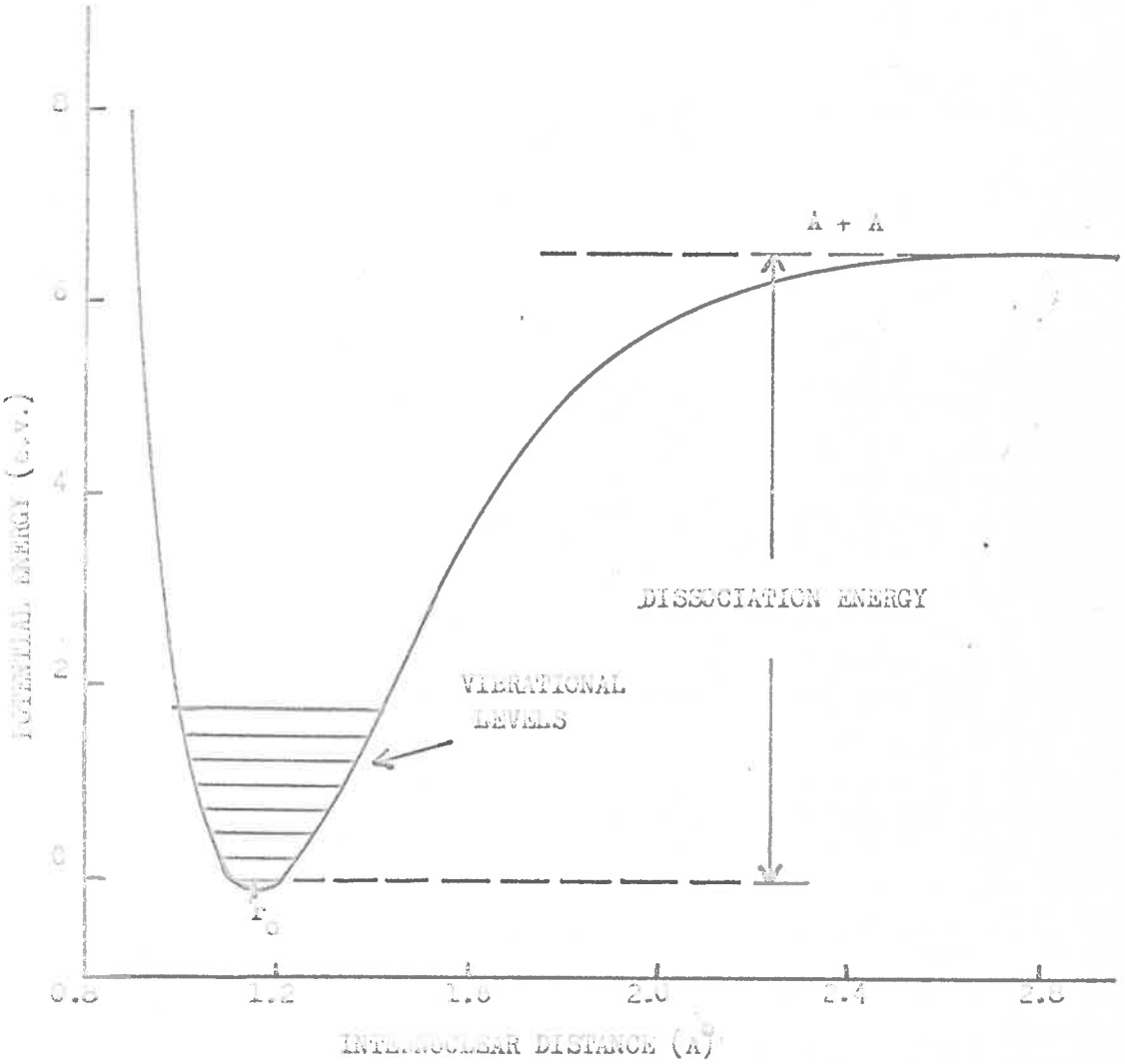

Fig. I.3 . Potential energy curve for a hypothetical diatomic molecule A_2 .

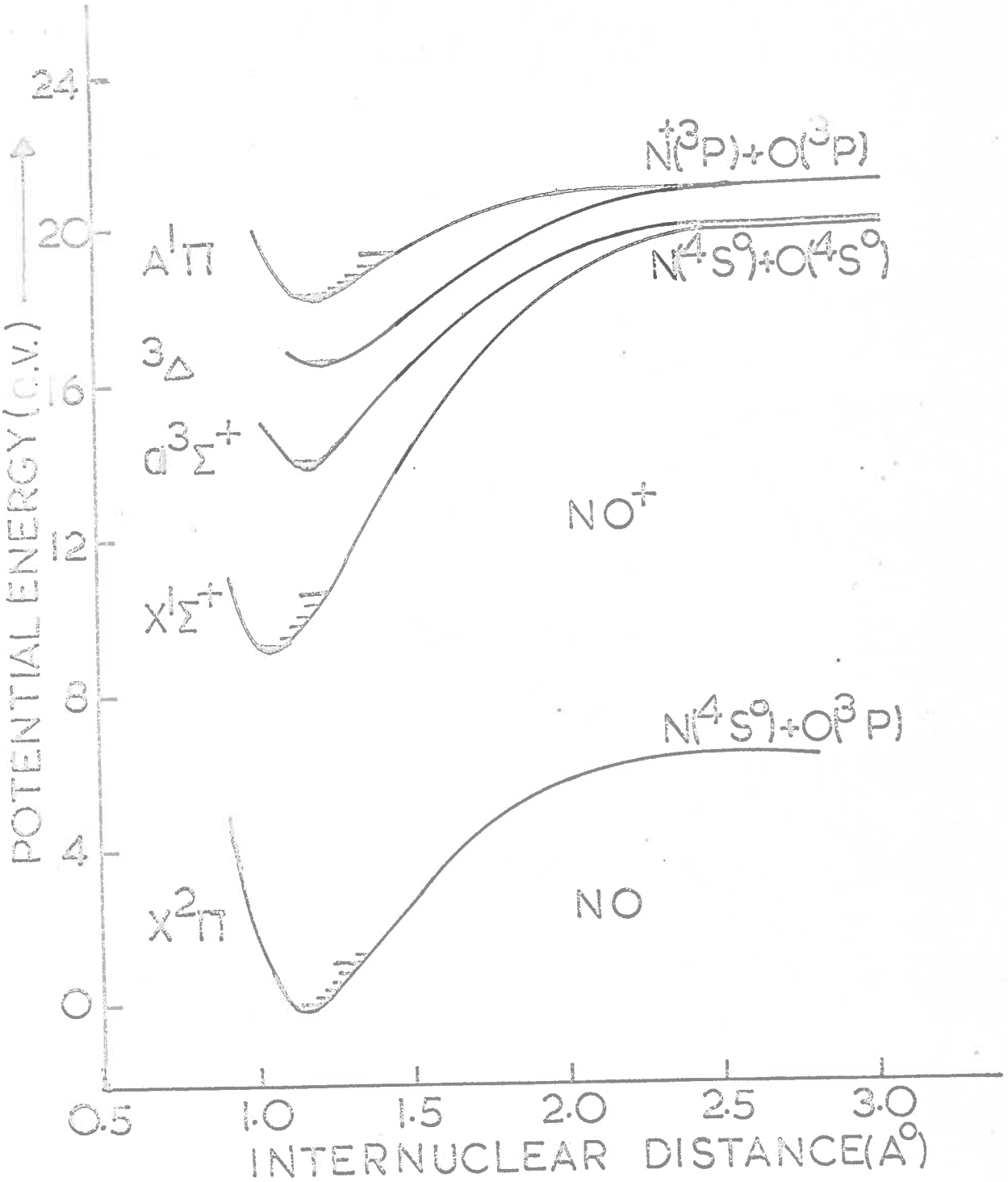

Fig. 1.4. Potential energy curves for NO (ground state only) and some of the NO^+ states (Gilmore, 1965).

a transition is unlikely to occur, since an electronic transition takes place so rapidly that the nuclei do not change their internuclear distance or momentum during the transition. The Franck-Condon principle also applies in polyatomic molecules. The most probable transition is one during which neither the positions nor the momenta of the nuclei change.

I.3b.1 Theoretical Cross-Sections for Molecules

Computation of accurate electronic wavefunctions for molecules is far more difficult than in atomic systems, leaving little scope for theoretical predictions of photoionization cross-sections. Some work, though, has been attempted for light molecules.

Exact electronic wavefunctions have been obtained only for the molecular hydrogen ion for which photoionization cross-sections were reported by Bates et al. (1953). Shimizu (1960) in his calculations of cross-sections for H_2 assumed that the orbital of the ejected electron was represented by a plane wave while the nuclei were supposed to be fixed at their equilibrium positions. The analytic wavefunctions of Weinbaum (1933) for the initial electronic state have been used by Flannery and Opic (1965) for computation of cross-sections for H_2. In the final state, the system has been taken to consist of

a H_2^+ ion in the $1s\sigma_g$ ground electronic state and a free electron moving in a field that included a contribution from the quadrupole moment of the ion. Simplifying approximations have been made in the treatment of the rotational and vibrational states.

Total photoionization cross-sections for O_2 and N_2 have been attempted by Tuckwell (Private communication) using dipole length matrix elements. Only the electron involved in the ionization process was taken into account. The initial states were described with L.C.A.O. wavefunctions of the appropriate symmetry, constructed from real Slater-type atomic orbitals. For the final states, the treatment of Flannery and Opic for H_2 was used. Computations for cross-sections were extended from 45Å to the threshold of the ground electronic states of the two ions.

Cross-sectional predictions for methane have been reported by Dalgarno (1952), using wavefunctions for the active electron appropriate to a spherically symmetric field.

Dissociation cross-sections for the weak Herzberg continuum of molecular oxygen have been computed by Ditchburn and Young (1962). In these calculations, the electronic transition moment was assumed to be constant. Jarmain and Nicholls (1964) extended the computations to the strong Schumann-Runge continuum of O_2.

I.3b.2 Comparison Between Experimental and Theoretical Cross-Sections

Computation of the accurate electronic wavefunctions of most of the molecules is quite difficult; thus a great deal of effort has been put into the experimental determination of ionization continua. So far, experiments have been limited to cold gases in which most of the molecules lie in the lowest vibrational level of the ground electronic state.

Total photoionization cross-sections may be determined by measuring the total absorption cross-section and the photoionization yield of the gas. These measurements, however, do not distinguish between different processes, e.g. different excited states of the ion and various fragments found because of dissociative ionization.

Much of the experimental data on cross-sections of different gases that has been reported so far, has been recorded with relatively low resolution instruments.

Experimental results of studies on the photoionization cross-sections of molecular hydrogen have been reported by Tanaka (1944), Lee and Weissler (1952) and Wainfan et al. (1965). Cook and Metzger (1964a) investigated the ionization continuum photoelectrically using

high resolution instruments. Their results seem to be in fair agreement with the theoretical calculation of Flannery and Opic (1965). A comparison between the two investigations is shown in Figure I.5.

Cross-sectional measurements of molecular oxygen over the region to the short wave side of 1050Å were recently made by Huffman et al. (1964). For molecular nitrogen, cross-sections were reported by Clark (1952), Weissler et al. (1952), Lee (1955) and Watanabe and Marmo (1956). The results were improved with higher resolution by Huffman et al. (1963) and Cook et al. (1965). The results obtained by Cook and Metzger for both the gases are in fair agreement with theoretical calculations of Tuckwell (Private communication) near the threshold but are considerably lower at higher photon energies.

Much experimental work has been done on other molecules such as NO, CO, CO_2, water vapour and ammonia (Astoin and Granier, 1955; Huffman et al, 1964; Sun and Weissler, 1955; Metzger and Cook, 1964; et al). Comparison is not possible because the cross-sections of these gases have not been calculated theoretically.

Ditchburn (1955), Sun and Weissler (1955), Metzger and Cook (1964) and Rustgi (1964) investigated methane

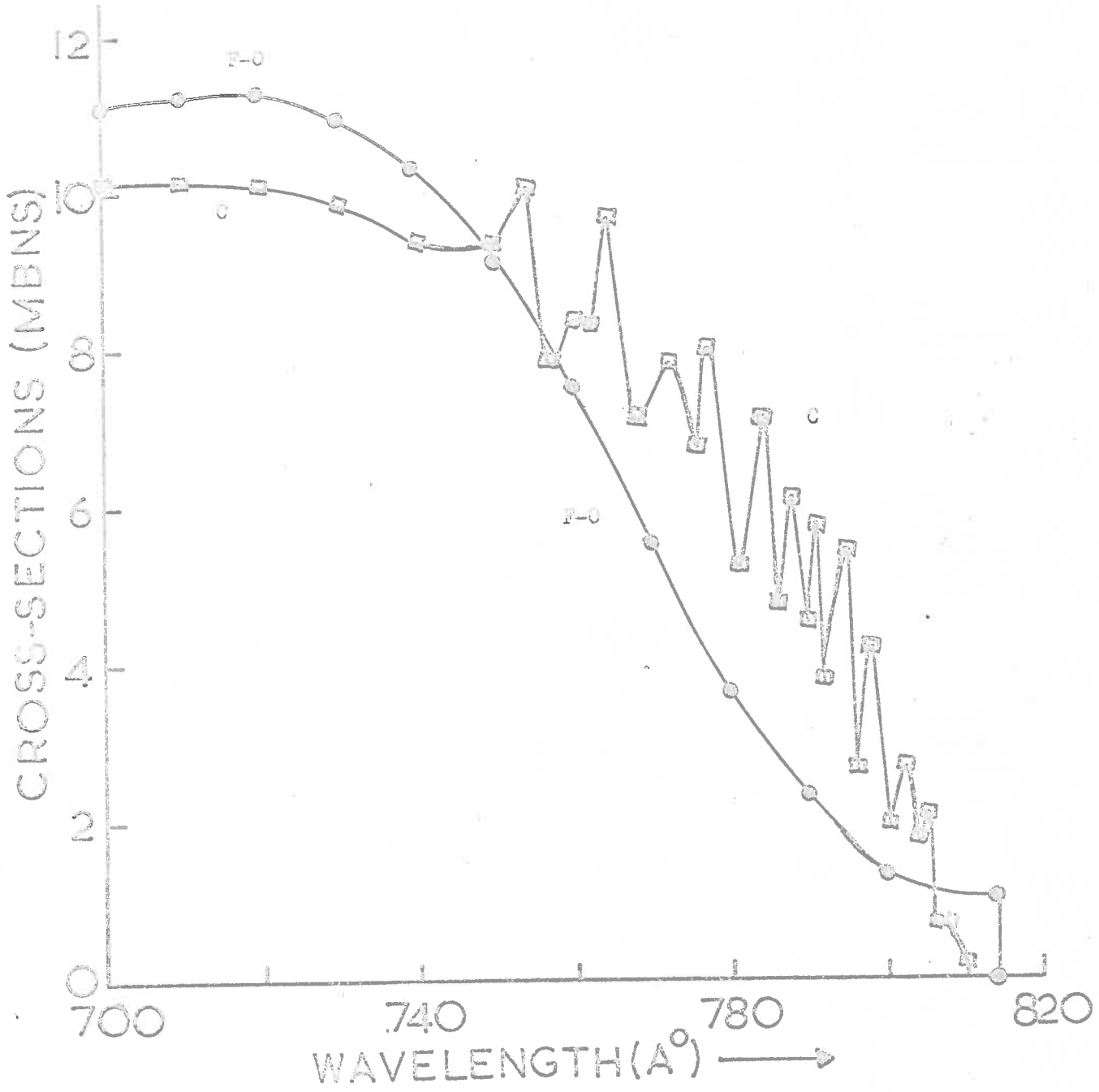

Fig. I.5. A comparison of photoionization cross-section for molecular hydrogen between theoretical calculations (Flannery and Opik, 1965; denoted by F-O) and experimental measurements (Cook et al, 1965; denoted in the figure by C).

experimentally. A comparison of these results with the theoretical calculations of Dalgarno (1952) showed the computed cross-sections to be much higher.

I.4 Ionization Potentials of Molecules

The spectroscopic determination of the ionization potentials of the molecular gases is possible from the Rydberg series limit in band spectra. This limit corresponds to transitions between the zero vibrational levels of the electronic ground states of the molecule and the ion and the resulting ionization potentials are referred to as the adiabatic potentials. The Rydberg series has, however, been identified in molecular spectra in a few cases only.

Ionization potentials which can not be determined by spectroscopic methods, may be found by electron or photon impact experiments. Electron impact methods employ a mass spectrometre for the identification and recording of the ions. Ion current measured as a function of the voltage accelerating the electrons, yields the so-called ion appearance curves from which ionization potentials may be determined. The main difficulty in this method is the fact that the ionizing electrons are not monoenergetic. Monochromatic electrons are produced by using magnetic

and electric filters (Nottingham, 1939; Clarke, 1954) but this technique yielded severely reduced electron currents. The method of quasi-monochromatization of electrons (Fox et al. 1951) was used to obtain the most reliable information on the ionization potentials of molecules. This was reported to remove the effect of the electron energy spread and did not exhibit the asymptotic tail as obtained in early experiments.

Lossing et al. (1956), Viselov et al. (1957) and Watanabe (1957) reported photoionization measurements of ionization potentials of molecules, using a mass spectrometer. In this method, a more closely monochromatic ionizing photon beam could be obtained and thus the accuracy of the measurement was higher than in electron-impact experiments. Studying the appearance curves, Watanabe (1954,57) associated the ionization potential with the point at which the curve changed abruptly. Nicholson (1963) associated the ionization potential with the steepest part of the appearance curve. The results obtained by the two interpretations were in fair agreement except that Nicholson's method seemed to be more accurate when the photon beam resolution was not very high. The first derivative of the photoionization cross-section curve near threshold (Hurzeler et al. 1957) was formed as a profile

of the probability distribution amongst the vibrational levels, the peak of which was associated with the vertical ionization potential and the sharp cut-off with the adiabatic ionization potential. There is some uncertainty in most of these interpretations, and the most reliable values are obtained when the vertical and the adiabatic ionization potentials are nearly the same. However, all this leads to the conclusion that in case of high beam resolution experiments, the probability of ionization of the molecules can be represented by a step-function; it is equal to zero for photon energy less than the ionization potential and is constant for photon energy greater than or equal to ionization potential. This is in accordance with what was predicted by Wigner (1948) for processes such as photoionization, where the products are oppositely charged.

Values of ionization potentials obtained by electron impact experiments have often been found to be slightly higher than those measured by photoionization methods. The assumption that electron impact methods lead to vertical ionization potential is true because of the fact that only low resolution measurements have been reported (Nicholson, 1963). The discrepancy can be explained by Wannier's model (Wannier, 1956) which says that the electron, being a charged particle, can not lose all of its energy during a collision.

The determination of threshold energies of the excited states is of considerable importance. These have been found spectroscopically to an accuracy of 0.001 e.v. In some cases, where Rydberg series have not been found, photoionization methods have again been used; the best values available are those determined by electron impact experiments (Frost and McDowell, 1955; 1958).

I.5 Partial Photoionization Cross-Sections

The study of the states of excitation of ions gives a measure of partial photoionization cross-sections and may be accomplished by measuring the kinetic energies of the charged particles released or by studying, if possible, the fluorescence of the ions.

Fluorescent radiation is emitted when the ions, produced in an excited state by photon impact, return to the ground state. The number of ions produced in a particular state is indicated by the intensity of fluorescent radiation. Total intensity of the undispersed fluorescent radiation as a function of incident photon wavelength was measured for several gases (Schoen et al. 1961). Huffman et al. (1963) observed the first negative and not the Meinel bands of the molecular nitrogen, using quartz and glass windows. This indicated that a considerable number

of ions were formed in the $B^2\ \Sigma^+$ state of the ion. Judge et al. (1963) dispersed the fluorescent radiation from several gases with low resolution and their reported data for N_2^+ confirmed Huffman's results. The second negative bands observed for oxygen at the incident photon wavelength of 703Å by Judge et al. indicated the production of ions in the $A^2\Pi_u$ state of O_2^+. They also observed the first negative band system at 630Å indicating that the ions were produced in the $b^2\Sigma_g^-$ state of O_2^+.

The partial photoionization cross-sections obtained by fluorescent radiation techniques are far from being accurate enough to help in the interpretations of many aeronomical processes. The reason is the low intensity of the fluorescent radiation and the presence of metastable states. It is also difficult to measure directly the number of ions in the ground state.

Partial photoionization cross-sections can be determined by an alternative method which involves the measurement of the energy distribution of the photoelectrons. The energy of the final state of the ion can be accurately determined by the difference between the photon energy and the photoelectron energy. Few experiments of this nature have been performed. Al-Joboury et al. (1963-65),

Turner and May (1966-67), Berkowitz et al. (1967), Samson (1966), Frost et al. (1967) and Spohr and Puttkamer (1967) recorded the photoelectron energy spectra for several gases by undispersed radiation from a helium discharge giving an intense emission line at 584Å. Berkowitz et al. and Spohr and Puttkamer used electron lenses with plane retarding potential systems while Frost et al. in their experiment employed spherical retarding grid geometry. A spherical grid system with focussing was used by Samson. These results, giving relative transition probability or branching ratio of some of the ions at a single wavelength, do not of course determine the variation of the cross-sections with energy. Vilesov et al. (1961), Schoen (1964) and Dolittle and Schoen (unpublished) estimated the photoelectron energy distribution at a number of wavelengths excited as emission lines from gas discharges. They used cylindrical retarding potential analyser. Blake and Carver (1967) using a helium continuum source and dispersing the incident radiation by use of a 1-metre monochromator, obtained relative transition probabilities and hence the partial cross-sections for N_2, O_2 and water vapour. A cylindrical retarding potential system was used in their experiment. The relative transition probabilities for various electronic states of N_2^+ at 584Å as reported by different

experimenters are shown in Figure I.6. The comparison shows slight variations in the values for different states. Partial photoionization cross-sections for N_2^+ as obtained by Blake and Carver (photoelectron spectroscopy) and Judge and Weissler (1968) from fluorescence experiment, are shown in Figure I.7.

The experimental measurements made so far, indicate that more detailed investigation of partial photoionization cross-sections is required. Blake and Carver used a low resolution spectrometer, with resolution of the order of 0·4 e.v. The low energy noise characteristic of the apparatus, in their work, was quite appreciable. This shows a need of performing the experiment with high resolution and better detection technique.

In chapters II and III, experiments are described in which partial photoionization cross-sections for CO, CO_2, NO, N_2O and NH_3 have been measured. The energy analyser is of spherical retarding grid geometry with a point source of photoelectrons. High resolution and better detection is also assured.

I.6 Autoionization

The existence of excited states, capable of autoionization, was first experimentally established from

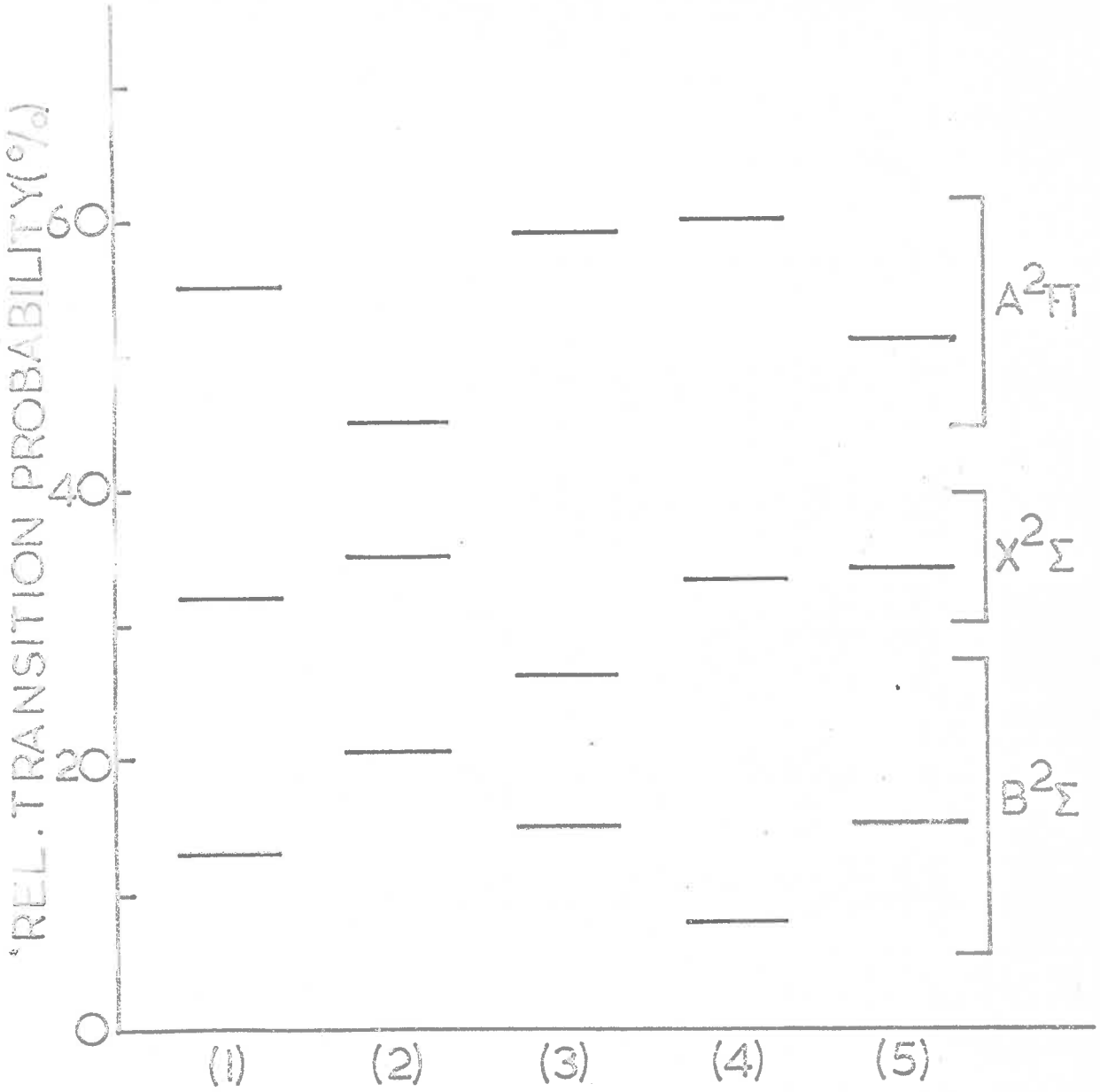

Fig. 1.6. Relative transition probabilities of exciting various electronic states of N_2^+ with 584 A^0 radiation.
(1) Samson, 1966. (2) Doolittle and Schoen, (unpublished), (3) Spohr and Putthamer, 1967. (4) Frost et al , 1967. (5) Blake and Carver, 1967 .

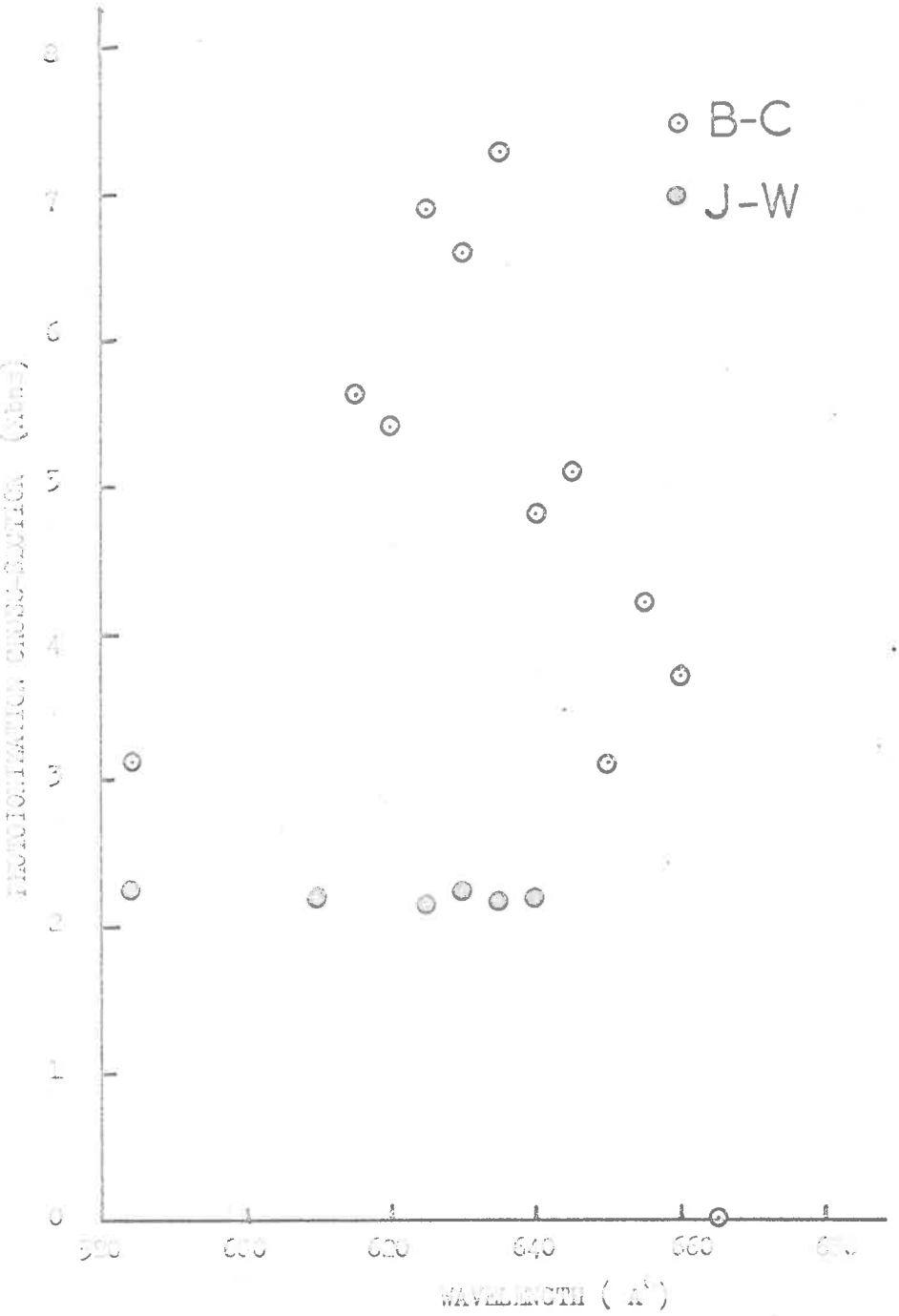

Fig. 1.7. Partial photoionization cross-sections of $B^2\Sigma_u^+$ state of molecular nitrogen as reported by Blake and Carver, 1967 (B-C) and Judge and Weissler, 1963 (J-W).

absorption of X-rays with atoms (Auger, 1925;26). The tracks produced in a Wilson cloud chamber due to absorption, seemed to diverge from the same point and the kinetic energy associated with the track seemed to vary with the energy of the incident X-ray photon. These tracks were assigned as due to primary photoelectrons. Other tracks observed to be coming from the same point did not have energies characterised by the incident photon but by the atoms involved in the interaction.

In the study of the absorption spectra of argon, krypton and xenon in the vacuum ultraviolet region near the first ionisation potential, Beutler (1935) observed numerous absorption lines attributable to excitation of inner electrons. These lines arising from autoionization were found to be broad and were asymmetrical in shape, tailing off towards shorter wavelengths.

The width of such lines was explained by assuming that an electron, other than the most loosely bound one, is excited to a continuum of states above the ionization potential, each state corresponding to different values of orbital angular momentum of the excited electron. Consequently, discrete absorption lines are observed in the midst of the photoionization continuous spectrum.

If there is an interaction between a discrete excited state and the continuum range of states of the lower level, the discrete states acquire the property of spontaneous ionization. A finite probability exists for a spontaneous radiationless transition to occur to the state of the ion with the emission of a free electron. If the probability of ionization is great, i.e. the time involved for the interaction of the atom with the radiation field is large, the energy value of the excited state becomes indistinct and the absorption lines associated with autoionization levels are broadened. The transitions involved in an autoionization process are illustrated in Figure I.8.

The asymmetric shape of the autoionization lines was explained by Fano (1935). He suggested that the asymmetry arises from the sharp variation in the coefficients of the various configurations as the energy value of the excited state passes through the stationary state. This qualitative explanation was extended in the form of a comprehensive analysis of the profiles of the autoionized absorption lines by Fano and Cooper (Fano, 1961; Fano and Cooper, 1965). The configuration interaction between a discrete state and an overlapping continuum was considered and it was found that the profiles of the

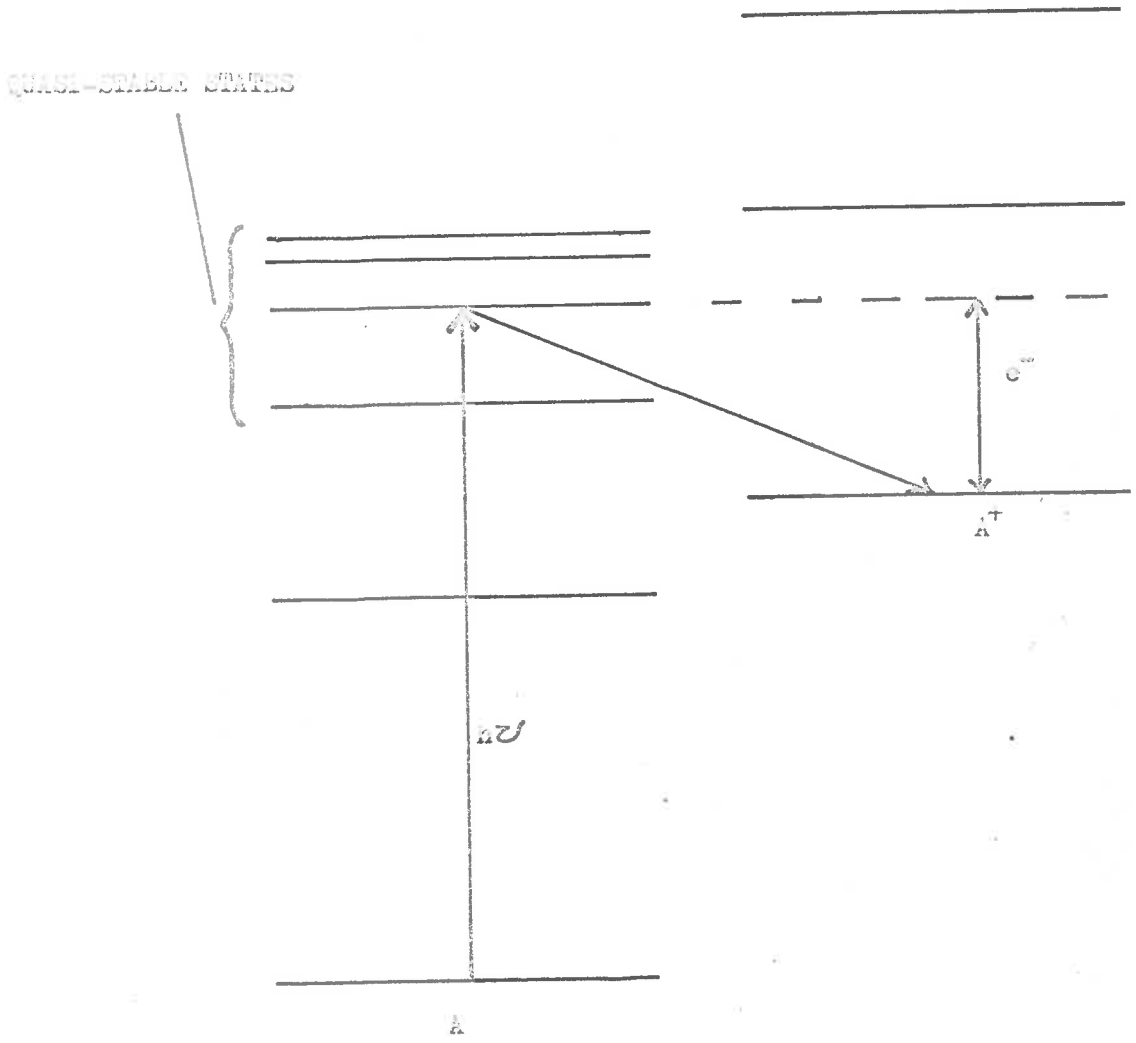

Fig. I.8. Energy levels of an atom A and the ion A^+, showing an autoionizing transition.

autoionization lines may be represented by

$$\sigma(\epsilon) = \sigma_a \left[\frac{-(q+\epsilon)^2}{1+\epsilon^2}\right] + \sigma_b$$

In this expression, ϵ is given by the difference between the photon energy and the unperturbed energy of the discrete states divided by the mean lifetime of the level with respect to autoionization. Out of the two components of absorption coefficient, σ_b refers to direct ionization. The numerical index q is characteristic of the line profile. Profiles for several values of q (0, ±1, ±2, ±3) are shown in Figure I.9. The maximum absorption, as can be seen from the figure, lies at ϵ equal to 1/q and the zero minimum at ϵ equal to -q. Changing the sign of q has the effect of producing a mirror image of the line.

Structure due to autoionization in case of argon and krypton was observed by Beutler (1935) between the $^2P_{1/2}$ and $^2P_{3/2}$ edges of the ionization limits. Perry-Thorne et al. (1960) and Huffman et al. (1963) in their quantitative analysis of kyrpton assigned oscillator strengths to the transitions leading to autoionization. Madden and Codling (Madden and Codling, 1963, Codling and Madden, 1964) observed another range of autoioniza-

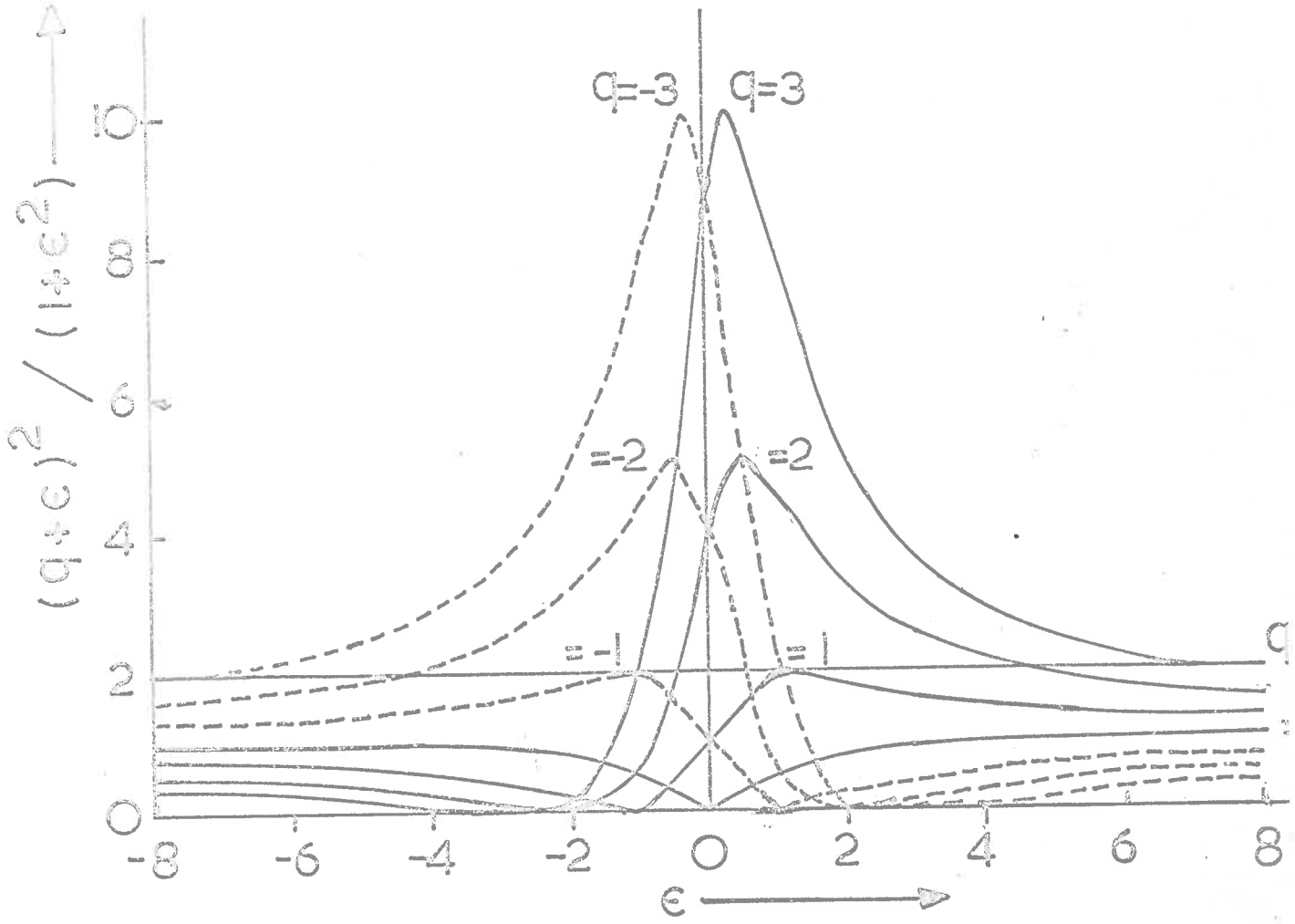

Fig. I.9. The autoionization line shapes (Fano,1961) for q = 0, ±1, ±2 , ±3 .

tion transitions towards the short wavelength side of 600Å for helium, argon, neon, krypton and xenon using the continuous radiation emitted from electron synchrotron as the background source of photons. The reported results are in good agreement with electron scattering measurements on inert gases (Samson et al. 1964).

Watsunaga et al. (1965) and Samson (1964) showed that the photoionization yield of the rare gases between the $^2P_{1/2}$ and $^2P_{3/2}$ limits, is equal to unity. This indicates that all of the atoms excited to autoionizing levels in this region undergo transitions to the ionization continuum.

I.6a Molecular Systems

Autoionization in molecular gases, sometimes known as preionization, was first reported by Henning (1932) with the observation of diffuse bands in carbon dioxide in the region of 750 to 785Å. Diffuse bands observed in the far ultraviolet absorption spectrum of molecular hydrogen (Beutler and Junger, 1936) and diffuse bands in oxygen with wavelengths shorter than 1000Å (Cook and Metzger, 1964b) were associated with preionization. A new Rydberg series in oxygen in the region of 500Å was reported (Codling and Madden, 1965) which converged to

a limit about 12 e.v. above the first ionization limit. The bands were found to be broadened and very asymmetrical. Tanaka et al. (1960) showed two new Rydberg series due to absorption in addition to those observed by Henning in the absorption spectrum of CO_2. These series converged to the excited states of the CO_2 ion.

Autoionization in molecules can be explained in the same way as for atoms. The overlapping of discrete energy levels and a continuous range of levels causes the radiationless transition to occur to the electronic state of the ion with the emission of an electron. This process causes the reduction of the lifetime of the discrete state followed by the broadening of the rotational lines. The end product in preionization is essentially the molecular ion and the ejected electron. For this to occur, stable discrete state of the molecule must lie adjacent to an electronic state of the ion.

Total photoionization cross-section measurements for O_2, N_2, NO and other gases (Cook et al. 1965) indicate the position of many sharp autoionizing resonances. These resonances which are superimposed on the photoionization continuum, have been thought to give some contribution to the photoelectron spectra of the gases.

The detailed study of the electron spectra of molecular oxygen, showed a low energy anomalous peak below the threshold of the ground state of the ion (Blake and Carver, 1967). This peak was assigned by the authors to fluorescent autoionization. This suggests a need for studying the fine structure in the spectra of gases on and off the resonance lines. Doolittle and Schoen (1965) studied the photoelectron spectra of molecular hydrogen on-resonance (780Å) and off-resonance (772 and 790Å) and showed that autoionization not only produced peaks in photoionization cross-section versus wavelength curves, but changed the energy distribution of the electrons emitted.

A more detailed investigation is needed to study the disintegration of a molecule excited to an autoionization state by observing the variation, if any, in the photoelectron spectra between one autoionized resonance and another and between an autoionized resonance and the neighbouring off-resonance continuum. The on and off line spectra for some selected autoionization states in molecular oxygen will be shown in chapters IV and V of this thesis. It will be shown that the spectra can be explained by Franck-Condon type calculations without the need to assume (Blake and Carver, 1967) radiative transitions in the neutral molecule.

CHAPTER II

PHOTOELECTRON SPECTROMETER

II.1 Introduction

Processes like autoionization, total and partial photoionization in photoelectron spectroscopy of gases are important for the interpretation of many astrophysical phenomena. The detailed study of these processes in the laboratory requires the design and construction of high resolution photoelectron spectrometers with improved detecting techniques. A spectrometer was constructed and its different parts are described in the following sections.

II.2 Photoelectron energy Analyzer

The measurement of energy distribution of electrons or other charged particles emanating within a small solid angle from their sources has been thoroughly studied by physicists through different experimental techniques.

Yarnold et al. (1948) employed a parallel plate analyzer to measure the energy distribution of the positive ions. The same technique was used (Harrower, 1955) for separation of electrons into discrete energy groups. The analyzer so developed had a resolution of 2% but very

small collecting efficiency. Also, it was found that this method suffered badly from spherical aberration (Klemperer, 1953).

Another important form of the energy analyzers quite commonly used for positive ions, was a small 180° magnetic field type selector. The same principle was employed for photoelectrons of gases by Turner and May (1966). The electrons with a definite energy were focussed at a definite spot due to the magnetic field applied. The varying magnetic field gave the energy distribution. In fact, the spectrum scanned this way was a momentum distribution curve. A correction had to be applied to get energy distribution.

The retarding potential technique for the investigation of energy distribution of electrons, has become a useful tool in the recent years. The system comprised of two cylindrical grids followed by a collector. The first grid was earthed so as to produce field-free region for electrons emanating from the source. A varying retarding potential with respect to earth was applied to the second grid. Electrons with energy greater than the retarding voltage passed through the second grid and collected at the collector electrode, giving a definite energy distribution of the electrons. The cylindrical grid geometry

was used by Kurbatov et al. (1961), Al-Joboury et al. (1963) and Schoen (1964) in their spectroscopic work. In this case, the collimation of electrons between the source and the grids was essential. The resolution of this system, being 0·1 to 0·3 e.v. did not permit accurate measurements on vibrational energy-level spacings or transition probabilities. Frost et al. (1965) built an analyzer wherein photoelectrons were produced in a small volume at the centre of a spherical grid system, so that the initial ejection of the electrons was always normal to the retarding field. Greatly improved resolution of the order of ~0·1% was claimed by this modified system.

II.2.1 Choice and Construction of the Analyzer

A retarding potential energy analyzer with a spherical grid system and a point source of photoelectrons at the centre of the system was selected for our electron spectroscopy experiments. A few modifications to the previous system (Frost et al. 1965) were introduced.

The analyzer was designed to give an energy resolution of 0·1 e.v., which was the order of separation of the vibrational levels of many molecules.

Experimental limitations for such an analyzer are the gas pressure used and the intensity of the ultra-

violet photon beam available. The gas pressure in the ionization region is limited because the mean free path for the electrons in the gas must be sufficient to allow the electrons to travel to the detector without having collisions with other molecules. This limits the gas pressure to about 10^{-2} m.m. of Hg. The maximum beam intensity obtainable from the ultraviolet lamp of the monochromator in the present experiment is typically of the order of 10^{9} photons per second. Taking an arbitrary set of values of the gas pressure as 10^{-3} m.m. of Hg, a beam intensity of 10^{9} photons per second and the absorption coefficient of 300 cm^{-1} for some arbitrary gas, the number of photoelectrons produced per centimetre path along the photon beam is of the order of 10^{6} electrons per second.

The angular distribution also affects the number of photoelectrons collected from the ionization region. The direction of emission of photoelectrons is defined by the angles θ and ϕ as shown in Figure II.1. Sommerfeld (1930) has shown that for electric dipole transitions, the probability of an electron being emitted in a direction (θ,ϕ) is independent of ϕ, but depends upon $\mathrm{Sin}^2\theta$.

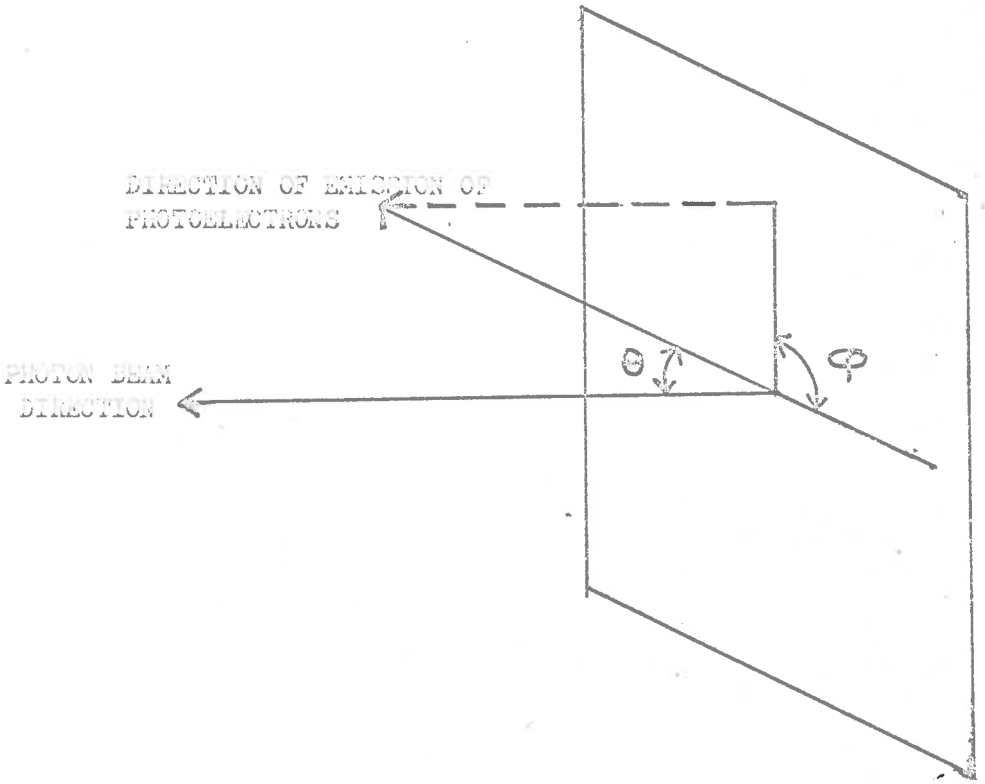

Fig. II.1 . Diagram defining the angles which describe the direction of emission of a photoelectron .

The analyser was designed for the energy resolution of 1%. Under these conditions, the maximum value of angle θ which defines the direction of energy component of electron emission, was calculated. θ was found to be $5^{o}44'$. This showed that the spread in the energy component was about 2%, giving the number of electrons to be collected as about 10^{3} per second.

II.2.1a Point Source of Photoelectrons

A twenty-eight cm. long metallic tube of two and a half cm. diameter was machined. The ultraviolet photon beam, dispersed by a one-metre monochromator was allowed to pass along one side of the tube. The width of the beam was restricted by appropriate baffles so as not to touch the sides of the tube giving scattered light. The gas under observation was allowed to flow in from the other end of the tube. With the interaction of the two, the photoelectrons were produced which emanated through a small hole in the centre of the tube, to the spherical grids, with the hole as the centre of a spherical grid system.

This system suffered from a few defects. Firstly, the electrons emitted in directions other than that of the hole, struck the walls of the tube and were reflected back through the hole to the grid system. These reflected

electrons which had lost some of their energy were also energetically analysed and then detected by the electron detector. Also the electrons coming out of the hole struck the edges and produced secondary electrons.

The first defect was removed by replacing the portion of the tube just opposite the hole with a two and a half centimetre long rectangular cylinder completely coated from inside with a solution of colloidal graphite in alcohol, commercially known as aquadag. The bottom side of the cylinder was made slanting at a small angle with the horizontal surface. Inside the cylinder was soldered an electron trap of honeycomb shape made of aluminium (Figure II.2). Due to multiple reflections inside, the electron would lose almost whole of its energy before coming out of the trap.

The secondary electrons being produced from the edges of the hole were stopped partially by making the edges of the circular hole conical, protruding towards the grid system. Also a thin coating of aquadag helped to reduce the production of secondary electrons.

The apparatus was arranged so that the hole sizes could be changed readily. A rectangular plate with the desired size of the hole at the centre could be screwed

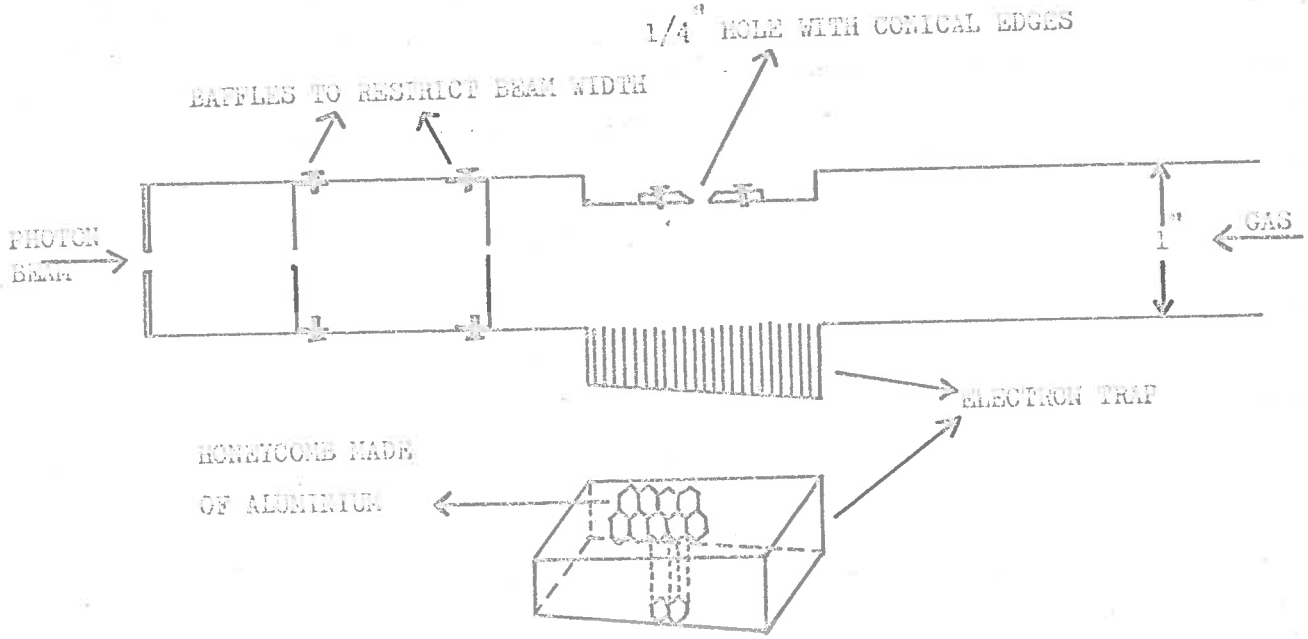

Fig. II.2 . Point source of photoelectrons and the associated electron trap .

into the tube.

II.2.1b The Spherical Grid System

Two concentric spherical and one plane grid were used. The spherical grids with the centre of the tube (Section II.2.1a) just below the hole, as centre were made of copper. The first spherical grid had a radius of about 6·5 cm. and the second about 8 cm. Ideally, the grids represent a spherical equipotential surface which is transparent to electrons. In fact, the potential in the space between any pair of grid wires is different from the potential of the wires when there is a potential gradient on either side of the grid. This potential variation may be reduced by placing the grid wires closer together but a compromise has to be reached between the resolution of the grids and their transparency to electrons. The wire mesh used for the spherical grids had a transparency of about 50% and the wire spacing was about 20 lines per inch. The plane grid made of knitted tungsten wire mesh (obtained from Metex Electronics, New Jersey), had a transparency of about 90%.

The spherical grids were designed to receive electrons over a cone of 60 degree angle. The spurious electrons coming from the hole at a greater angle were

stopped to pass through the grid system as secondary electrons, by fitting a cone at the lower end of the first spherical grid (Figure II.3).

These grids were supported by four metallic rods screwed in a blanking plate which again was fitted with glass-covar seals for electrical connections. The grids were insulated from these rods and from each other with small teflon insulators. A photograph of grid-mounting and other small details is shown in Figure II.4.

The number of electrons passing through the grid system was calculated taking into account the transparencies of the three grids. This gave a number of the order of 1000 electrons per second. These electrons, as expected, required a better detection technique with high gain and low noise.

II.3 Photoelectron Detectors

The photoelectron detectors can be chiefly divided into two categories, one which can be used for the detection of a beam of electrons constituting a maximum current of 10^{-12} amperes; the second type of detector is useful only when the detection of single electrons is required. In the determination of partial photoionization cross-sections of O_2, N_2 and water vapour, the

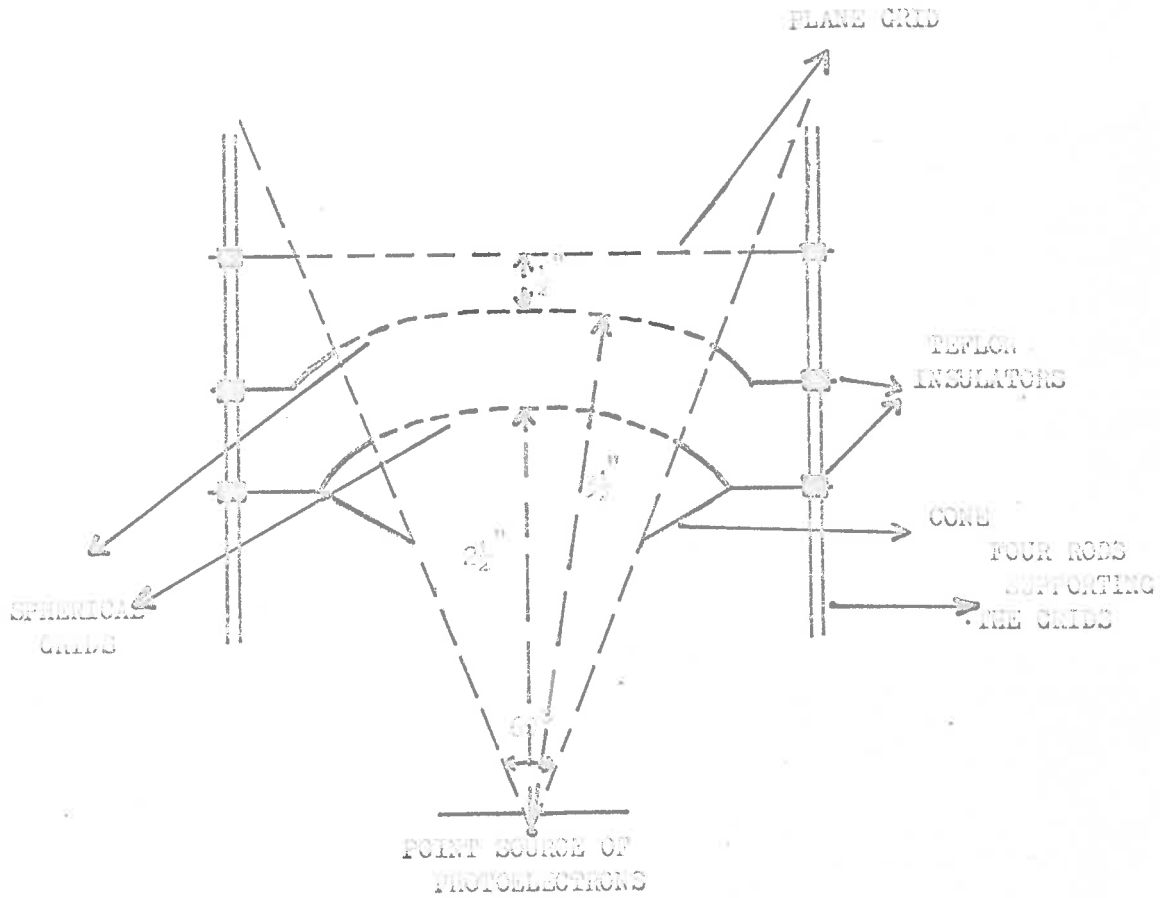

Fig. II.3 . The spherical grid analyser with some technical details .

Fig. II.4a Photograph showing spherical grid analyser clamped to the blanking plate.

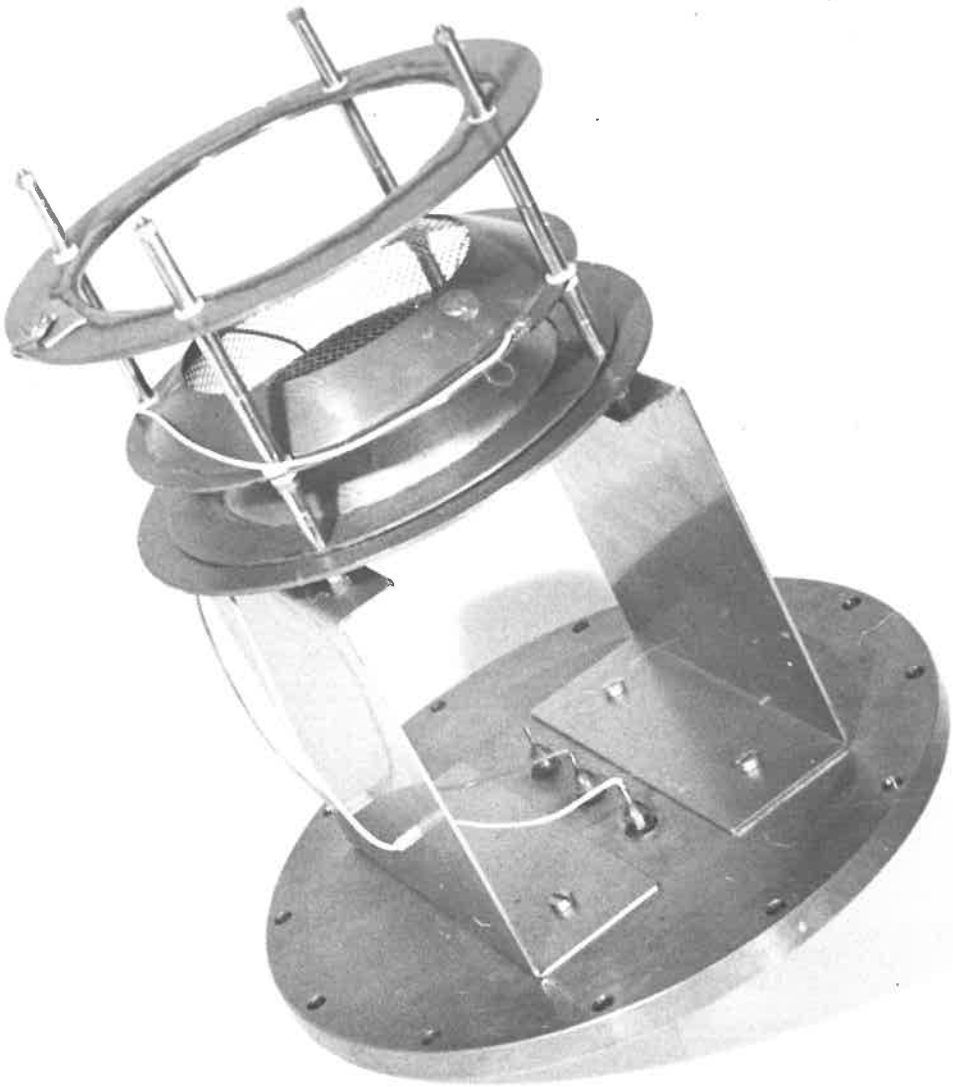

Fig. II.4b Photograph showing point source of electrons.

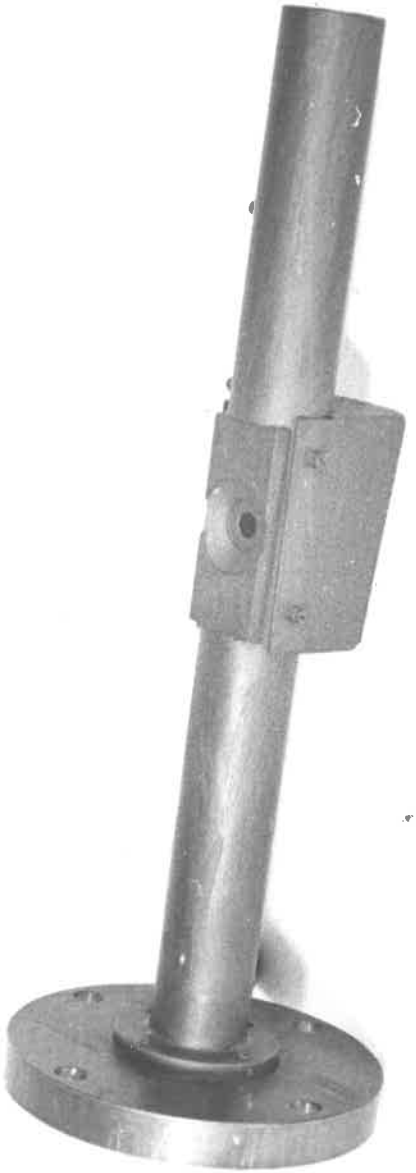

photoelectrons giving a current of 10^{-12} amperes were detected with a Wayne-Kerr electrometer (Blake and Carver, 1967).

In the photoelectron spectrometer used in the present work, the photoelectrons produced are of the order of 1000 per second (Section II.2) which rules out the possibility of its detection by the methods given above. The detectors mostly used for this purpose are electron multipliers with separate dynodes or with a continuous dynode.

II.3.1 Requirements of an Electron Detector

The photoelectron detectors with a sufficient sensitivity to count a small number of electrons should have broadly the following specifications:

1. Capable of repeated exposure to atmosphere,
2. high signal to noise ratio,
3. a time response of less than 10^{-6} second,
4. a reasonable sensitivity for electrons with energies between less than 10 e.v. and 1000 e.v.,
5. pressure independence of the charge multiplication factor etc.

In the electron multipliers with separate dynodes, the electron to be detected is caused to impinge upon a

cathode surface and liberate secondary electrons. These electrons in turn are caused to strike a succession of dynodes, each giving a secondary electron yield greater than unity. The process results in a number of electrons large enough for easy detection of the current by a vacuum tube voltmeter. This type of detector inherently meets requirements 1, 4 and 5. The signal to noise ratio is quite high but not high enough for our purposes. The time response is also quite appreciable.

In magnetic electron multipliers (Smith, 1951), the electrons are directed from dynode to dynode by the action of crossed electric and magnetic fields. This does not meet the requirement 4 due to deflection of electrons in high magnetic field.

Goodrich and Wiley (1961) developed a new electron multiplier by using a continuous surface of high resistance semi-conductor material. The detector consists of two plane parallel surfaces located a few m.m. apart made of a conductive coating on an insulating base. The same potential difference is applied across the long dimension of each surface to obtain the same potential gradient along each surface. The upper surface is maintained more positive than the lower surface. The entire structure is

placed in a uniform magnetic field perpendicular to the plane of the surfaces. The electron impinging at the cathode gives rise to secondary electrons and due to crossed electric and magnetic fields, more secondary electrons are produced along the surface. But again due to high magnetic field, a 5 to 10 e.v. electron cannot reach the cathode. Leffel (1964) reduced the magnetic field by taking out one bar magnet behind the entrance grid. This detector using Leffel's suggestion was tried by us but still it did not meet the requirement 4 to electrons of lower energies. The magnetic field was further reduced by using different layers of iron, netic and conetic around cathode, but still it did not match our requirements.

Farnsworth (1930) first proposed an electron multiplier consisting simply of a resistive tube. Oschepkov (1960) gave details of such a tube made of a special type of ceramic. Goodrich and Wiley (1962) developed a multiplier of glass with a resistive coating on the inner surface of the tube. When a potential of about 2·5 kv is applied between the ends of the tube, an electron entering the low potential end will initiate the cascade of secondary electrons from the walls (Adams and Manley, 1965). The detector called channel electron multiplier meets the

requirements 1, 2, 3, 4 but its undesirable feature is the pressure dependence of charge multiplication factor.

II.3.2 Choice of the Detector

The channel electron multiplier was thought to be the best to suit our purposes. Although it had a smaller collecting area than the resistance strip magnetic electron multiplier, its collecting efficiency was found to be about ten times greater than the latter's.

The Mullard's channel electron multiplier (No. B318 BL) was selected to be used. It had an internal diameter of 1·25 m.m. and is planar in geometry. It has input ends flared out to about 5 m.m. more than the internal diameter. This is made of lead containing glass.

The details of the geometry of the multiplier are shown in Figure II.5.

II.3.3 The Detector Mounting

Because of the detector being used at quite a high voltage, its perfect insulation from the rest of the apparatus was necessary. The detector was mounted with two teflon clamps rectangular in shape with small semi-circular holes at the centres of their long sides. These clamps with the detector in, were screwed on a circular

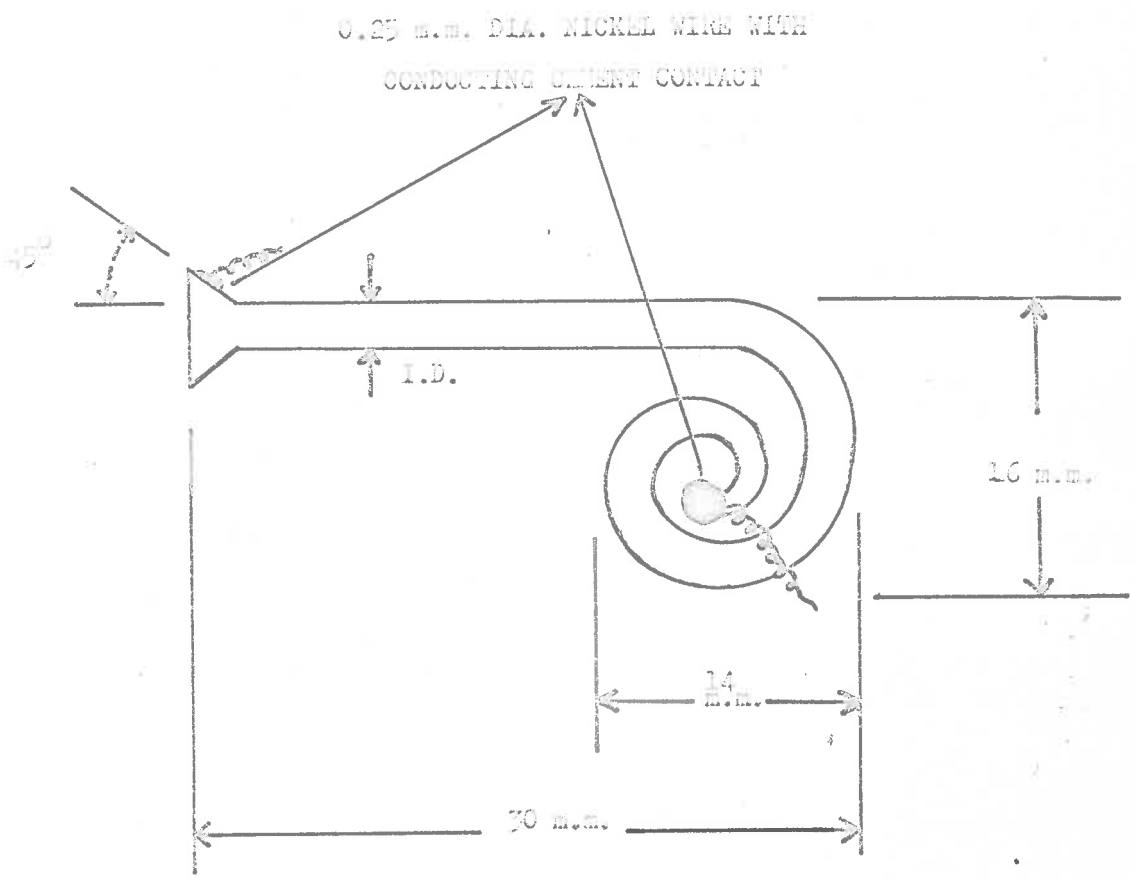

I.D. 1.25 ± 0.15 m.m.
O.D. 1.95 ± 0.25 m.m.

Fig. II.5 . Details of Mullard's channel electron multiplier no. B 313 BL.

copper disc with a hole in the centre. The horn of the detector passing through this hole, was kept on one side of the copper disc and the rest of the detector on the other side. This disc was supported with the help of two mounts screwed on one side to the disc and on the other side to the blanking plate which rested on the top of the vacuum chamber. The whole system could slide in the chamber without touching any part of it. This way, the detector was kept at a distance of about four inches from the plane collecting grid of the energy analysing system. The two wires, one at the horn and the other at the end of the multiplier were taken out for electrical connections through the glass-cover seals soldered in the blanking plate (Figure II.6).

II.3.4 Performance of Channel Electron Multiplier

Different combinations of voltages were tried at the two ends of the detector. The most suitable set of voltages, giving a high count rate for electrons of all energies at the gas pressure of 10^{-3} m.m., was 200 volts and 3 kv at the lower and the top ends respectively. Count rate versus voltage curve gave a starting voltage of 4 kv. At the voltages used in the present work, the typical value of the gain was found to be of the order of 10^7.

Fig. II.6 Photograph showing the mounting of the channel electron multiplier.

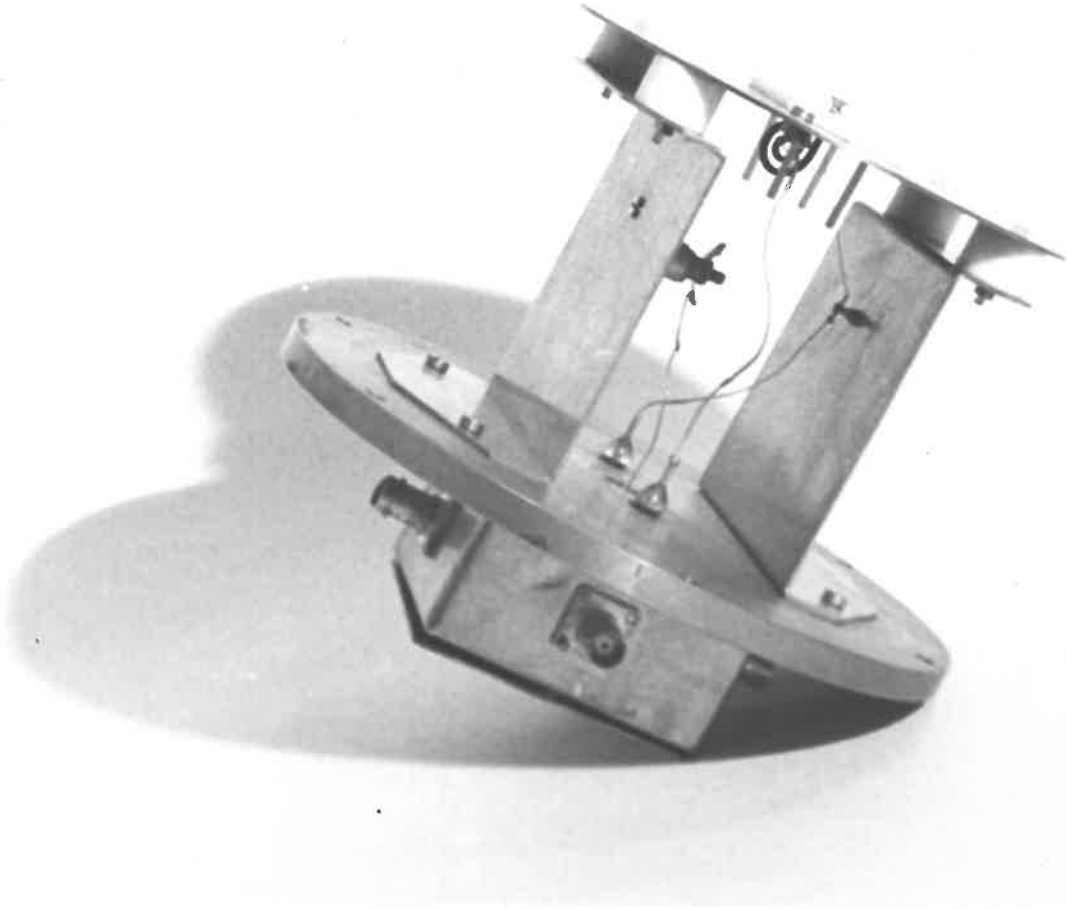

The plot of pulse height on X-axis and the frequency of occurrence of that pulse height gave a distribution which was roughly triangular. This agreed to the specifications of the manufacturers.

Count rate was found to depend slightly on pressure for pressures more than 5×10^{-4} m.m. but more rapidly for pressures more than 10^{-3} m.m. of Hg. At pressures below 5×10^{-4} m.m. of Hg. the count rate did not seem to show pressure dependence.

The background count rate was found to be small, of the order of 5 to 10 per second.

It was difficult to measure the highest count rates because this multiplier is faster than many of the currently available pulse counting equipment. It is advisable to find out whether the detector count rate is saturated at any stage. Saturation count rate would be different for different gases in the vacuum chamber. Argon gas was used for this purpose with the incoming photons from the monochromator of wavelength 743Å. The lamp current was varied so as to vary the intensity of light in vacuum chamber. The photoelectrons produced were detected by the multiplier and were counted by some pulse counting techniques for each value of lamp current.

Figure II.7 shows a plot of count rate against the lamp current or light intensity. The graph shows a linear relationship between the two quantities in a region of 40 m.A. to 120 m.A. for the values of lamp current. With a further increase of current the count rate starts saturating, showing that the appropriate value of current to operate the lamp was between 110 to 120 milliamperes.

II.4 Other Details of the Spectrometer

II.4.1 The Beam Trap

As gases under investigation flowing through the tube which is used as a point source of electrons are generally at a very low pressure, i.e. 10^{-3} m.m. of Hg. approximately, only a small fraction of the ultraviolet beam is absorbed. The remainder of the beam could be allowed to pass through a beam trap, a cylinder coated from inside with aquadag and kept at a positive potential, or such other similar arrangement. The alternative arrangement used by us is a photomultiplier tube screwed on to the vacuum chamber with its cathode facing the incoming photons.

The photomultiplier used (EMI 9514S) was made sensitive to ultraviolet radiation with a coating of sodium salicylate, a fluorescent material (Johnson et al. 1951).

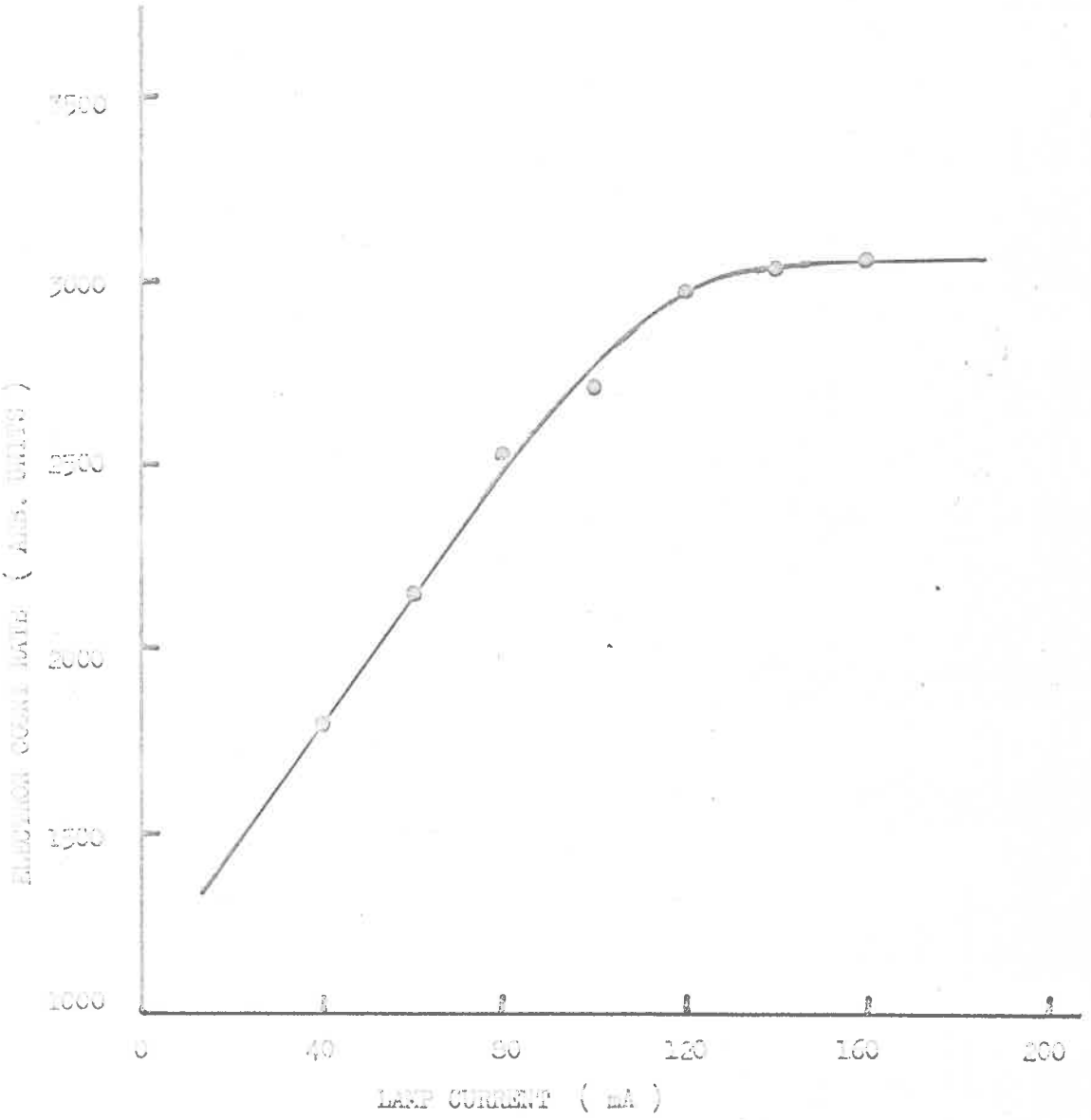

Fig. II.7 . Graph of count rate versus lamp current .

A glass plate coated with this material was placed in front of the photomultiplier. The spectral distribution of the fluorescent radiation from sodium salicylate has a maximum at about 4250Å which corresponds well with the spectral sensitivity of S-type photomultiplier cathodes (Allison et al. 1964).

The cathode of the photomultiplier tube was given a voltage of 1400 volts from a power supply and the current at the anode was measured using a d.c. amplifier (Hewlett-Packard, model 425 A).

II.4.2 The Vacuum Chamber

The vacuum chamber (Figure II.8) was constructed of copper tubing six inches in diameter. The top and the bottom parts were the detachable blanking plates with the detector and the analysing systems mounted to them. Electrical connections to the grids and the channel electron multiplier were made through the glass-covar seals in the blanking plates of the vacuum chamber which was windowless. The ultraviolet beam entered from the adjustable exit-slit of the monochromator into a long narrow tube, the other end of which was fitted with the photomultiplier tube. The gas entered the chamber from the other side of the tube through a needle valve, which was adjusted to maintain a constant pressure in the chamber.

Fig. II.8 The vacuum chamber with spectrometer inside and light source on the one-metre monochromator. The photograph shows a part of the differential pumping system in the background.


DO NOT
SCAN MANUALLY BELOW 6Å OR ABOVE 600Å

A two inch oil diffusion pumping system was used to evacuate the vacuum chamber to a pressure of 10^{-6} m.m. of Hg. A liquid air cooled trap was included to remove condensable impurities from different gases under investigation.

Facilities were provided for attaching an ionization gauge head (Edwards) and a pirani gauge head (Speedivac, Model 3B) to the vacuum chamber. When the chambers were evacuated, the residual gas pressure was measured with the ionization gauge and the pirani gauge was used to monitor the gas pressure during the experiment.

II.4.3 The Monochromator

The study of autoionization (chapters IV and V), partial photoionization cross-sections (chapter III) of different atmospheric gases was done using the one-metre near normal incidence monochromator (McPherson, Model 225) with Bausch and Lomb replica grating (1200 lines per inch), blazed for 1000Å. The entrance slit could be adjusted to give a slit width of 10, 50 and 100 microns. An exit slit width of 1000 microns was used to give a beam resolution of about 8Å for some experiments but for others, 200 microns slit was used giving 1·6Å resolution.

The light source used (section II.4.4) was isolated

from the monochromator by a two stage differential pumping system. The first stage was pumped by a mechanical booster pump (Godfrey KB/V400/28) and a backing pump while the second stage was pumped by an oil booster (DynavacOB 1500) and a backing pump. With the light source running and the entrance slit width 100 microns, the main chamber of the monochromator could be maintained at a pressure of less than 10^{-4} m.m. of Hg. with the use of this differential pumping assembly.

A general view of the experimental arrangement with the one-metre monochromator is shown in Figure II.9.

II.4.4 Light Source

A requirement for an ideal ultraviolet light source is its capacity to emit a continuous range of wavelengths with a uniform intensity distribution. Radiation from an electron synchrotron is such an ideal source (Madden and Codling, 1965).

A high current discharge of different gases through a narrow tube would provide a 'many-lined' spectra with a continuous range of wavelengths. But the large fluctuations of intensity with wavelength would be a great limitation against our requirement.

Fig. II.9 General view of the apparatus used to record photoelectron spectra.

The excitation of the emission continua of the rare gases (Tananka et al. 1958, 1962; Huffman et al. 1965; Wilkinson et al. 1965) was found to provide lamp sources close to the ideal ones. In a discharge through different rare gases at pressures of the order of 50 m.m. of Hg, diatomic molecular ions are formed in their bound first excited state. The continuum is due to the transitions between this state and the unstable ground state of the ion. The Hopfield continuum of helium (Hopfield, 1930) has a useful intensity in the range 600 to 1000Å, neon in the range 740 to 1000Å, argon 1070 to 1600Å, krypton 1240 to 1700Å and xenon 1470 to 1900Å.

The light source used in the present work was emission line of helium at 584Å and the Hopfield continuum of helium. For both cases, a high current density was required and this was supplied to the lamp source in two different modes. For producing helium 584Å line, A.C. mode was used (Figure II.10a). In this, the lamp was supplied with a high voltage, 15 k.v. through a series resistance used for stabilizing the discharge. For producing the emission continuum of helium, high current density was provided by using a condensed spark discharge. The circuit diagram showing this is given in Figure II.10b. A few condensers in parallel were charged through a series

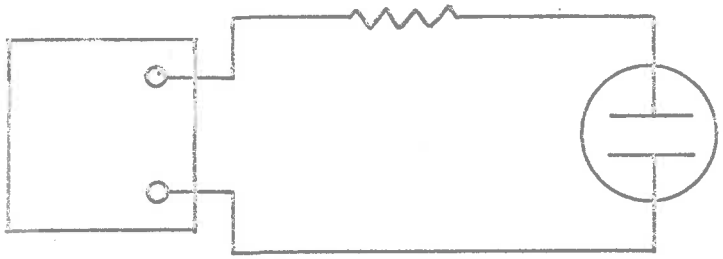

(a)

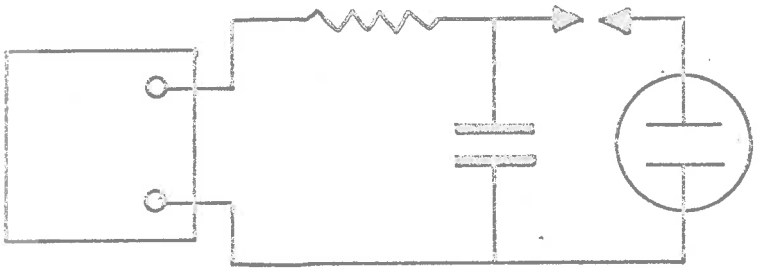

(b)

Fig. II.10. Circuits for supplying power to the capillary discharge lamp (a) A.C. mode (b) condensed spark discharge mode .

resistance and dischargedthrough the lamp via a spark gap between two rounded tungsten electrodes. The spark was stabilized by injecting a jet of compressed air through the gap and by illuminating the gap by UV radiations from a quartz mercury lamp.

The emission continuum of helium observed is shown in Figure II.11.

II.5 Operation of the Spectrometer

II.5.1 Grid Voltages

The first spherical grid was kept at an earth potential so as to provide for the photoelectrons emitted from the point source, a field free region between the grid and the source. A sweeping retarding voltage ranging from a slightly positive voltage to -15 volts was applied to the spherical grid. This grid, due to the nature of the potential applied to it, would be called from now on the retarding grid. To the third grid, which was plane, a positive potential was applied to ensure that all the electrons which penetrated the retarding grid, were collected, so the name collecting grid.

To have a knowledge of saturation characteristics of the collecting grid, measurements of electron count rate corresponding to different collecting voltages for

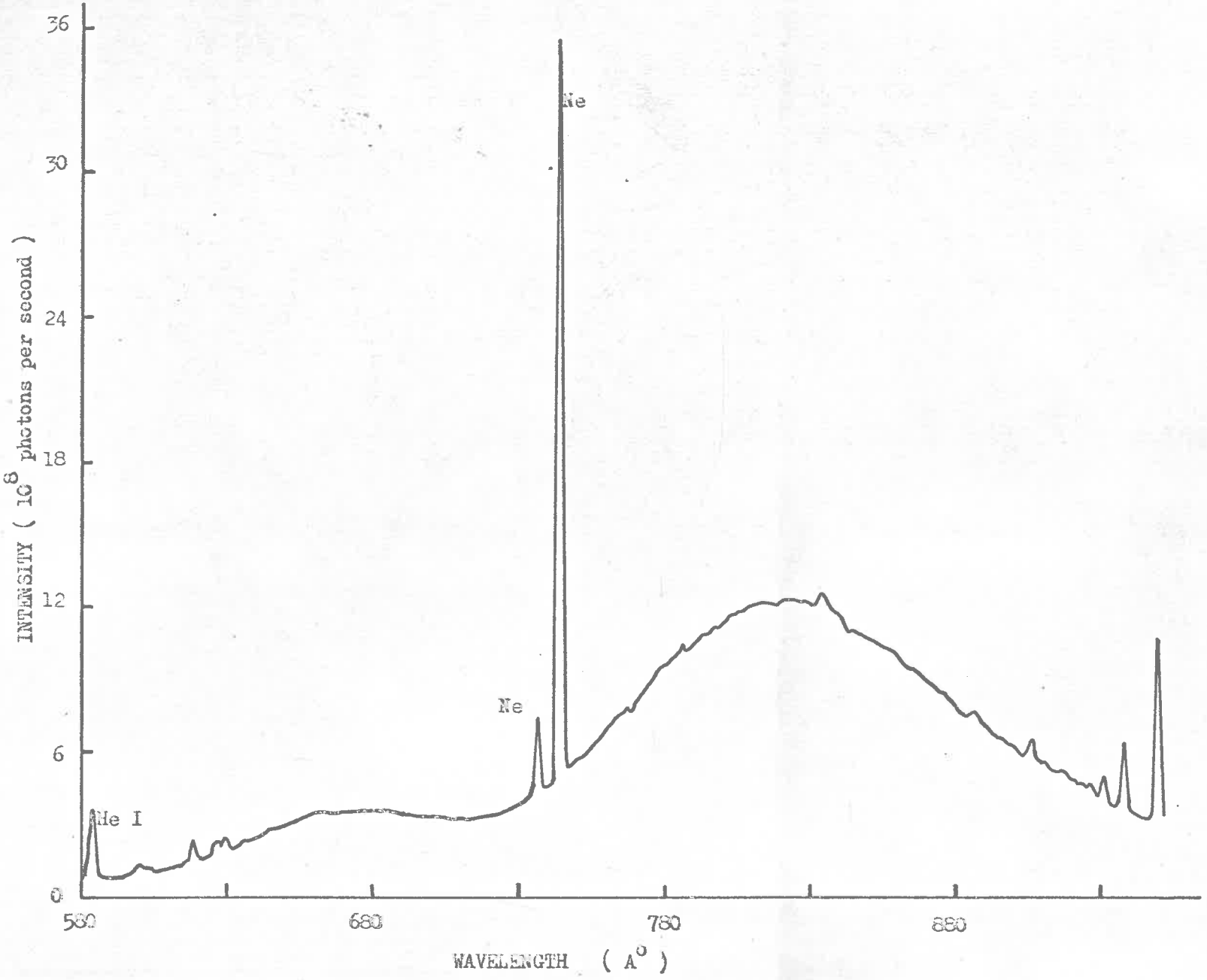

Fig. II.11. Hopfield continuum of helium excited by a spark discharge in 50 m.m. of Hg of gas pressure .

zero retarding potential were made. A plot of the two variables (Figure II.12) shows that the electron current was fairly constant for the collecting potentials between 12to 17 volts. So during all the experiments, the collecting potential was kept at 17 volts.

The retarding potential applied to the retarding grid was in the form of a negative going staircase with 100, 200 or 400 steps of variable heights in accordance with the number of channels used for storing the energy spectra of electrons in the 400-channel pulse height analyser (RIDL model 34-12 B). One step corresponded to one channel and as the step of the staircase advanced, an arrangement was made to advance the channel simultaneously. This could be achieved easily by using the multi-channel analyser in time mode.

The broad principle of the operation of the spectrometer is shown in Figure II.13. The spectrum of electron energies for xenon gas was scanned by sweeping the staircases linearly with time. The curve stored is shown in Figure II.14. This curve, a plot of electron current as a function of retarding potential, is the integral of the electron energy spectrum because all electrons with energies greater than the retarding potential are detected. The curve consists of two steps, one step for each discrete

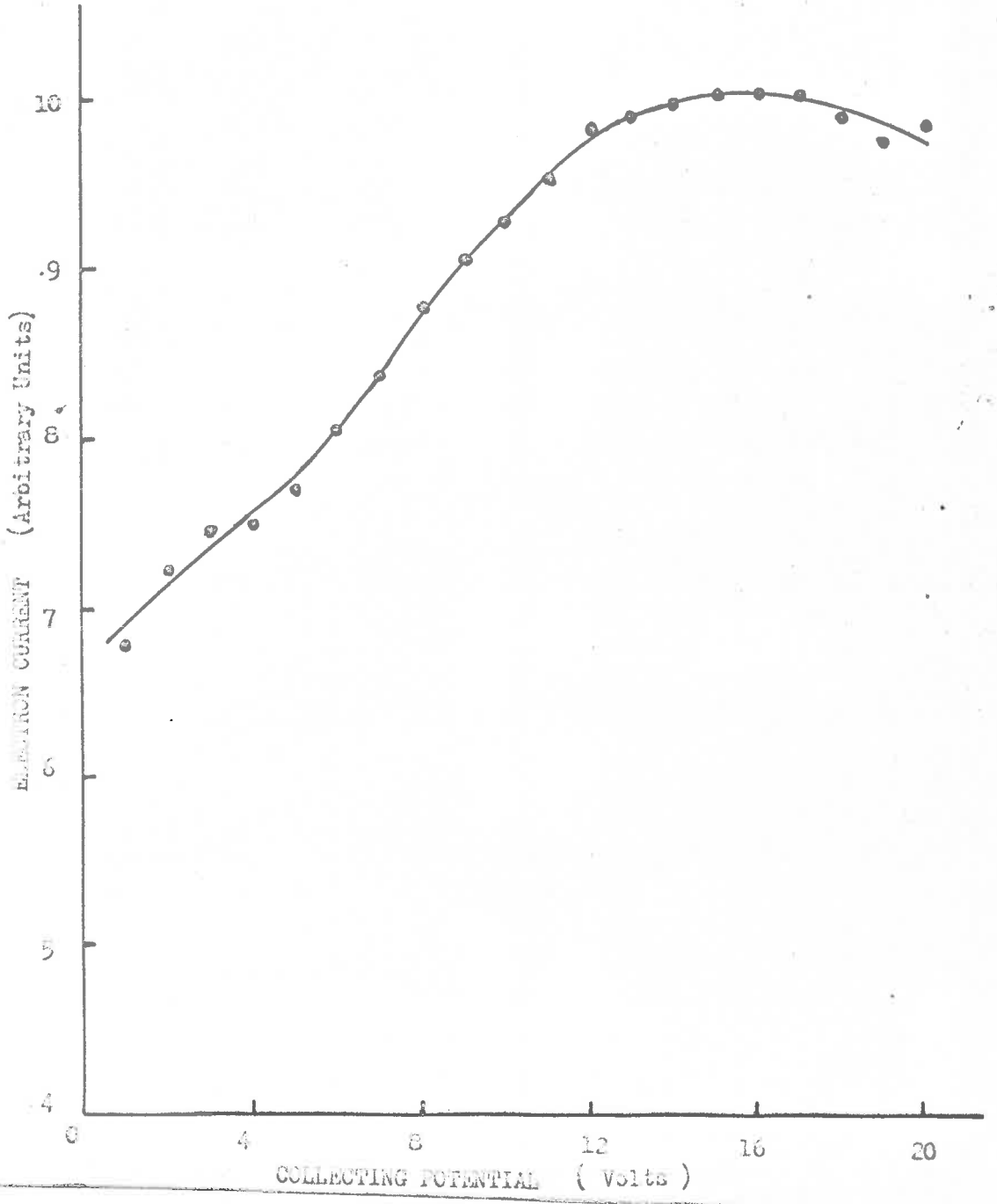

Fig. II.12. Saturation characteristics of the photoelectron spectrometer.

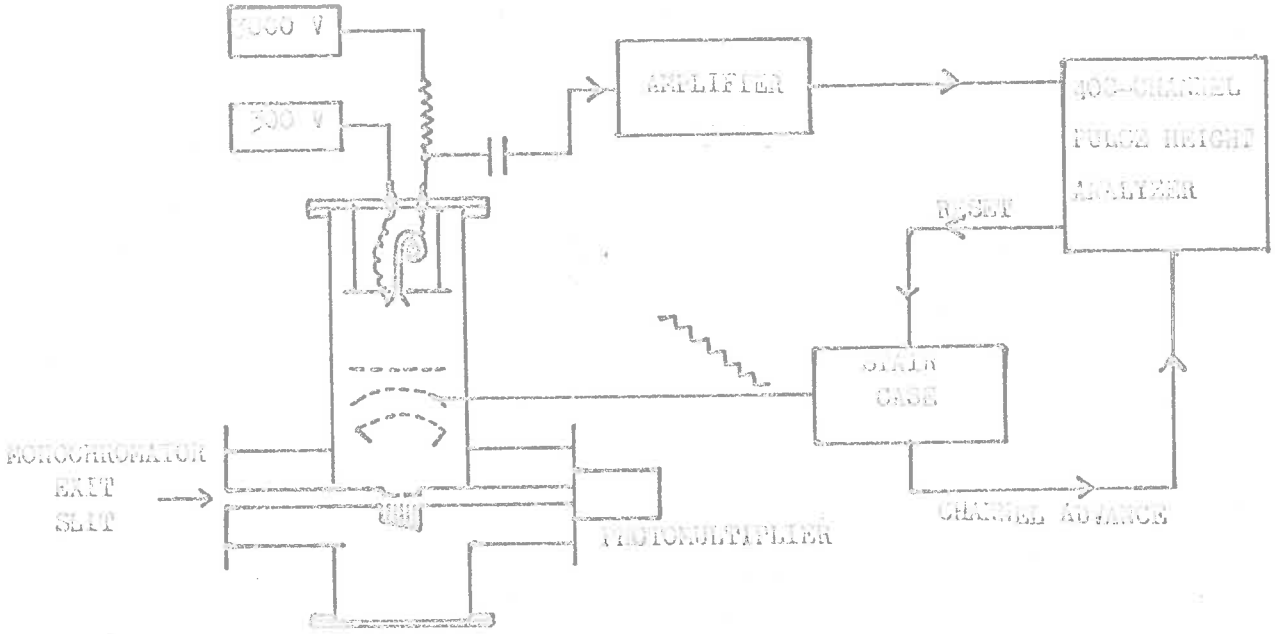

Fig. II. 13 . Diagram showing the principle for the operation of photoelectron spectrometer .

Fig. II.14. Integral spectra of xenon at 584 A°.

energy present in the spectrum.

The integral spectrum does not give a fair idea of the low energy noise of the spectrometer. So the differential spectrum is required. The numerical differential being tedious and time consuming, the electronic differentiation has been attempted.

II.5.2 Electronic Differentiation of the Integral Spectrum

A square wave was superimposed on the steps of the staircase symmetrically with the step passing through the centre of the square wave. Two pulses of same dimensions and frequency as the square wave but opposite in phase to each other were fed to the add and subtract modes of the multi-channel pulse height analyser. To have a better understanding of the electronic differentiation, suppose one step of the staircase corresponds to 2 volts of retarding potential. A square wave is superimposed on this step so that 1/4 of a volt is on each side of the step. This step corresponds to a certain channel. In this channel, the number of electrons coming out with energy between 2 and 2 1/4 volt will be added and number of electrons with energy between 2 and 1 3/4 volt will be subtracted, the number of add and subtract operations

depending upon the speed of the channel advance. The same will be repeated in the next channel which corresponds to some other value of the retarding potential and so on.

To ensure that no spurious counts are recorded during add-subtract charge or channel advance, a gated pulse is required to feed the detector gate input of the pulse height analyser. Figure II.15 shows a 20 microsecond pulse used to gate the detector. Halfway through the 20 microsecond period, the flip-flop is fired to charge the add-subtract mode and advance the channel address. Thus the detector gate is 10 microsecond ahead of the add-subtract and channel advance front edges and is 10 microsecond behind if the time for these front edges is neglected (Figure II.16).

The differential spectrum for xenon was recorded using the electronic differentiating technique. The spectrum shown in Figure II.17 is the result of many scans. The spectrum from only one scan would be of poor quality because of large amount of noise generated at the spark gap of the power supply for the monochromator lamp. Sufficient averaging of the noise was achieved by having several scans. This was done by resetting the staircase automatically after each scan using a reset pulse from

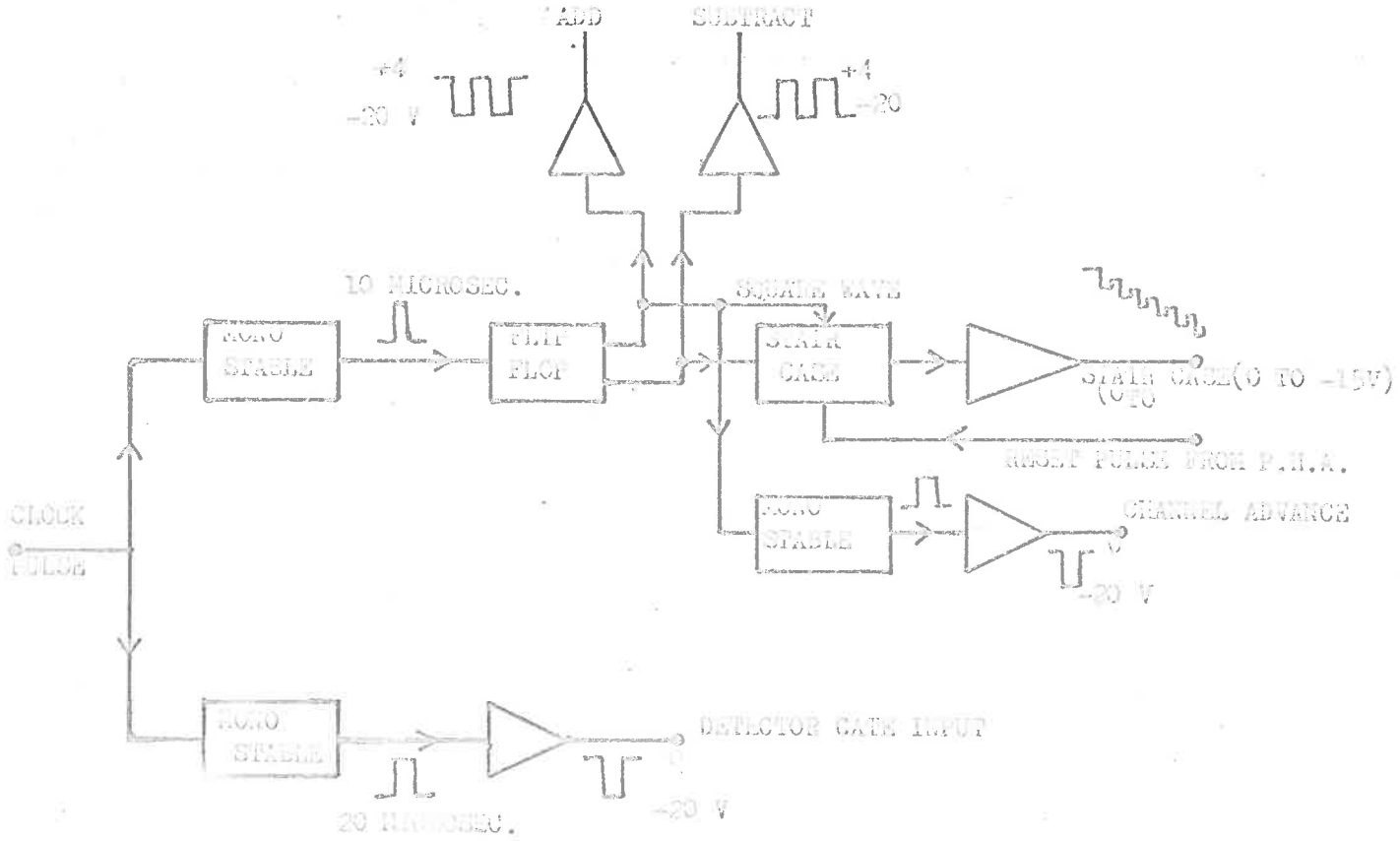

Fig. II.15. Block diagram of the electronics used to produce the required
[illegible] ording stair case .

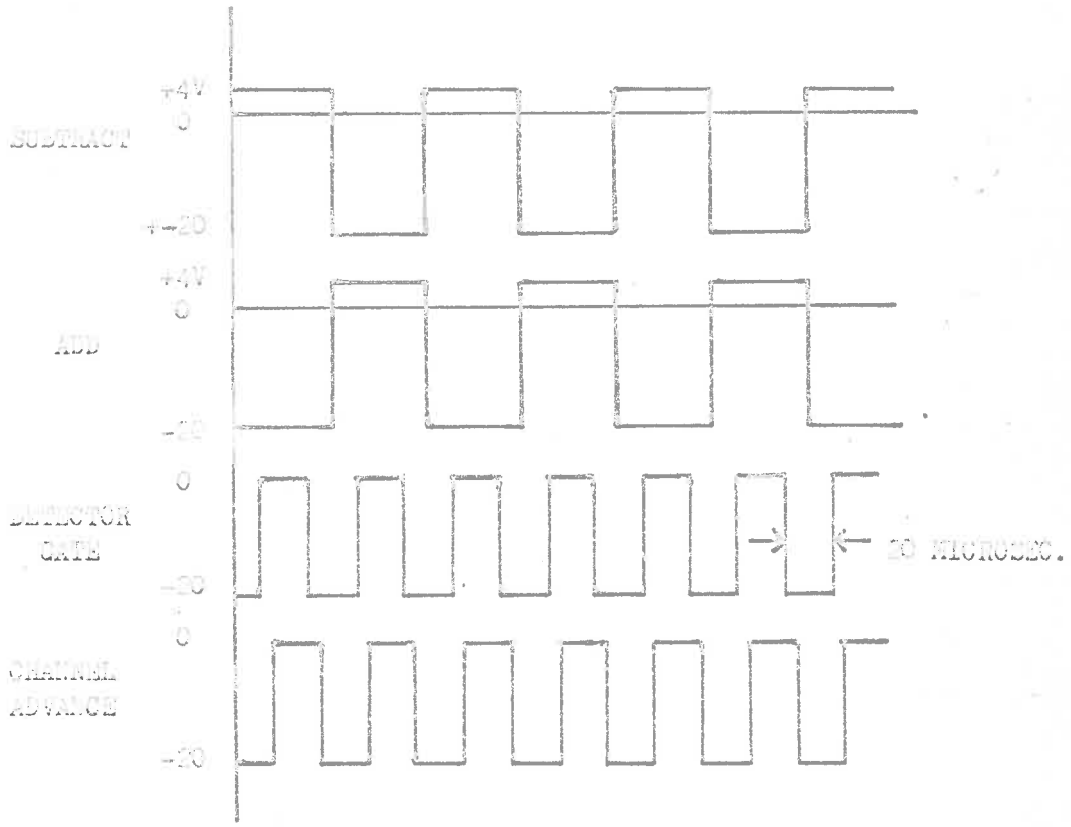

Fig. II.16 . Add-subtract , detector gate and channel advance pulses.

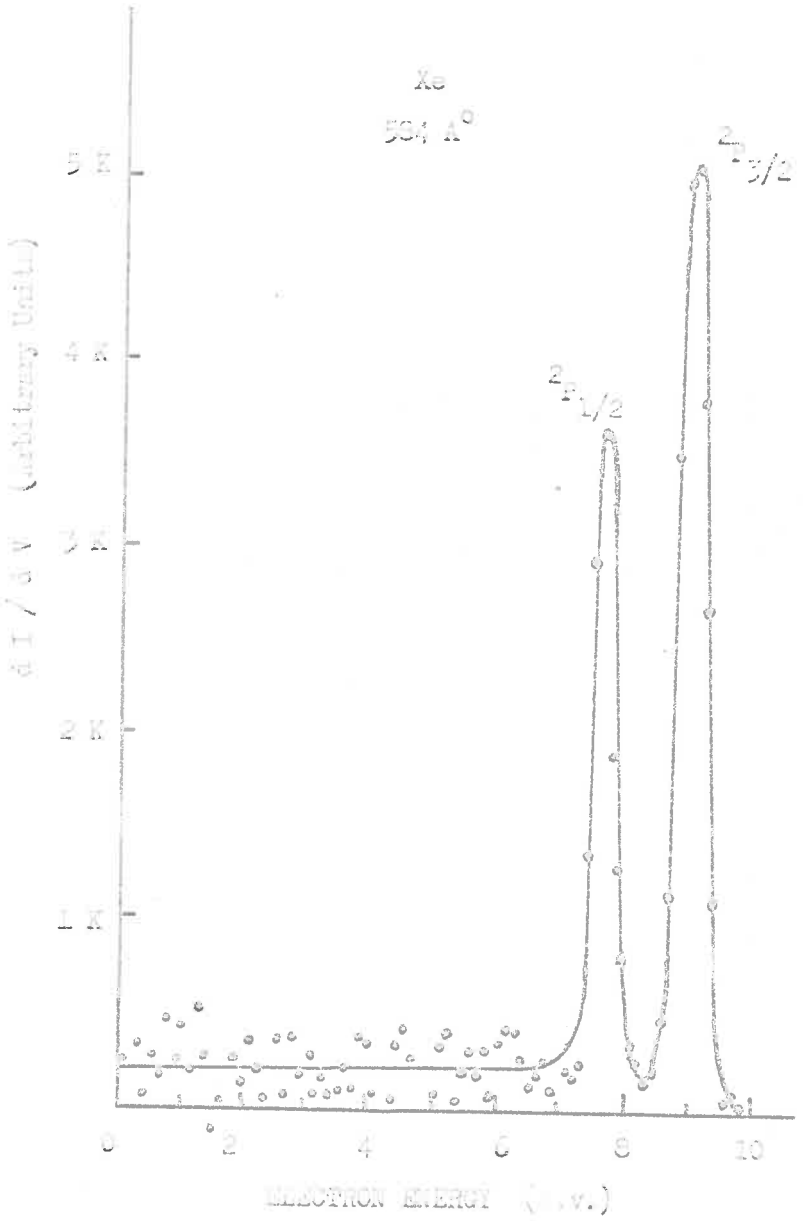

Fig. II.17. Photoelectron energy spectra (differential) of xenon at 584 A° .

the pulse height analyser which resets the binaries of the staircase after 100, 200 or 400 channels as required.

II.6 Performance of the Spectrometer

The spectra of different gases for the two experiments, partial photoionization cross-section and autoionization phenomena described in chapters III and IV respectively, could be interpreted only after several characteristics of the spectra had been studied. These included resolution of the spectrometer, its collecting efficiency and calibration of the energy scale.

II.6.1 Resolution

The resolution of the spectrometer was defined as the full width at half maximum of the peak produced by a monoenergetic electron source. The half width of the two xenon peaks was taken as a measure of the resolution. This was found to be ~ 0.4 volts in each case (Figure II.17) with 584Å photon radiation incident on the gas, giving peak energies of 7·7 and 9·0 e.v.

This resolution was obtained with the best operating conditions of the experiment available. The exit slit of the monochromator was 200 microns wide, giving a beam resolution of 1·6Å which corresponded to an energy spread of 0·08 e.v. at 584 Å. The small beam resolution limited

the height of the square wave superimposed on the staircase step, which affects the resolution, to a minimum of 0·1 volts. But to increase the electron count rate for better statistics, the square wave height could be increased up to 0·2 volts without much loss of resolution.

Many other factors were also affecting the resolution of the spectrometer. The fundamental assumption for constructing better resolution spherical grid systems was to produce photoelectronsin a small volume at the centre of the spherical grid system so that initial ejection was always perpendicular to the retarding field. Every care was taken to produce electrons in a small volume making the diameter of the hole (Section II.4.1a) in the best limits of our theoretical calculations. But there was a slight possibility that the spherical grids due to the problem of their mounting were not exactly aligned with the electron source as the centre.

Other factors with different effects on the resolution were the contact potential in the grid wires and their mounts, negligibly small distortions of the grids from spherical forms and the variation of the potential of the space between the grid wires from that of the wires.

For the investigation into the autoionization phenomenon, the spectra obtained for different gases were under the same experimental conditions as quoted above. But for the measurements of partial photoionization cross-sections, some of the resolution was sacrificed in order to improve the noise to signal ratio in the spectra. The monochromator exit slit was increased to 1000 microns, giving a beam resolution of about 8Å (0·33 e.v. energy spread at 584Å).

II.6.2 Analysis of the Monoenergetic Spectrum

The photoelectron spectrum of argon as shown in Figure II.18 showed a single peak at the energy equal to the difference of the photon energy and the ionization potential of argon. The resolution of the spectrometer was adjusted to get only one peak, a combination of the two from the doublet ground state $^2P_{1/2,3/2}$ of the argon ion. The spectrum obtained had also a small area of low energy. Many possible reasons for this low energy portion of the spectrum were investigated. Effects such as electron collisions with gas atoms, existence of magnetic fields were positively negated by the different experimental approaches used. The remaining possible origin of the low energy part of the spectrum was reflection of electrons at the grid surfaces and the secondary emission.

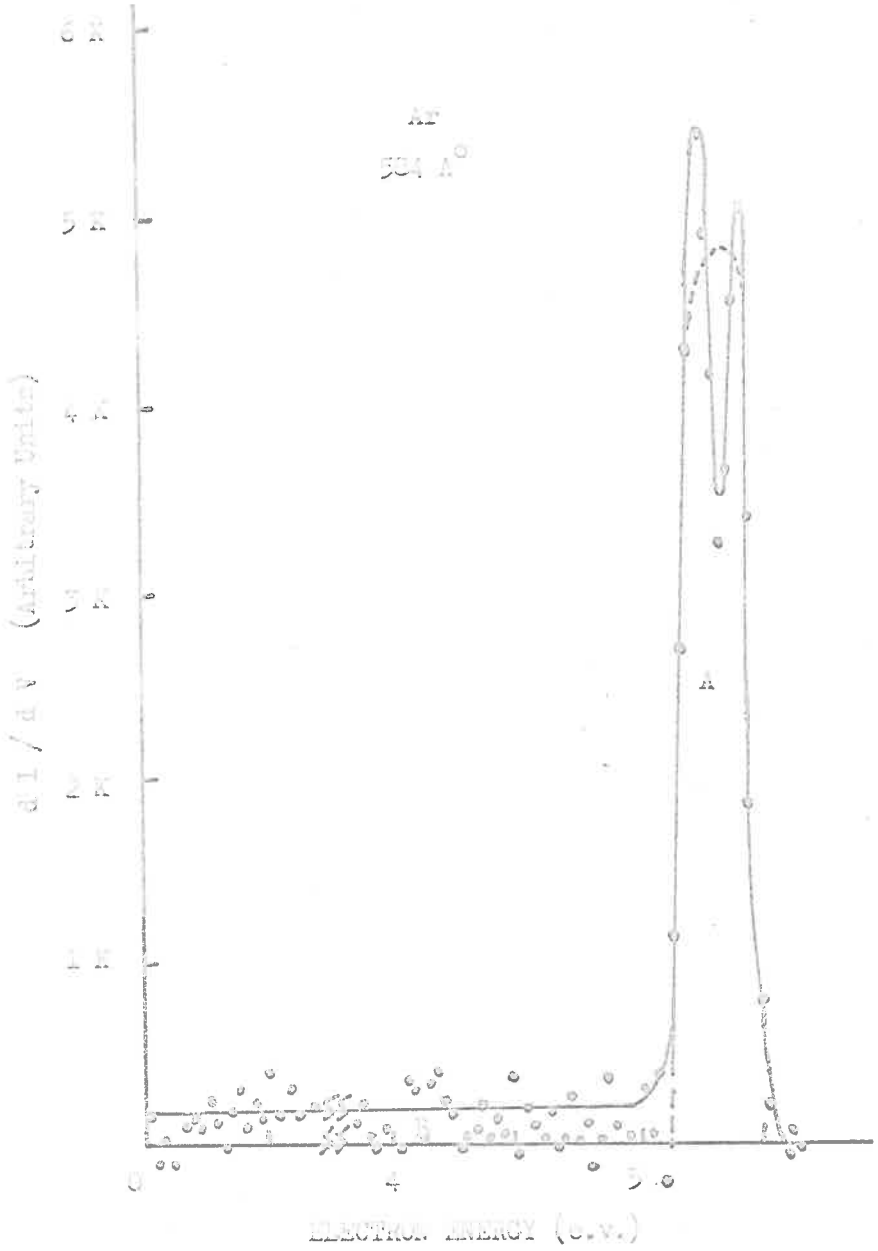

Fig. II.13. Photoelectron energy spectra of argon at 504 A° showing the two areas, under the peak (A) and the low energy area associated with the peak (B).

For the purpose of assigning the low energy part to the different peaks of the spectrum of various gases, the spectrum of argon was divided into two parts. The first was a symmetrical peak, marked A and the second was the remaining low energy part, marked B, which was thought to be due to electron reflection and secondary emission from grid surfaces. With the assumption that the peak shape depended mainly on the peak energy, the ratio of areas B and A was measured over a range of peak energy (Figure II.19). This calibration curve is a good tool for unfolding complicated spectra. The plot of B/A against peak energy of argon was compared with that of zenon and molecular hydrogen. They were found to be in good agreement showing that the spectrum shape does not depend on peak width.

The energy scale of the spectrometer also needed some sort of calibration. This was again done using the argon peak as a standard. In Figure II.20, the predicted peak energy was plotted against measured peak energy over a range of photon energy.

II.6.3 Electron Collecting Efficiency

One of the possible sources of error in spectra is the variation of electron collecting efficiency with

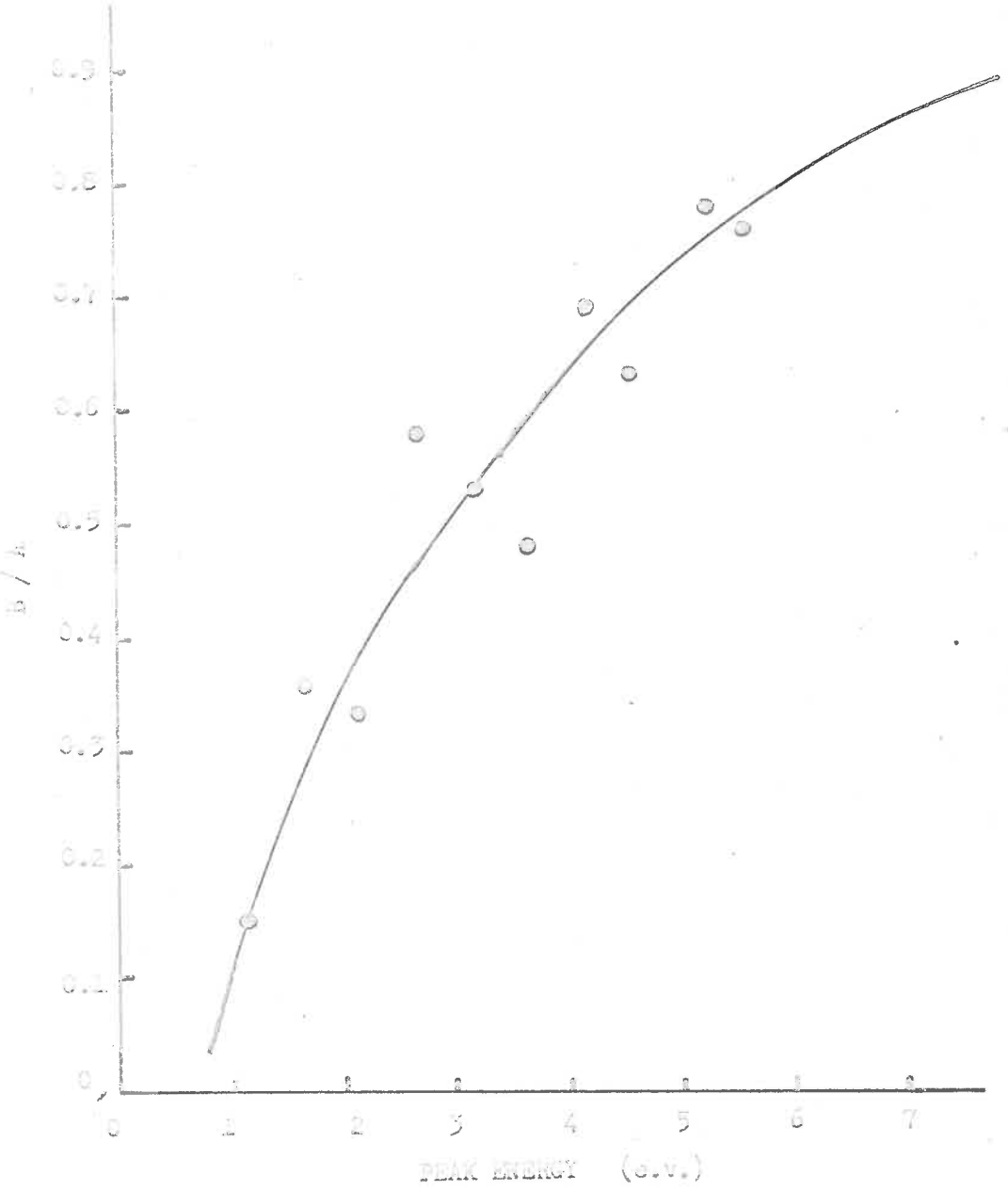

Fig. II. 19 . The calibration curve for unfolding complicated spectra of molecular ions.

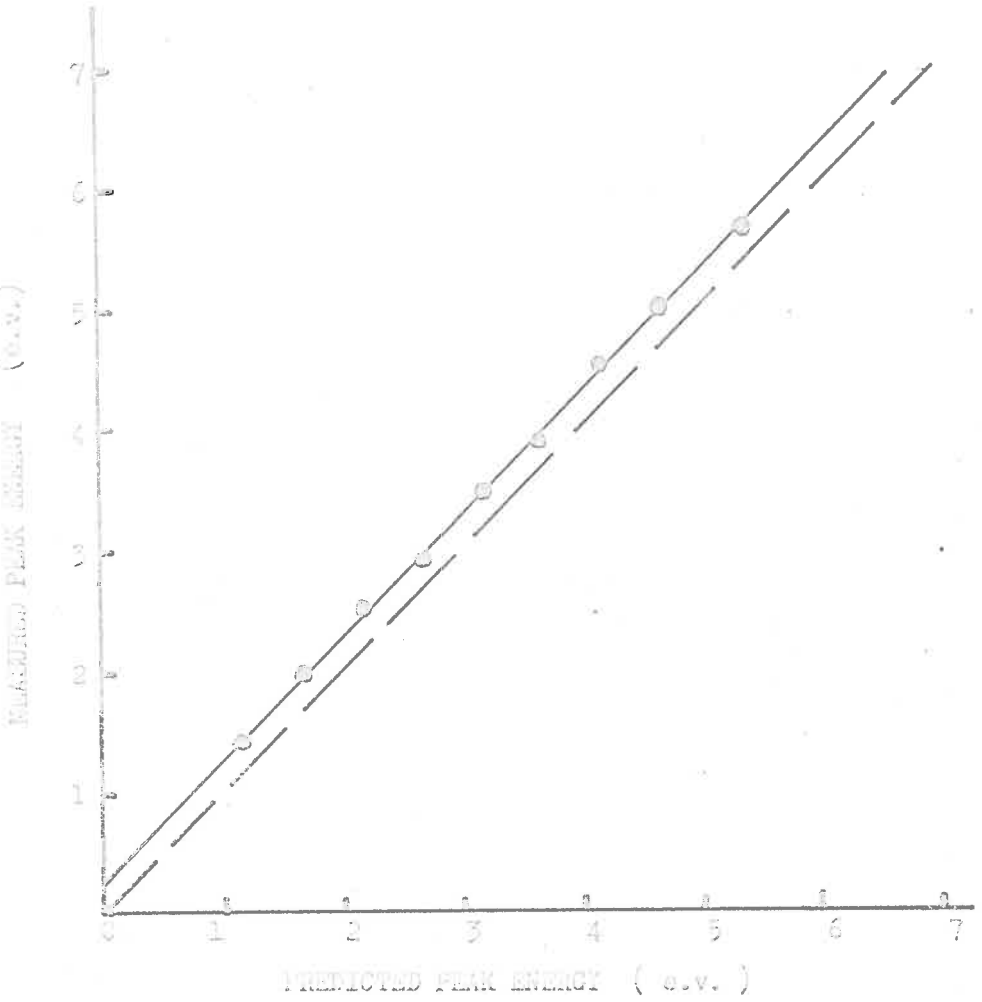

Fig. II.5 . Calibration of energy scale using argon gas .

electron energy. In order to avoid this error, the collecting efficiency has been measured as a function of incident photon wavelength, using argon as the source of monoenergetic photoelectrons. Photoionization yield of argon being constant (Samson, 1964), the apparent changes in the yield would affect the electron collecting efficiency of the spectrometer.

As shown in Figure II.21, the photon beam intensity I_3 measured at the end of the tube can be calculated in terms of incident photon beam intensity I_0 and the different distances x_1, x_2 and x_3. This is given by

$$I_3 = I_0 \, e^{-k(x_1 + x_2 + x_3)}$$

The number of electrons produced in the target area is calculated as

$$\begin{aligned} n_e &= I_1 - I_2 \\ &= I_0[e^{k(x_2 + x_3)} - e^{kx_3}] \end{aligned}$$

where k, the absorption coefficient of argon, depends upon the incident photon wavelength and the pressure which is kept constant throughout the experiment. The ratio of the number of electrons collected by the channel electron multiplier to the number of electrons produced in the target area, would give electron collecting

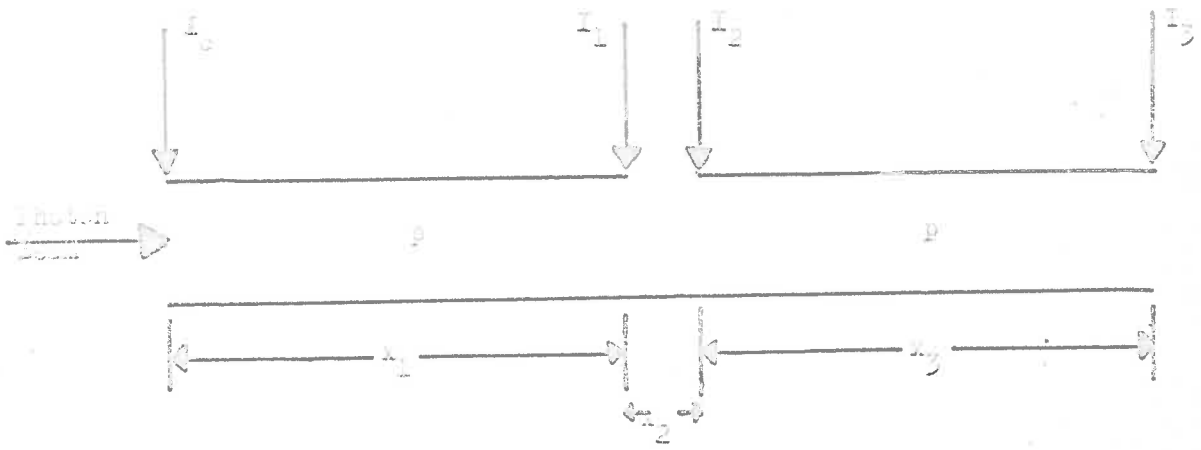

Fig. II.C1. Point source of photoelectrons showing the intensity of light at different distances from the exit slit of the monochromator .

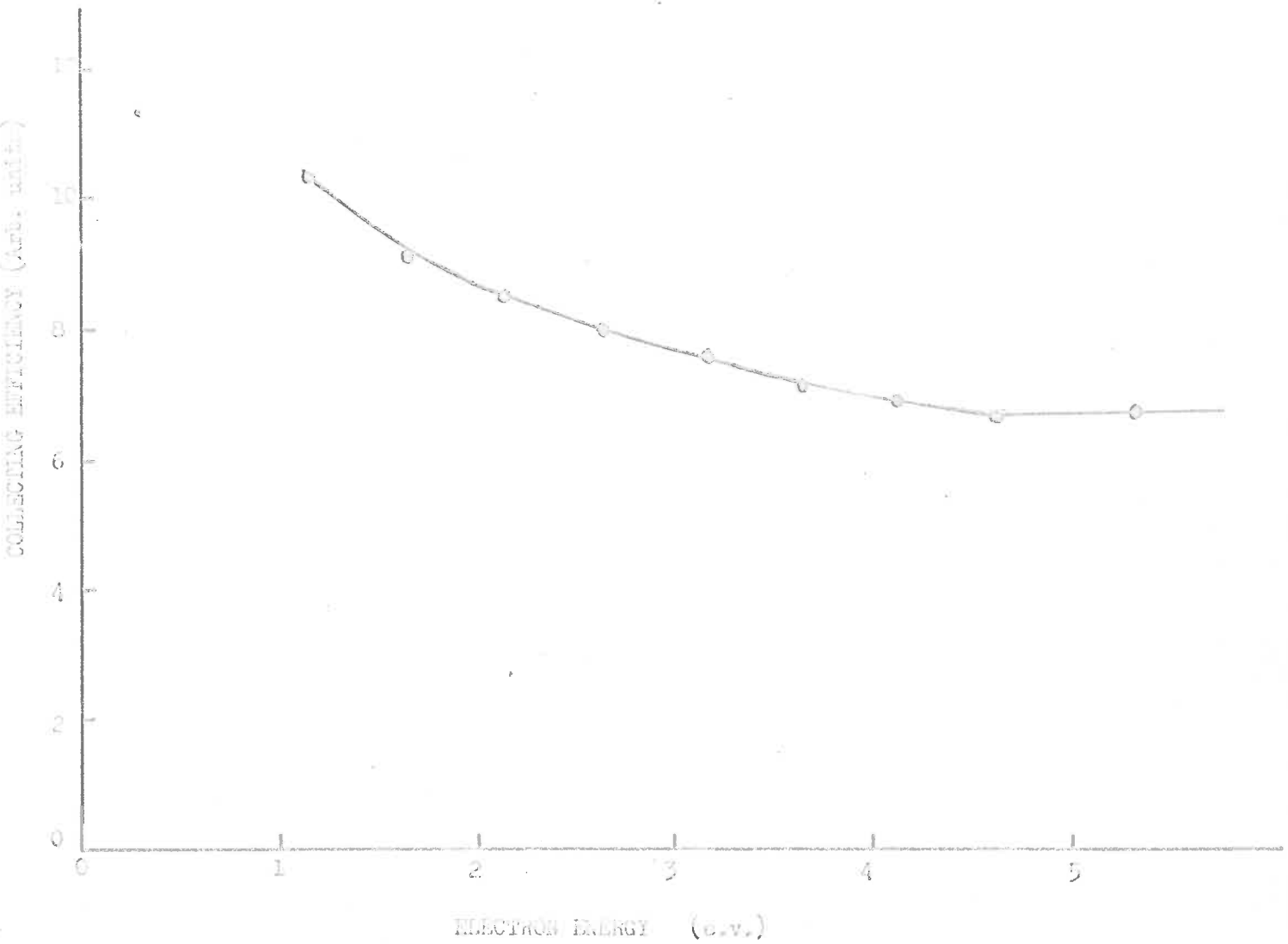

Fig.II.22. The plot of electron collecting efficiency against electron energy.

efficiency. Its variation with electron energy is shown in Figure II.22. The collecting efficiency of low energy electrons as shown in the figure is slightly higher than that of the high energy electrons. The small variations which occurred indicate that no correction factor is necessary.

CHAPTER III

PARTIAL PHOTOIONIZATION CROSS-SECTIONS

III.1 Carbon Dioxide

The presence of carbon dioxide as one of the major constituents in the Venusian atmosphere (Shimizu, 1966) necessitates the experimental investigation into the photoelectron spectroscopic aspect of the gas. This will assist to have a better understanding of various aeronomical phenomena occurring in this planet viz. the partial photoionisation rates at different altitudes of the Venusian ionosphere and electron temperatures.

The photoelectron spectrometer described in chapter II was used to obtain the energy spectra of the ion. The spectra obtained, in general, consist of several peaks which can be identified as the ground state and other excited states of the molecular ion. These spectra were analysed to obtain partial photoionization cross-sections for the different states of the ion, i.e. the contribution of different states to photoionization. The variation of partial photoionization cross-sections with photon wavelength was also obtained by recording spectra at different wavelengths.

III.1.1 Photoelectron Energy Spectra

The photoelectron spectra for CO_2 were recorded at 584Å and at wavelengths between 600Å to 720Å. This was achieved by using the Hopfield continuum of helium as the light source. The beam resolution was kept at 8Å but the spectra were taken at 5Å intervals. The carbon dioxide was of 99·9% purity and was used without any further purification. The operating pressure in the spectrometer chamber, as measured by an ionisation gauge, was 9×10^{-4} m.m. but the pressure inside the tube used as the source of photoelectrons was considerably higher ($\sim 9 \times 10^{-3}$ m.m.).

As an example, the spectrum at 605Å, recorded under the above conditions is shown in Figure III.1. This spectrum shows four photoelectron peaks, each one of which was identified with one of the states of the singly charged molecular ion. The peak position of each state, the photon energy and the energies of the different electronic states of the ion, as measured by other experimentalists or predicted by theoretical calculations, serve to identify the peak. The half-width of the different peaks was found to be about 0·5 e.v., indicating that the vibrational structure of the different bands was unresolved.

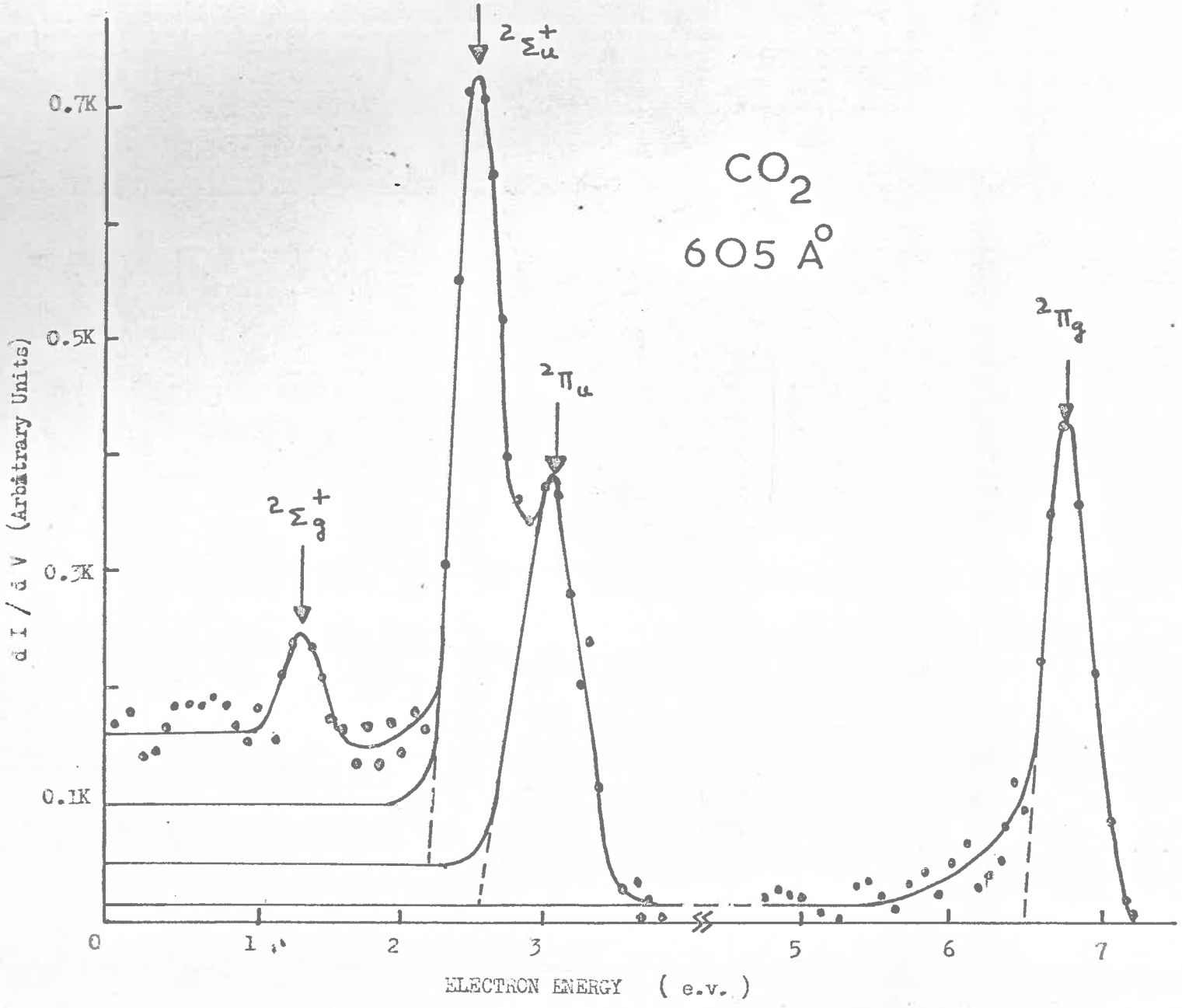

Fig. III.1. Photoelectron energy spectra of carbon dioxide at 605 A° .

Some resolution had to be sacrified in order to get a satisfactory signal to noise ratio. The maximum of the unresolved bands may or may not correspond to the lowest vibrational level of the state, giving adiabatic or vertical excitation potentials of the states respectively (Franck-Condon principle).

The energies of different electronic states of the ion were measured experimentally by Tanaka et al. (1960), Al-Joboury et al. (1965) and Turner and May (1967). Tanaka et al. found the energies of the $^2\Pi_g$, $^2\Sigma_u^+$ and $^2\Sigma_g^+$ states as 13·78 e.v., 18·06 e.v. and 19·39 e.v. respectively. Slightly different results for these three states were reported by Al-Joboury et al. who observed energies at 13·68 e.v., 18·08 e.v. and 19·29 e.v. respectively.

Strong evidence for the existence of the $^2\Pi_u$ level was given by Mrozowski (1941, 1942, 1947) with 17·32 e.v. as the reported energy value of the state. Mulliken (1942) also suggested the existence of this state but the energy value quoted by him was quite vague (>17·1 e.v.). Turner and May (1967) confirmed experimentally Mrozowski's results and reported the adiabatic excitation potential of the state at 17·32 e.v.

The spectrum of carbon dioxide at 605Å (Figure III.1)

shows the peak positions to be in reasonable agreement with those of Al-Joboury et al., Tanaka et al. and Turner and May. The highest energy peak occurs at 6·8 e.v. It is assumed that the zero vibrational level of this band occurs at the peak position in accordance with Turner and May's findings. The 6·8 e.v. peak corresponds to the ground electronic state $^2\Pi_g$ of the ion, giving 13·7 e.v. as the energy of the ground state of the ion from the ground state of the molecule. The second peak has an energy of 3·2 e.v., giving the energy of the electronic state of the ion as 17·3 e.v. This confirms the predicted state $^2\Pi_u$ of Mrozowski and shows a good agreement of the excitation potential of the state observed in the present experiment with the results of Mrozowski and Turner and May. The third peak at 2·5 e.v. corresponds to $^2\Sigma_u^+$ state and is about 3% in accuracy with other results. The fourth peak in the spectrum at 1·3 e.v. corresponds to the $^2\Sigma_g^+$ state of the molecular ion.

III.1.2 Unfolding the Spectra

The interpretation of the photoelectron energy spectra of carbon dioxide in terms of partial photo-ionization cross-sections required the measurement of area under the spectrum associated with each peak. It

was assumed that the spectrum was equivalent to the sum of several monoenergetic spectra with the shape shown in Figure II.18.For purposes of unfolding the spectra the area (A) under the most energetic peak was measured with a planimeter. Knowing the peak energy from the spectrum, the area under the low energy side (B) associated with this peak was calculated. This was achieved with the help of the curve of B/A against peak energy (Figure II.19). In this way, the area equal to the calculated value of B, was fitted to the low energy side of the peak by a trial method, keeping the shape of the low energy side of the peak the same as in Figure II.18. Each successive peak in the spectra of carbon dioxide was treated in the same manner.

Assigning the total areas of two peaks just resolved, as $^2\Pi_u$ and $^2\Sigma_u^+$ states in this case, is quite complicated. For this, the knowledge of the shape of the two peaks is essential. This was achieved by taking the spectra with the retarding potential on the grid between -2V and -4V, spreading the two peaks over 100 channels of the multi-channel analyser. The shapes of the peaks now being known in detail, the areas under low energy side of the peaks could be easily determined.

III.1.3 Branching Ratios

The number of ions produced in each state was assumed to be directly proportional to the area of the spectrum which was associated with the corresponding peak. The measurement of areas associated with different peaks as a function of total area under the whole spectrum would give the percentage of ions in their respective electronic states. This was defined as the branching ratio of the state.

For better understanding of the branching ratios, the spectra of carbon dioxide at different wavelengths needs to be discussed. Figure III.2 shows spectrum at 625Å. This spectrum contained peaks corresponding to all four electronic states of the ion. As the photon wavelength increased, the peaks tended to shift towards the low energy side of the spectrum, keeping constant energy difference between different peaks. At 655Å (Figure III.3), the peak corresponding to $^2\Sigma_g^+$ state seemed to vanish, indicating the threshold energy of the state to be between 19·2 to 19·3 e.v. Figure III.4 shows the energy spectrum at 700Å which indicates the presence of only two peaks corresponding to $^2\Pi_g$ and $^2\Pi_u$ states. At 720Å (Figure III.5), only ground electronic state $^2\Pi_g$ is shown to exist.

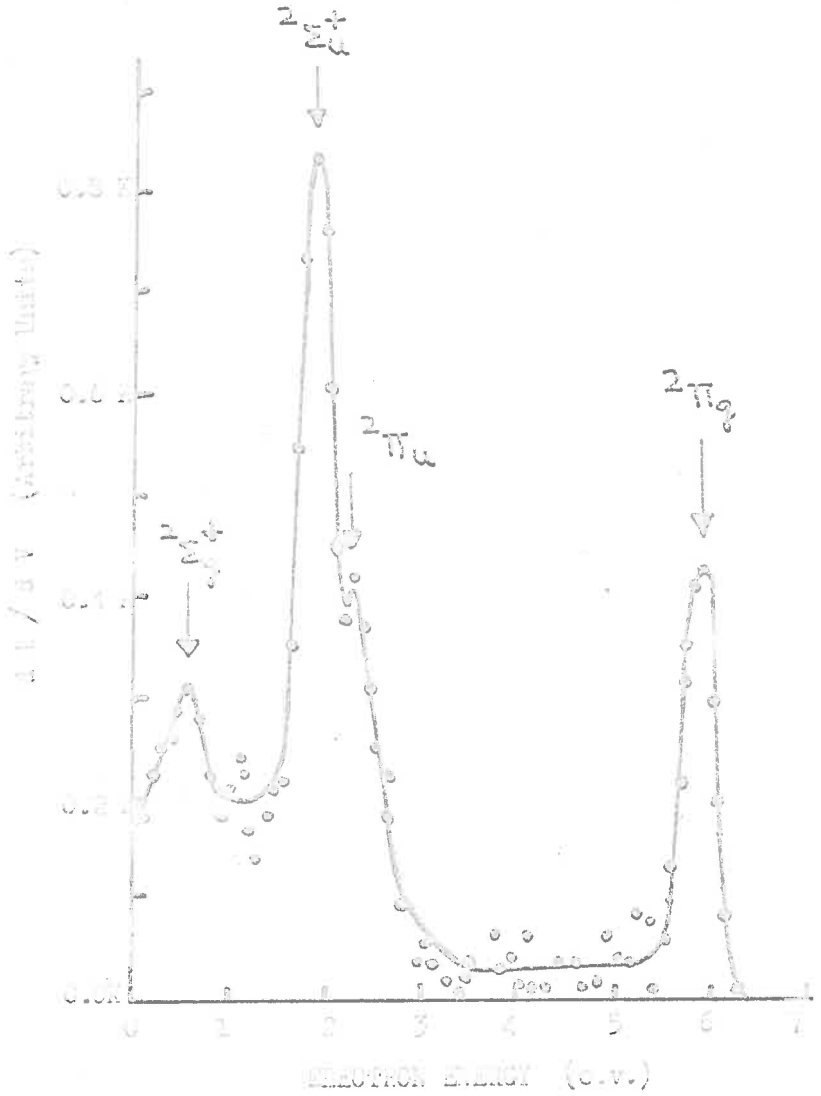

Fig. III.2 . Photoelectron energy spectra of carbon dioxide at 625 A^o .

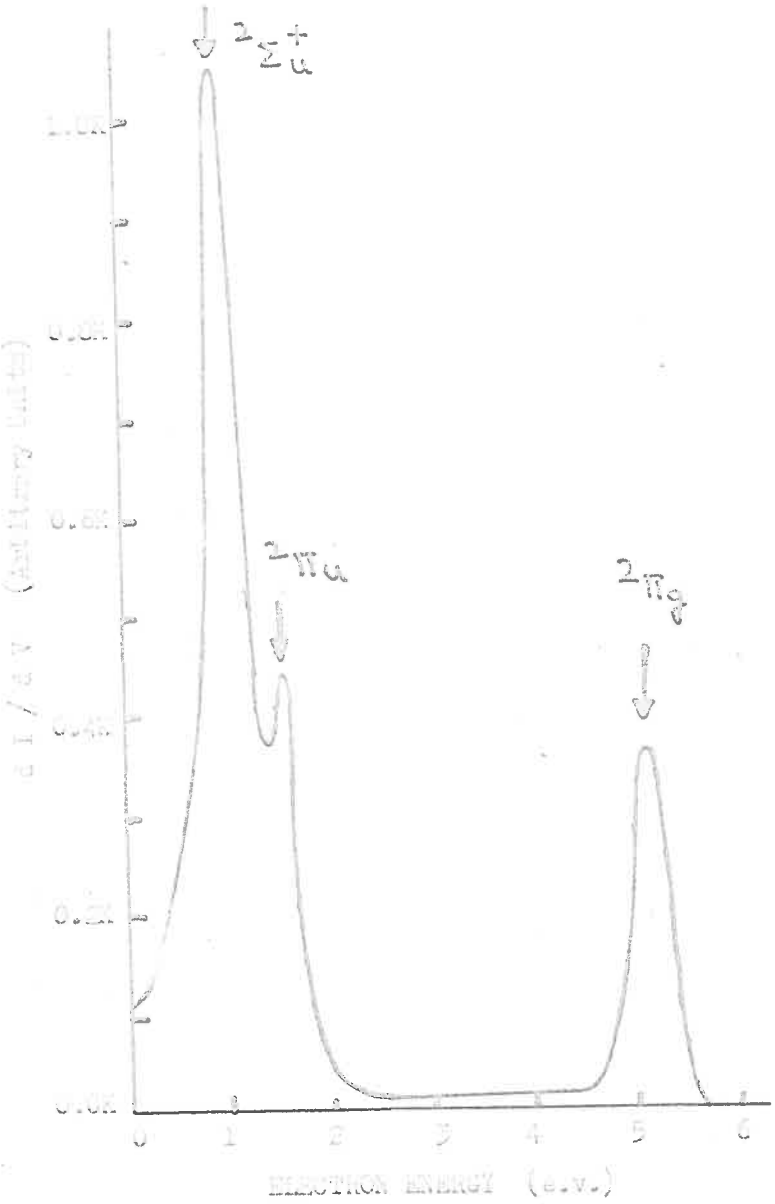

Fig. III.3. Photoelectron energy spectra of carbon dioxide at 655 A^o .

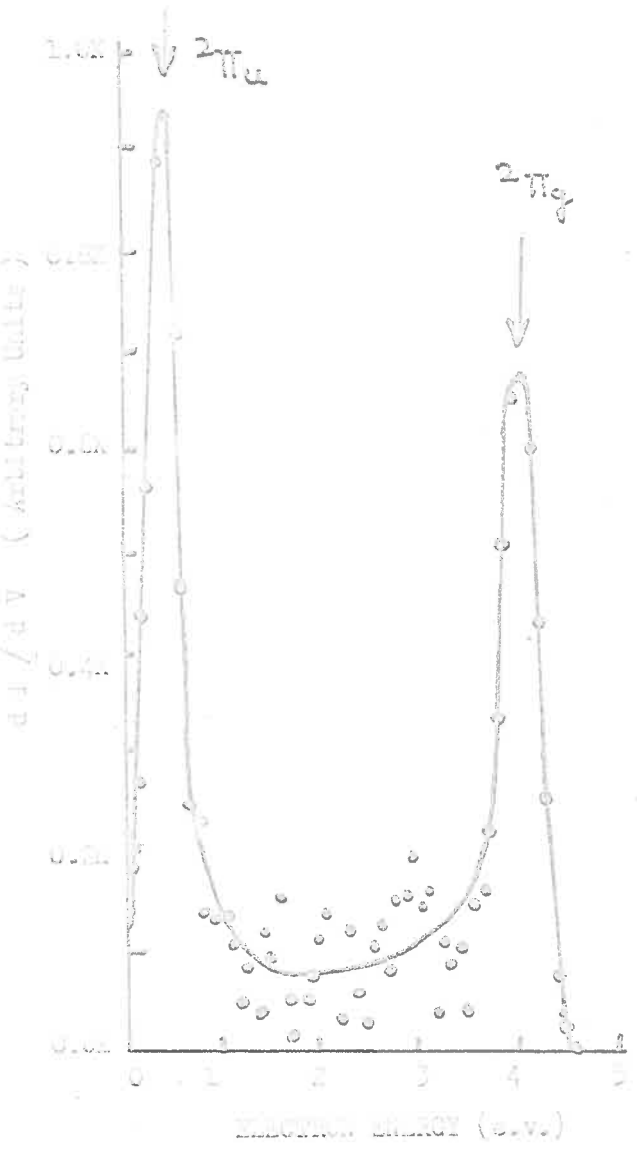

Fig. VII.4 . Photoelectron energy spectra of carbon dioxide at 700 A^0.

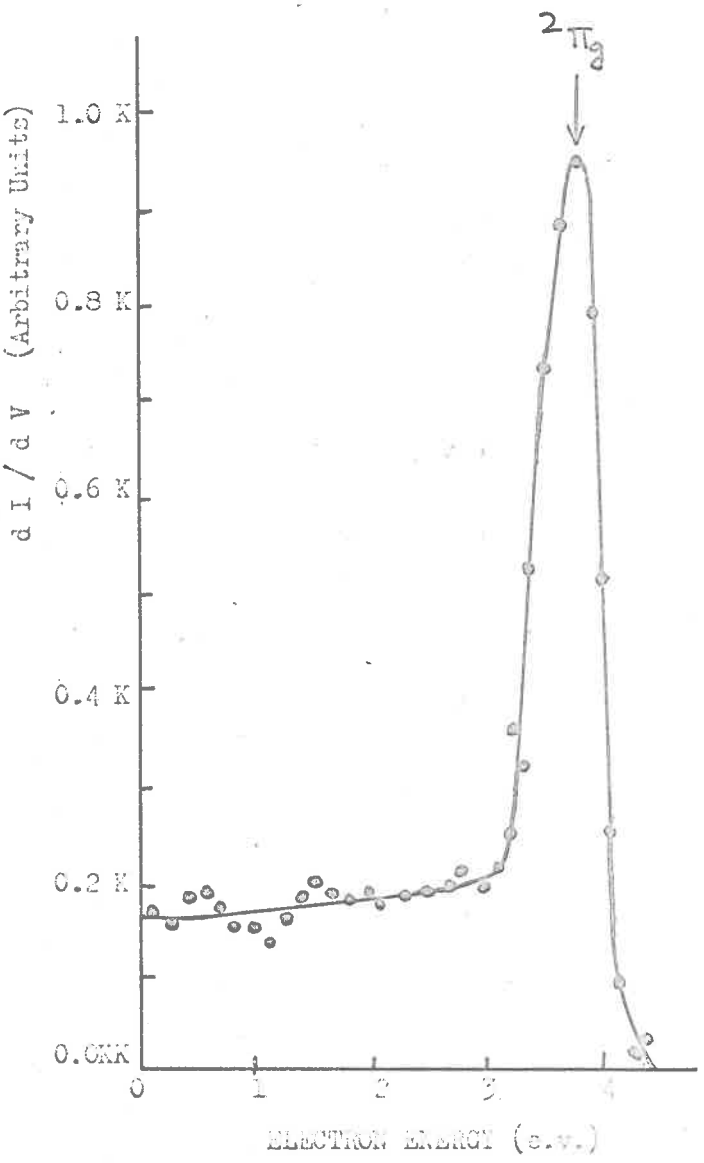

Fig. III.5. Photoelectron spectra of carbon dioxide at 730 A° .

The plot of branching ratios against wavelength is shown in Figure III.6. The branching ratios of the ground state of the molecular ion ($^2\Pi_g$) were found to be fairly constant in the wavelength region of 584Å to 675Å. In this region, the branching ratios varied from 24% to 28%. As the wavelength increased, the percentage of ion formation in the state started increasing almost exponentially. From 720Å to the threshold energy of $^2\Pi_g$ state, the contribution of ion formation is limited only to the ground state. In the $^2\Pi_u$ state, the branching ratios varied from 19% to 23% in the wavelength region of 584Å to 675Å. The maximum for this state (50%) corresponded to the photon wavelength of 700Å. The relative ion formation in $^2\Sigma_u^+$ state increased slowly up to 670Å which corresponded to the maximum relative transition probability. The branching ratios of $^2\Sigma_g^+$ state varied from 10 to 12% in the wavelength region of 584Å to 625Å after which they decreased rapidly.

III.1.4 Partial Photoionization Cross-Sections

The partial photoionization cross-sections of different ionic states of CO_2 were obtained by combining the branching ratios of Figure III.6 with the total photoionization cross-sections. The total cross-sections of CO_2 reported by Cook, Metzger and Ogawa (1966) were

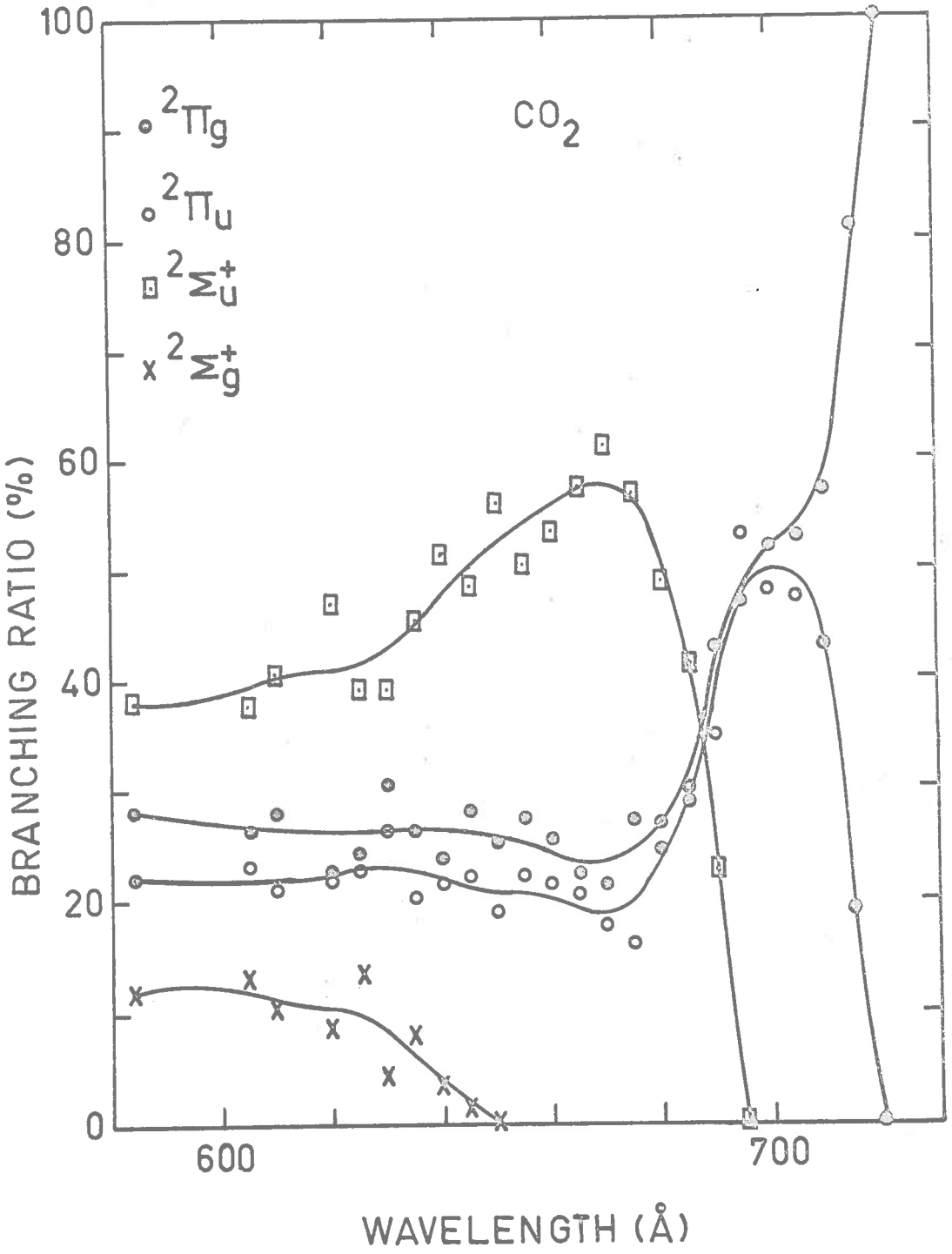

Fig. III.6. Branching ratios for different competing processes in CO_2^+.

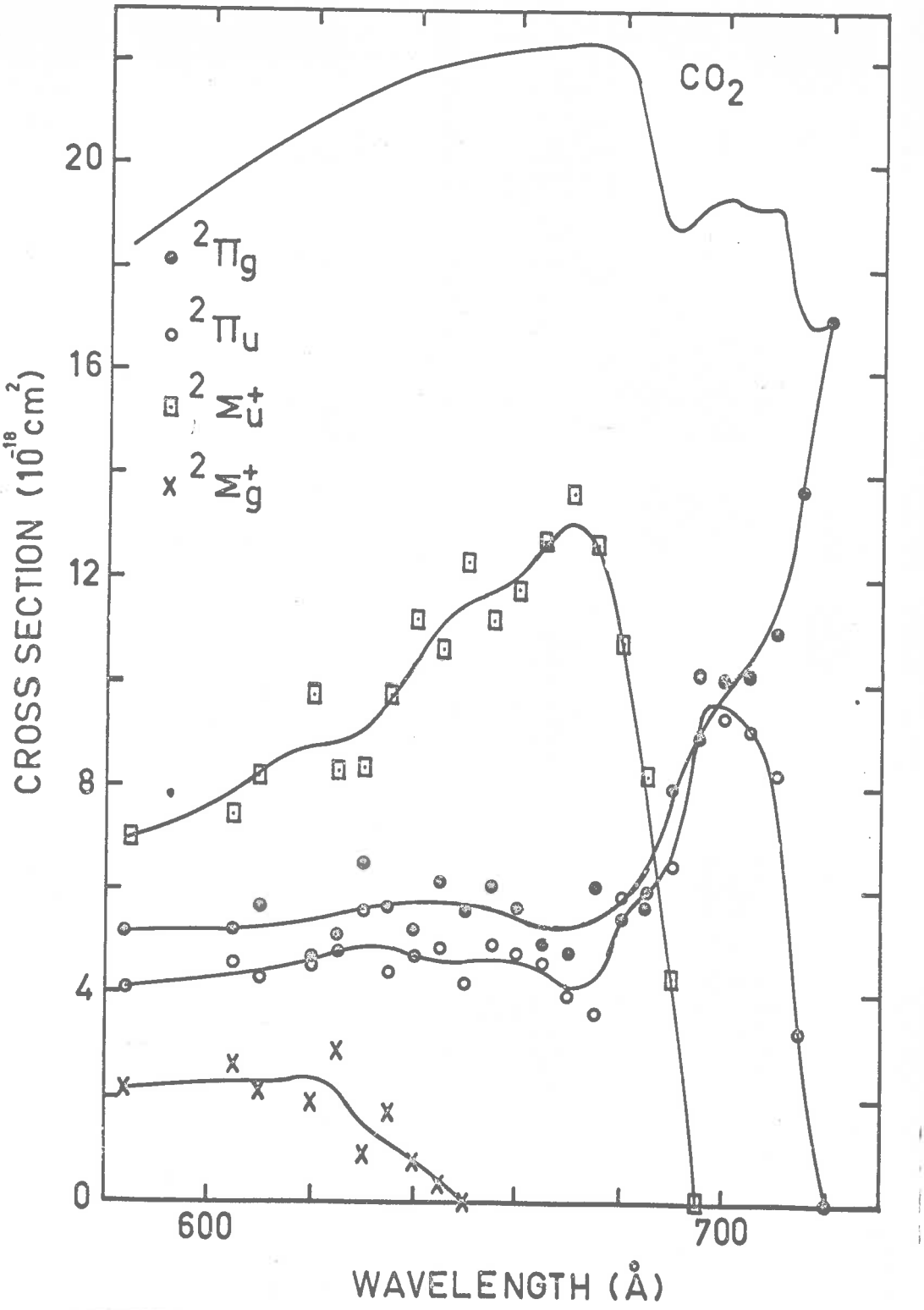

Fig. III.7. Partial photoionization cross-sections for different competing processes in CO_2^+ . The upper curve is the total cross-sections of carbon dioxide obtained by averaging the results of Cook, Metzger and Ogawa, 1966 over 8 A^o intervals .

averaged over 8Å intervals to obtain a resolution equivalent to that used in the present work. The total photoionization cross-sections so obtained and partial cross-sections as a function of wavelength are shown in Figure III.7.

III.2 Carbon Monoxide

Photoelectron spectra of carbon monoxide were obtained in the range of 600Å to 855Å at an interval of 5Å and also at 584Å. The different processes occurring are given in Table III.1.

TABLE III.1

Carbon Monoxide Photodisintegration Processes

Process	Appearance Potential (e.v.)			
	Turner et al. (1966)	Fox et al. (1954) (b)	Spectroscopic (a)	Present Work
$CO\ (X^1\Sigma^+) + h\nu$				
$\rightarrow CO^+\ (X^2\Sigma^+) + e^-$	14·00	14·1	14·01	14·0
$\rightarrow CO^+\ (A^2\Pi) + e^-$	16·54	16·4	16·53	16·5
$\rightarrow CO^+\ (B^2\Sigma^+) + e^-$	19·65	19·0	19·67	19·7

(a) Tanaka (1942)
Takamine et al. (1943)
Lindholm (1954a)

(b) Electron impact experiment

Table III.1 shows the values of appearance potentials for $X^2\Sigma^+$, $A^2\Pi$ and $B^2\Sigma^+$ states obtained in the present work to be in fair agreement with those of Turner et al. and Takamine, et al. The electron impact experiment (Fox et al.) gives low values for the three states.

A photoelectron spectrum of carbon monoxide at 584Å is shown in Figure III.8. The $X^2\Sigma^+$ state was found to have a band width of the same order of the beam resolution, indicating the presence of only $0 \rightarrow 0$ vibrational state. The $A^2\Pi$ and $B^2\Sigma^+$ bands had unresolved vibrational structure. The fourth peak which was obtained only in a few spectra at photon wavelengths 584Å, 600Å and 605Å, appeared at 0·5 e.v. corresponding to appearance potential of about 20·7 e.v. This peak could not be identified. It may be associated with the phenomenon of dissociative photoionization with a process similar to the following:

$$CO(X^1\Sigma^+) + h\nu \rightarrow C^+(^2P) + O(^3P) + e^-$$

Weissler et al. (1959) reported the appearance potential of $C^+(^2P)$ as 22·3 e.v. ± 0·4 e.v. A similar dissociative photoionization process is thought to explain the fourth peak.

The photoelectron spectrum of the isoelectronic

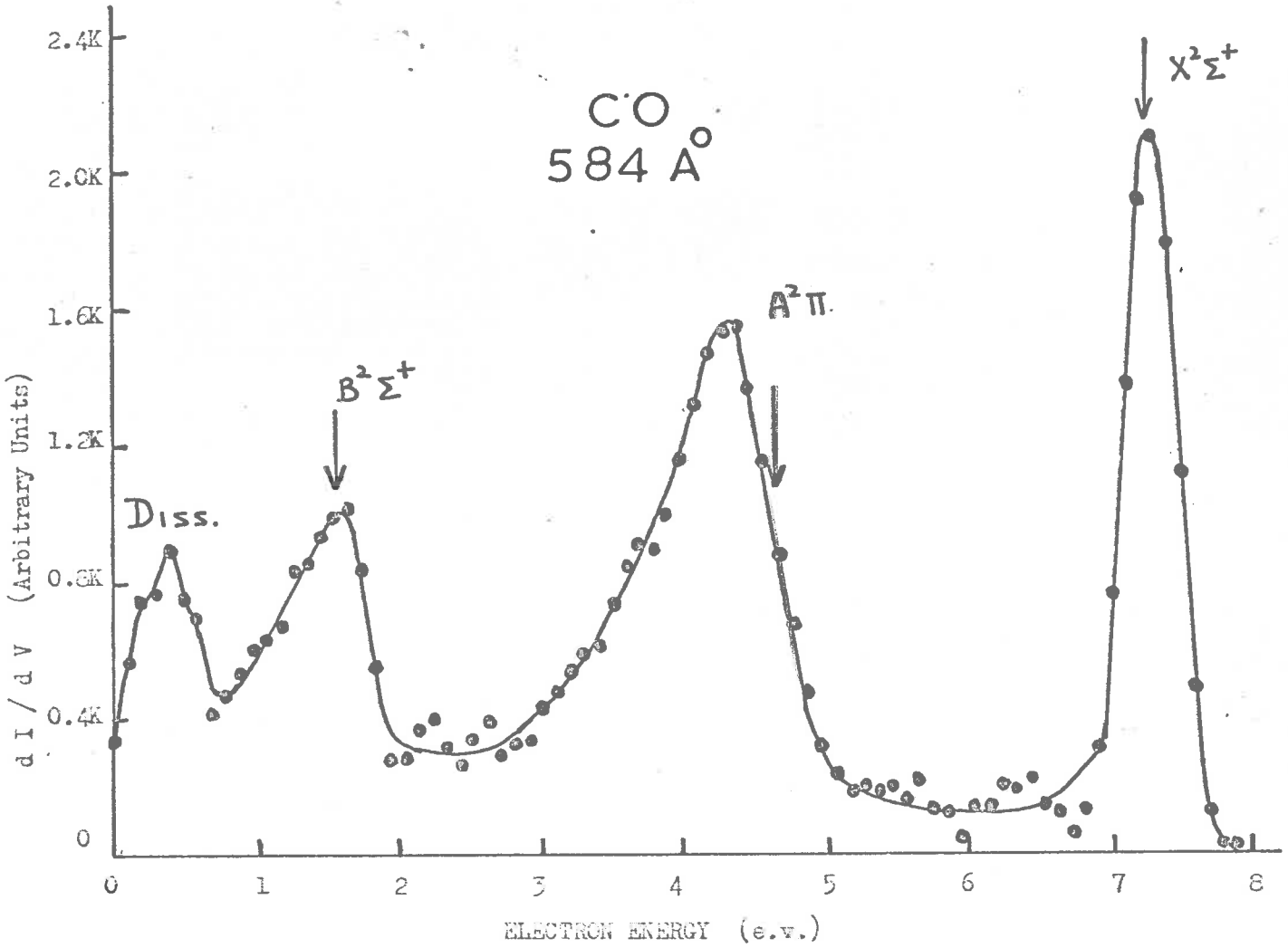

Fig. III.8. Photoelectron energy spectra of CO at 584 A° . The vertical ionization potential of $A^2\Pi$ state (16.9 e.v.) is different from adiabatic potential (16.5 e.v.).

molecule, nitrogen at 584Å is shown in Figure III.9. The close resemblance of this spectrum to that of carbon monoxide (Figure III.8) at 584Å can be seen except for the peak assigned as due to dissociative ionization.

In Figure III.10 is shown the photoelectron spectrum of carbon monoxide at 670Å. Only two peaks, corresponding to the $X^2\Sigma^+$ and $A^2\Pi$ states, can be seen. Figure III.11 being the spectrum of CO at 730Å, shows the $X^2\Sigma^+$ state and a narrow band of the $A^2\Pi$ state comprising of a few vibrational levels existing at this photon wavelength.

III.2.1 Autoionisation Processes

At photon wavelengths shorter than 855Å there was a low energy contribution to the photoelectron spectrum. This could be attributed to transitions in which, for a particular final state of the ion, all the excess energy is carried by photoelectrons. Between 755Å and 855Å, the photoelectron spectra showed a strong peak at about 0·3 e.v. which did not seem to vary in position with incident photon energy. Some of these spectra are shown in Figures III.12 and III.13. This peak was found to be present in spectra between 740Å to 750Å but was not resolved from $A^2\Pi$ state. Careful investigations showed

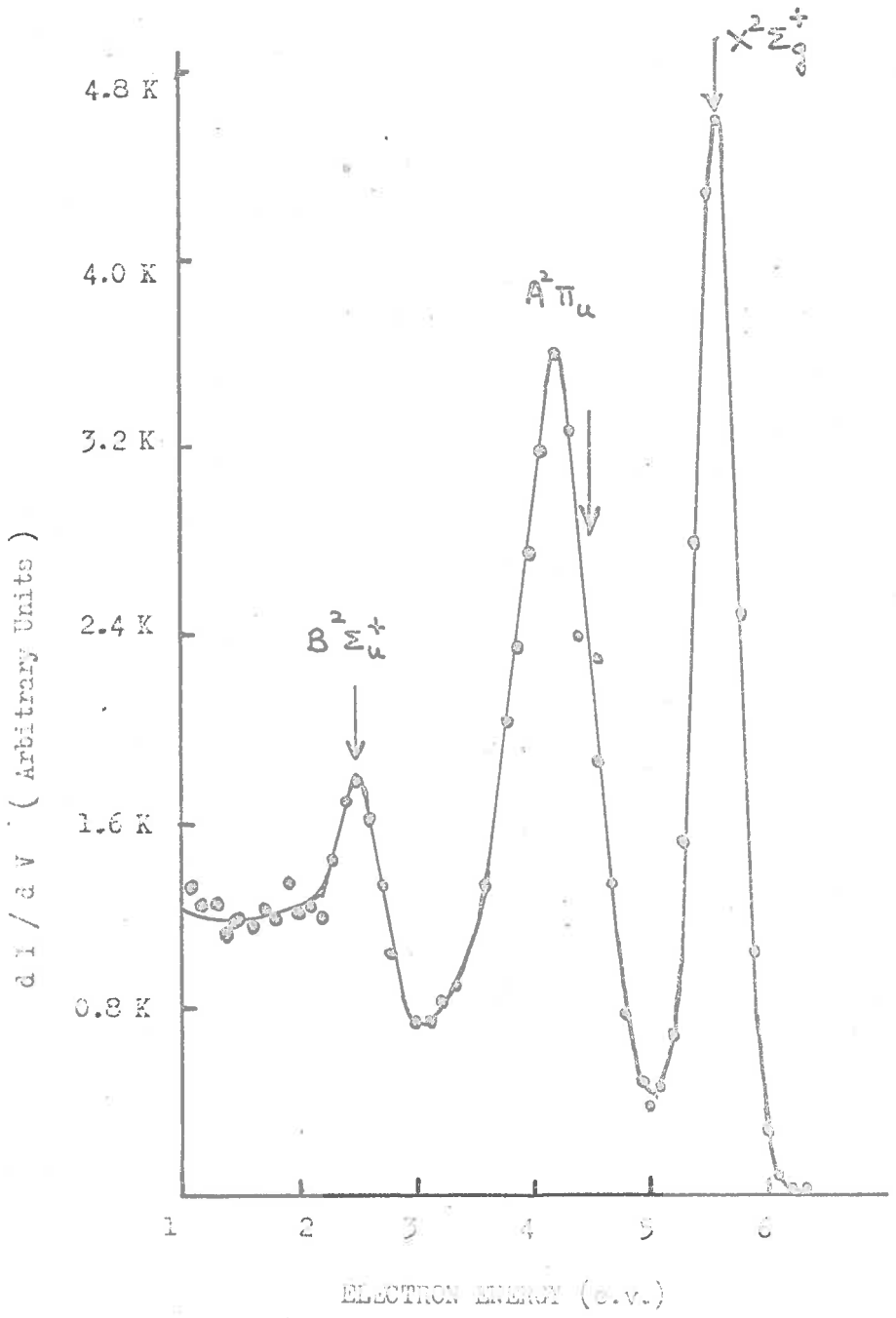

Fig. III.9 . Photoelectron energy spectra of molecular nitrogen at 584 A° .

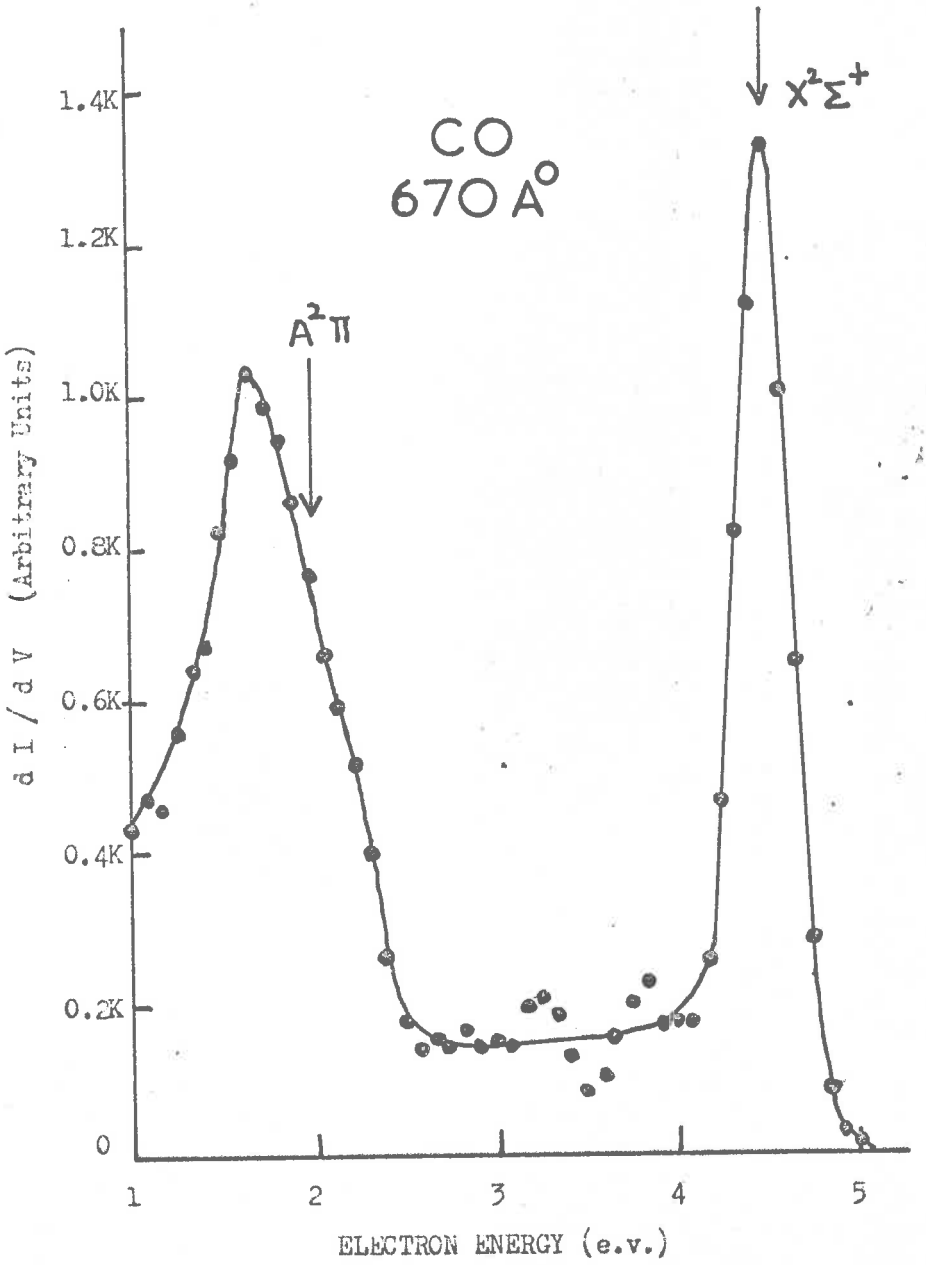

Fig. III.10. Photoelectron energy spectra of CO at 670 A°.

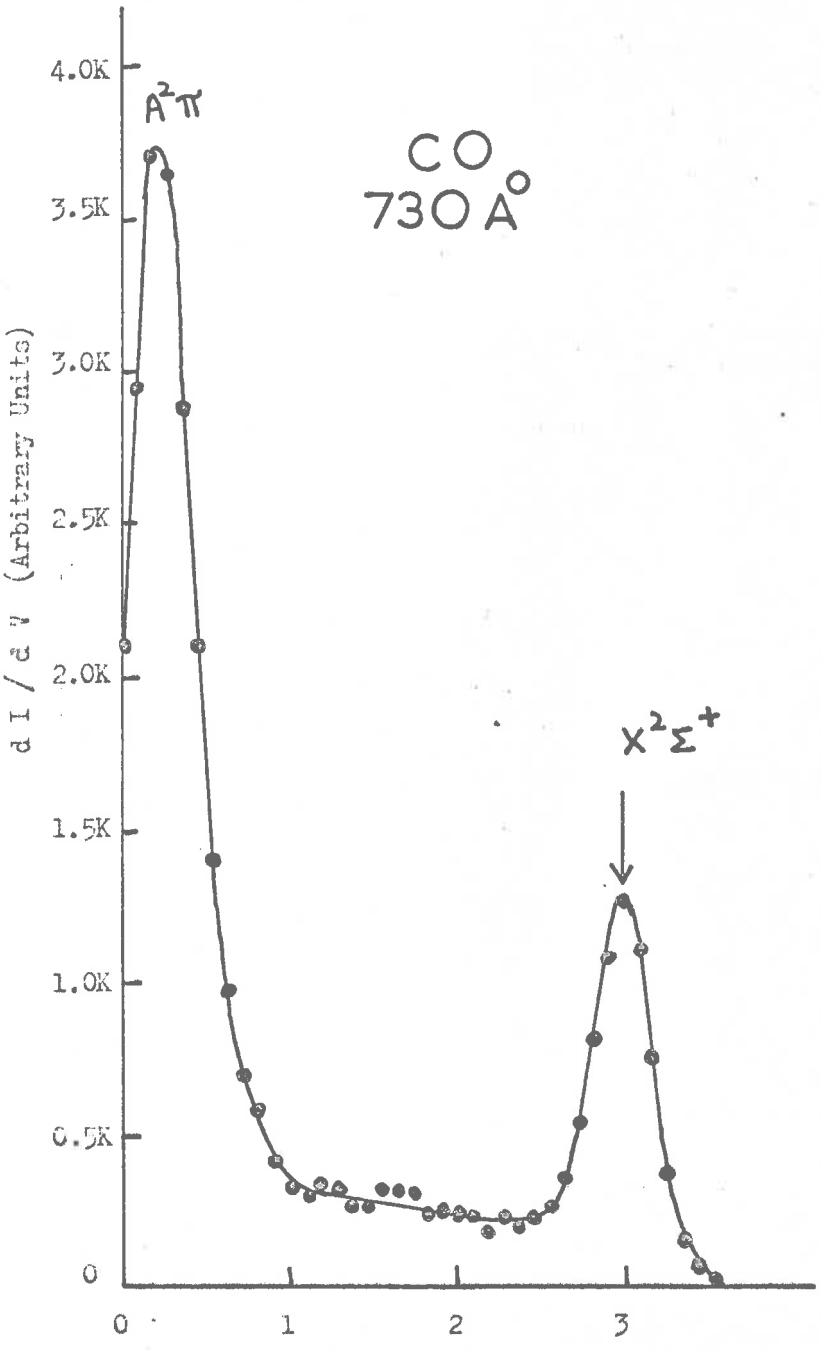

Fig. III.11. Photoelectron energy spectra of CO at 730 A°.

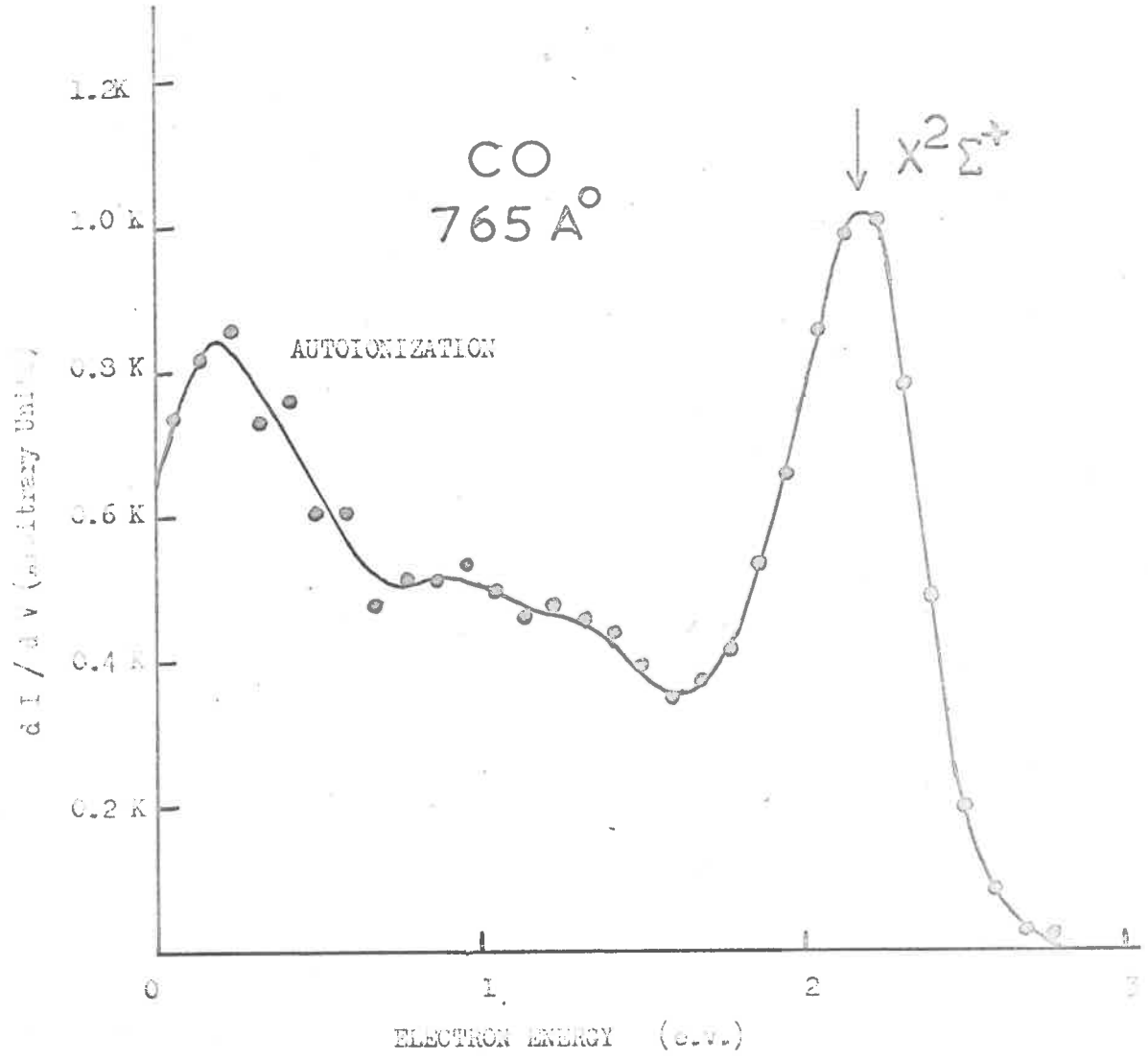

Fig. III.12 . Photoelectron energy spectra of carbon monoxide at 765 A° .

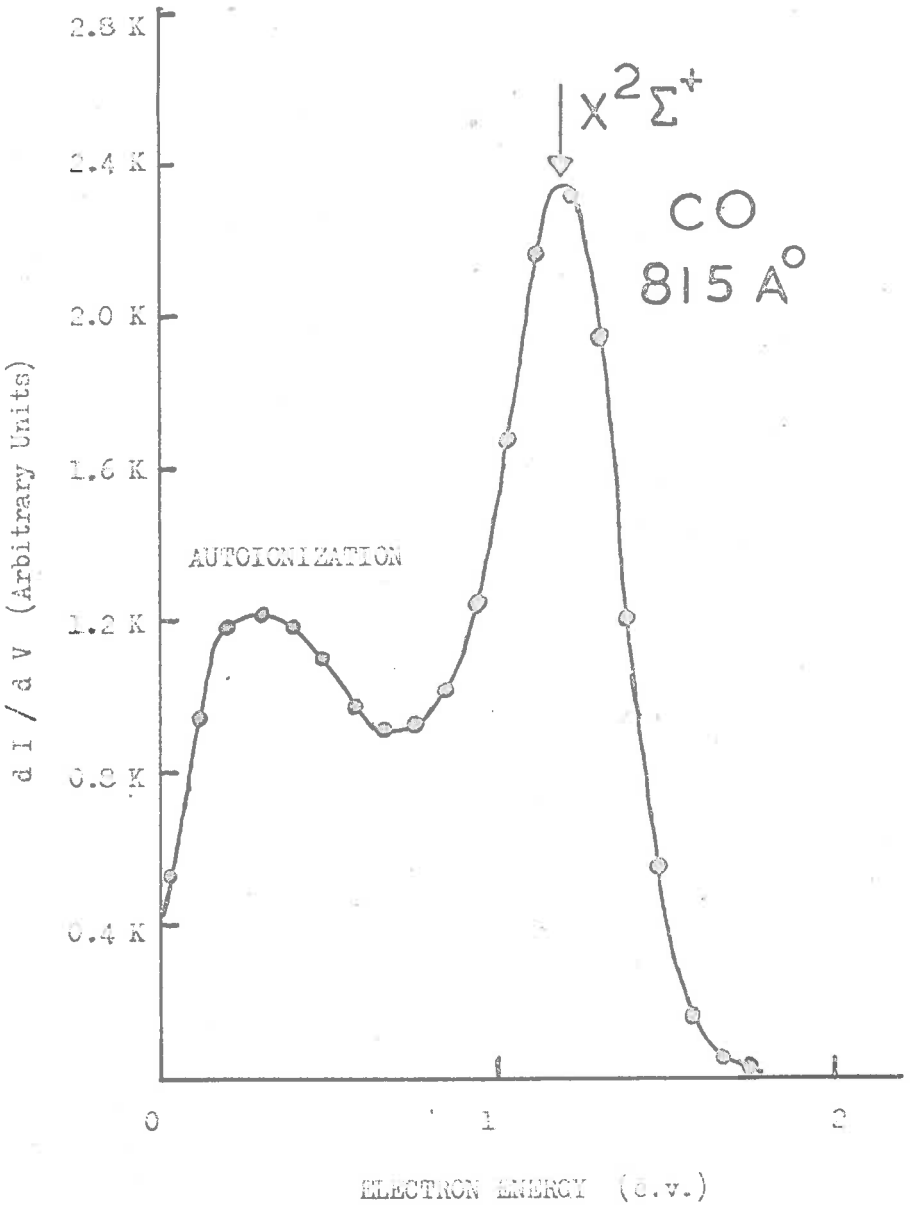

Fig. III.13 . Photoelectron spectra of carbon monoxide at 815 A° .

that this low energy anomalous peak was not an instrumental effect. It was observed for CO under all experimental conditions, including a variety of CO pressures but was not present for other gases such as CO_2, Ar, Xe etc.

The explanation for the low energy anomalous peak also observed in some of the spectra of molecular oxygen was given by Blake and Carver (1967). This peak was assigned as due to a fluorescent autoionisation process in which part of the energy was dissipated in the form of a photon with the subsequent emission of an electron to the nearest electronic state of the ion. This was considered to be the only possible explanation because it was thought that there were no energy levels available which corresponded to the position of the low energy anomalous peak. On the basis of a new argument now suggested, this previous explanation seems to be unnecessary.

The new explanation for the low energy anomalous peak is based on the assumption that the autoionizing state lies just above one of the electronic states of the ion and has got the same shape and depth as that of the ionic state. In Figure III.14 are shown the ground states $X^1\Sigma^+$ and $X^2\Sigma^+$ of CO molecule and CO^+ ion. The CO autoionisation state is shown approximately 0·3 e.v. above the

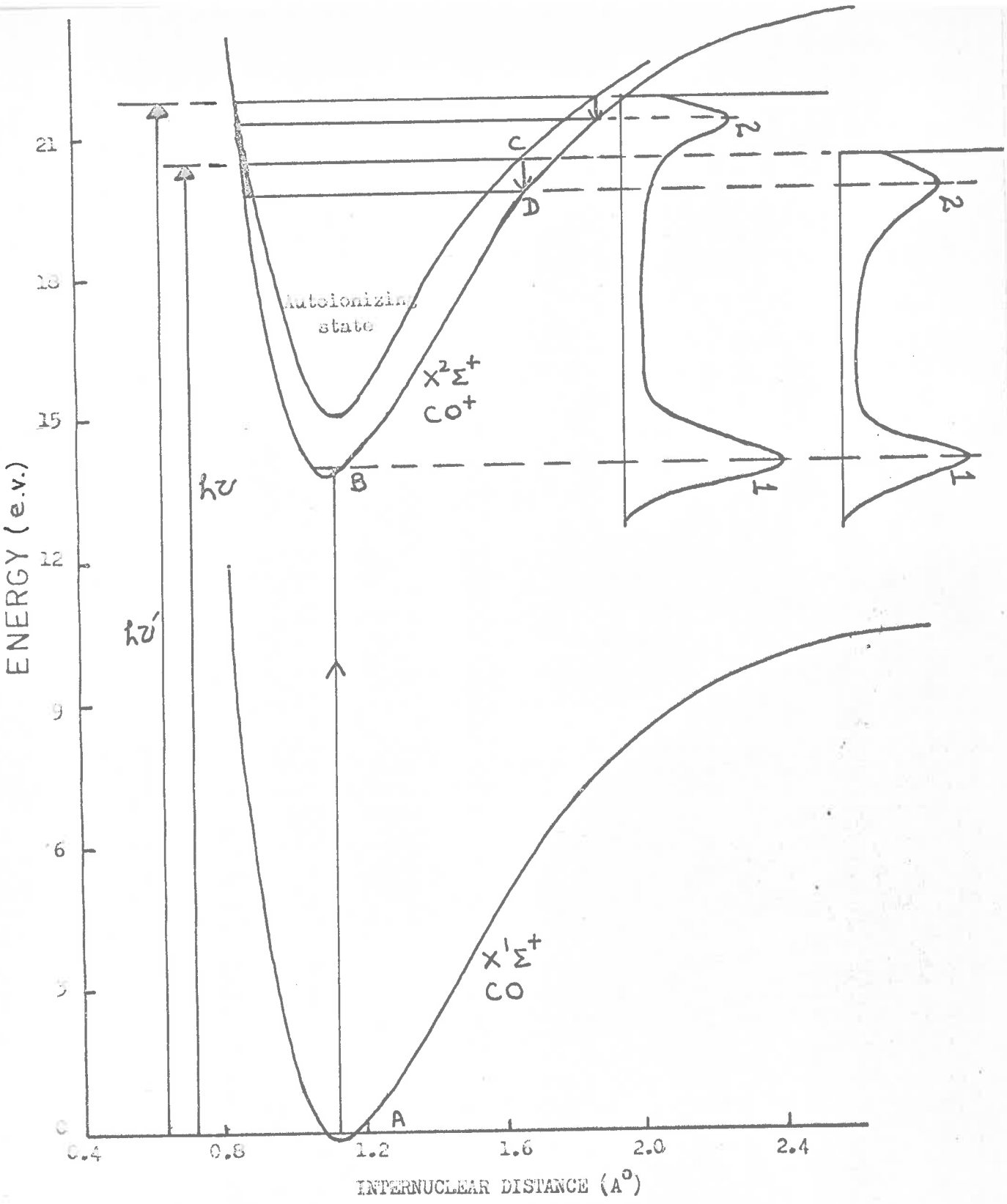

Fig. III.14. Figure explaining low energy anomalous peak on Franck-Condon principle. The ground states of CO molecule and ion are computed from Morse potential function but the autoionizing state is arbitrary .

$X^2\Sigma^+$ state of the ion. For direct ionization not involving autoionization state, the transition from A to B is most likely in accordance with the Franck-Condon principle and transitions like this give the most energetic of the peaks (peak I). Other transitions involve the autoionizing state which is excited in one of the vibrational levels. On autoionization, the transition C to D is most probable. Another transition with different photon energy is also considered which gives rise to peak 2.

Cook et. al. (1965) reported total photoionization cross-sections for CO showing many peaks over the photoionization continuum. Some of these peaks are thought to correspond to the vibrational levels of the autoionizing states. It is only when the photon energy coincides with that of a vibrational level that excitations to give transitions as explained above can occur. [The measurement of high resolution spectra on and off the autoionisation resonances is being attempted to establish the above explanation. Franck-Condon factors to reproduce these spectra are also being calculated as in the case of molecular oxygen (chapters IV and V)].

III.2.2 Partial Photoionization Cross-Sections

The branching ratios of carbon monoxide ion plotted

against wavelength are shown in Figure III.15. The electronic ground state ($X^2\Sigma^+$) of the ion has branching ratios varying from 32% to 42% in the range of wavelength 584Å to 730Å. Beyond 730Å, there is a rapid increase of the branching ratios with a maximum of 760Å. A decrease between 760Å and 780Å is noticed but beyond this, there is a rapid increase of branching ratios. At 855Å and higher wavelengths up to the threshold of $X^2\Sigma^+$ state, the branching ratio is 100% indicating the presence of the ground state only in the photoelectron spectra.

The branching ratios of $A^2\Pi$ state of the ion are seen to increase slowly in the range of 584 Å and 725Å with a broad maximum near 720Å. After 725Å there is a rapid decrease of branching ratios. At 760Å and beyond the $A^2\Pi$ state does not exist.

In the case of $B^2\Sigma^+$ state, the branching ratios seem to vary between 11% to 18% in the range of 584Å to 620Å while from 625Å onwards a rapid decrease is observed.

The branching ratios of the autoionising state are also shown in Figure III.15. A maximum at 780Å is observed and from 785Å onwards a slow decrease up to 850Å, followed by rapid decrease, is noticed.

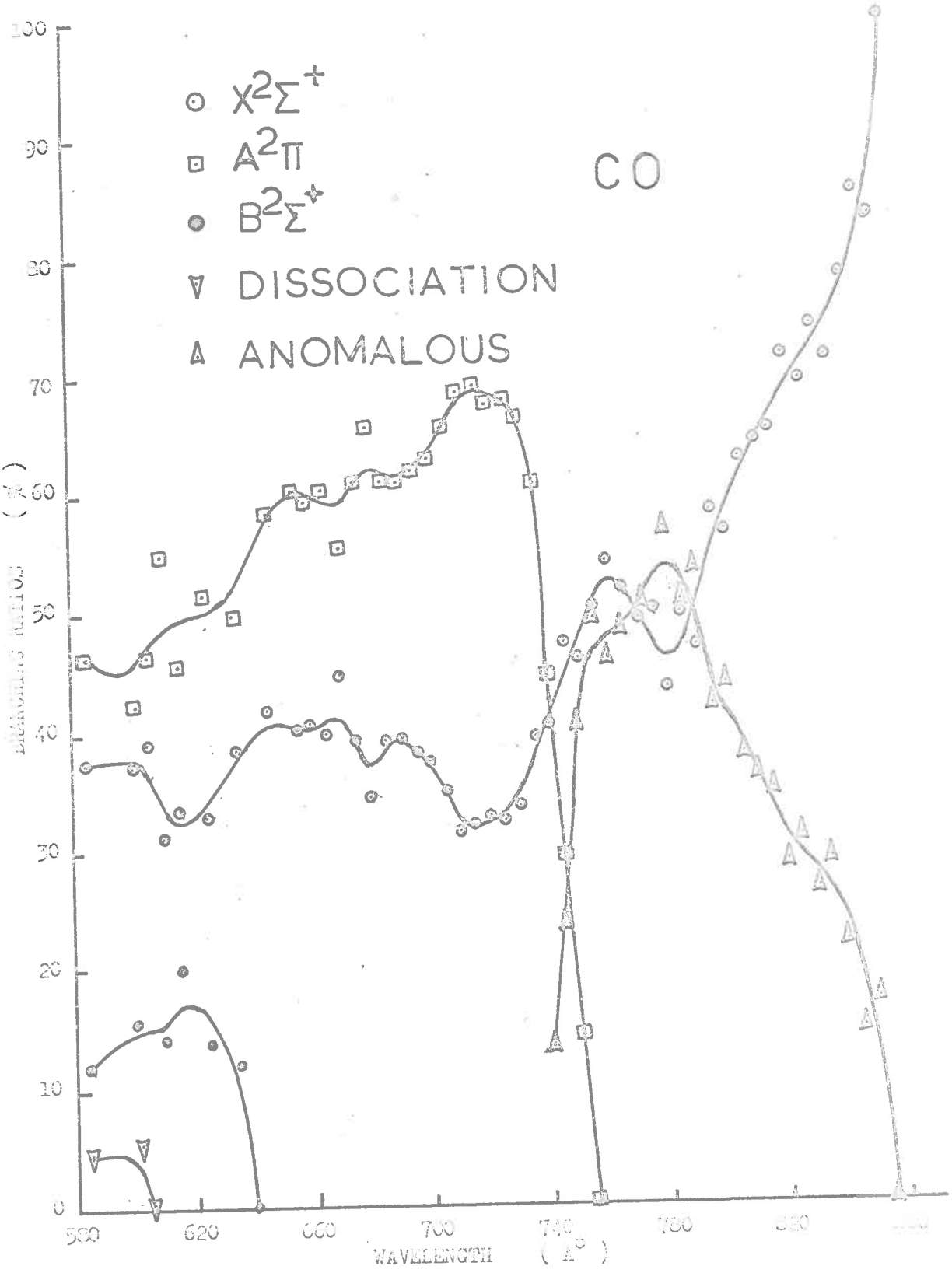

Fig. III.15. Branching ratios for different competing processes for CO .

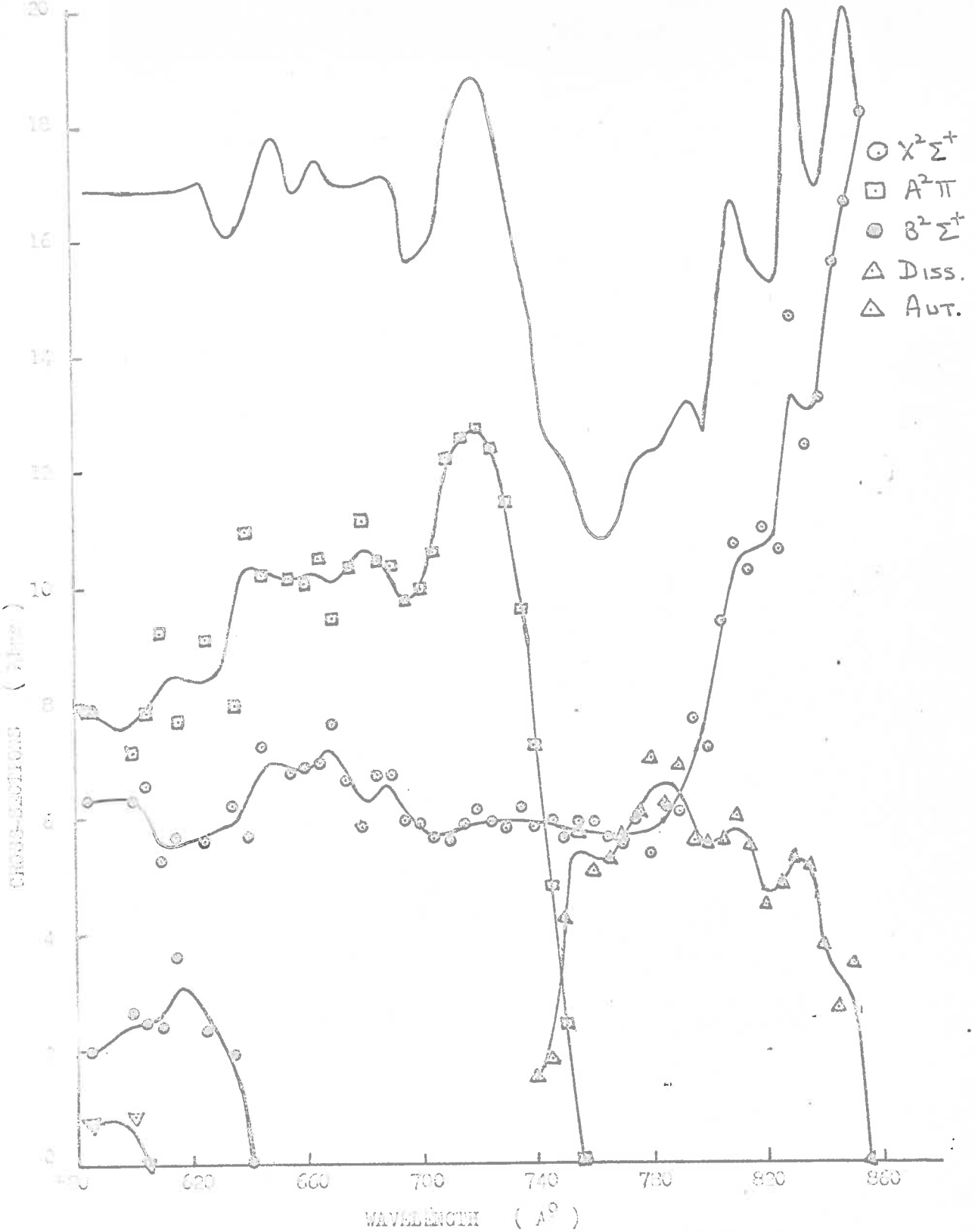

Fig. III.16. Partial photoionization cross-sections for different competing processes for CO. The upper curve shows total X-sections of Cook, Metzger and Ogawa, 1965 averaged over 8 A° intervals.

Partial photoionization cross-sections for the different processes are calculated by combining total cross-sections (Cook, Metzger and Ogawa, 1965) averaged over 8Å, the beam resolution used in the present work, and the respective branching ratios of different processes as shown in Figure III.15. The plot of the partial photoionization cross-section against wavelength is shown in Figure III.16.

III.3 Nitric Oxide

Photoelectron spectra of nitric oxide were recorded at 584Å and at 5Å intervals throughout the wavelength range 590Å to 805Å.

The energy levels of the nitric oxide ion which are energetically accessible are listed in Table III.2.

TABLE III.2

Nitric Oxide Photodisintegration Processes

Reaction	Threshold Energy (e.v.)		
	†*Gilmore (1965)	†**Turner and May (1966)	‡**Present Work
$NO(X^2\Pi) + h\nu$			
$\rightarrow NO^+(X^1\Sigma^+)+e^-$	9·24	9·24	9·7
$\rightarrow NO^+(a^3\Sigma^+)+e^-$	14·20	15·65	Not observed
$\rightarrow NO^+(^3\Delta)+e^-$	16·54	16·52	16·5
$\rightarrow NO^+(A^1\Pi)+e^-$	18·31	18·26	18·3

* Theoretical
** Experimental
T Adiabatic excitation potentials
‡ Vertical excitation potentials

Some of the photoelectrons may have resulted from processes of dissociative photoionization which occurred when the ion was left with an amount of vibrational energy greater than the dissociation energy of the electronic state of the ion. The ion then dissociated within a time of the same order of magnitude as the period of vibration. Dissociative ionization with the production of $N(^4S^o)$ and $O^+(^4S^o)$ fragments is a possible source of some photoelectrons at photon energies exceeding 20·1 e.v. Photoelectrons produced by dissociative ionization would be difficult to distinguish in the present experiment where they will make a low energy contribution to the photoelectron peak corresponding to the $NO^+(A^1\Pi)$ ion.

Table III.2 shows that the excitation energies of the $^3\Delta$ and $A^1\Pi$ states of the NO ion observed in the present work correspond fairly well with other published works. The vertical ionization potential of $X^1\Sigma^+$ state (9·7 e.v.) corresponds to the average of the $1 \leftarrow 0$ and $2 \leftarrow 0$ vibrational level. The nature of the photoelectron spectrum from nitric oxide is illustrated in Figures III.17, 18 and 19. There is a good deal of disagreement

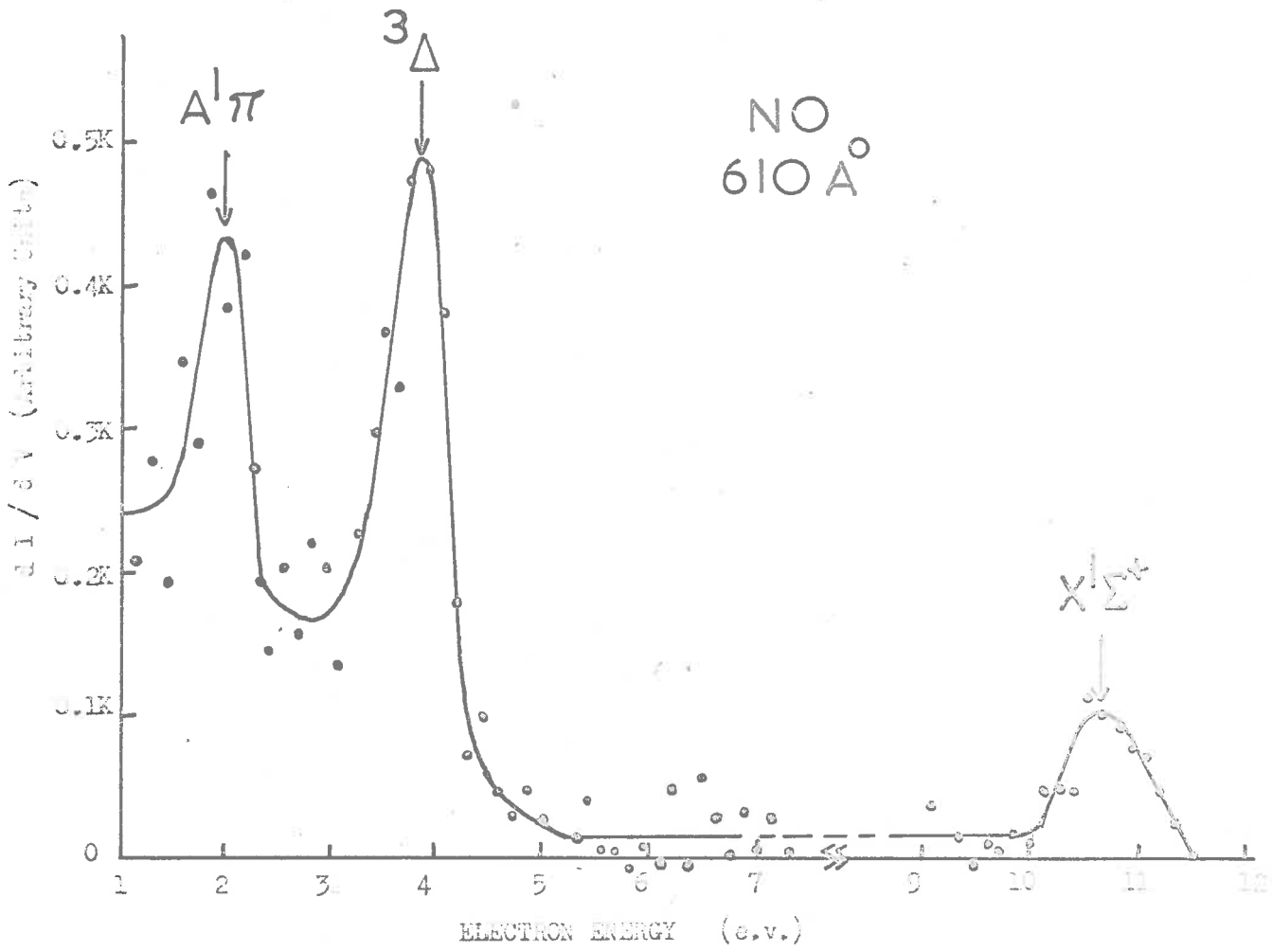

Fig. III.17. Photoelectron energy spectra of nitric oxide at 610 A°.

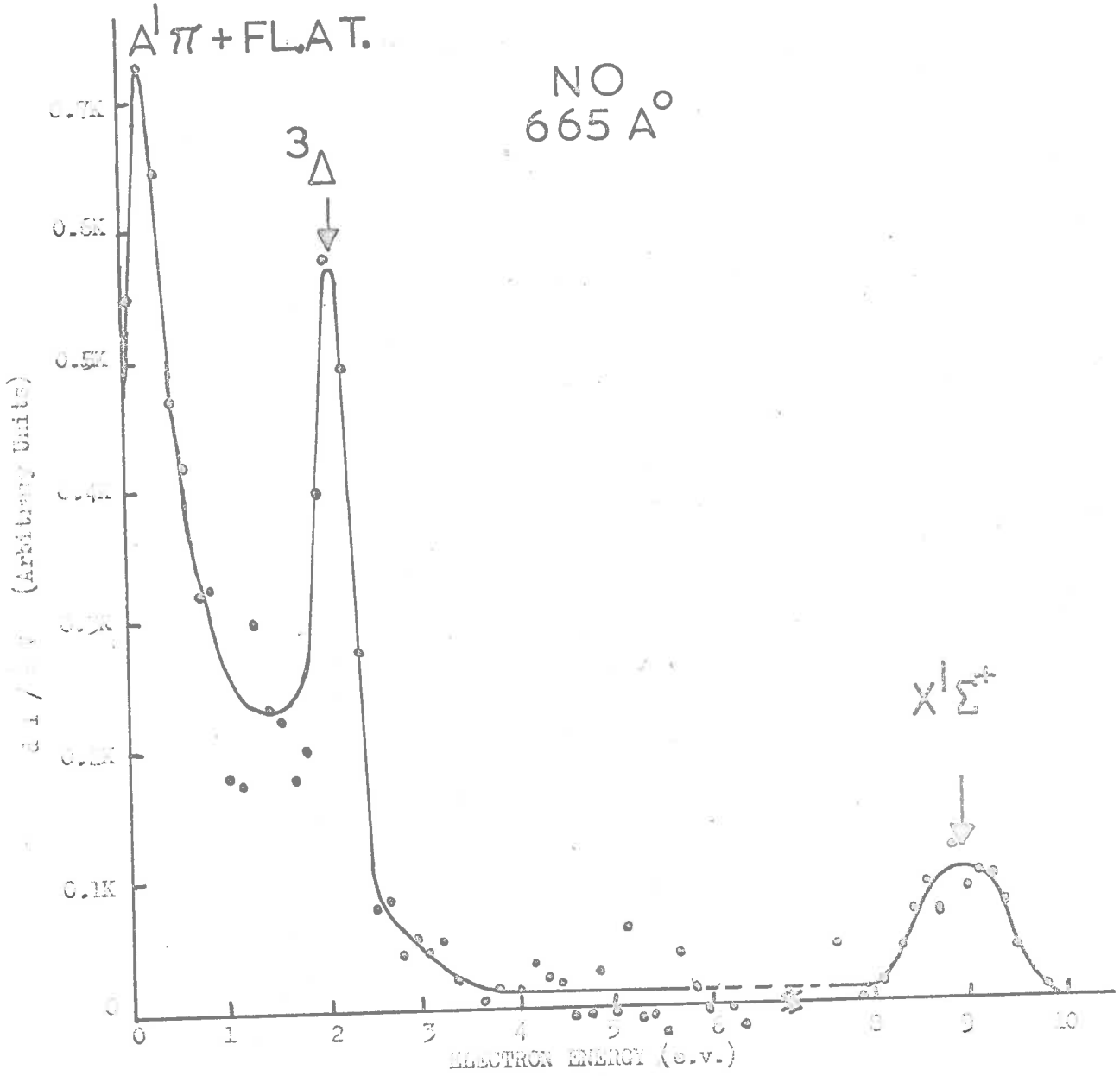

Fig. III.18. Photoelectron spectra of NO at 665 A°.

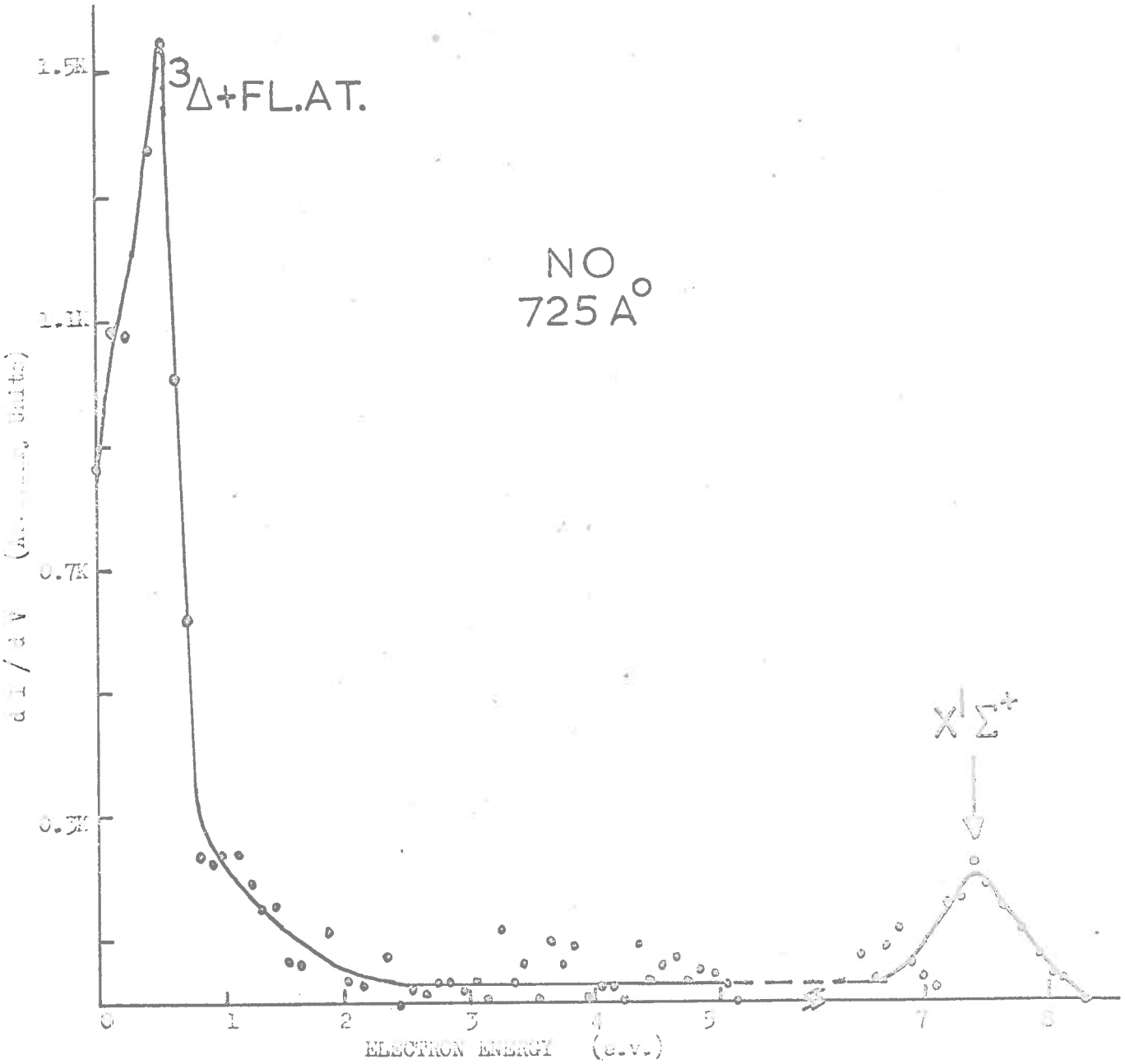

Fig. III.19. Photoelectron energy spectra of nitric oxide at 725 A°.

in literature about the $a^3\Sigma^+$ state. Turner and May (1966) assign this state as $^1\Sigma^+$. Samson (unpublished) has reported an energy of 15·0 e.v. to the $a^3\Sigma^+$ state. The photoelectrons have been identified with particular transitions on the basis of their energies. Photoelectron groups corresponding to transitions to the $X^1\Sigma^+$, $^3\Delta$ and $A^1\Pi$ states of NO^+ were clearly resolved in all spectra where they were energetically possible. No photoelectron peak corresponding to transition to the $a^3\Sigma^+$ state of NO^+ was distinguished in any of the observed spectra despite the fact that a peak with this energy lying between the $X^1\Sigma^+$ and $^3\Delta$ peaks should be easily identified.

Photoelectron spectra of NO at 610Å is shown in Figure III.17 which illustrates the $X^1\Sigma^+$, $^3\Delta$ and $A^1\Pi$ states of the ion. Approaching wavelengths higher than 590Å, the peak corresponding to $A^1\Pi$ state of the ion starts disappearing (Figure III.18) as seen in the spectra at 665Å. At wavelengths greater than 600Å, peak due to $^3\Delta$ state also starts disappearing as shown in Figure III.19 at 725Å. At wavelengths greater than 730Å only the ground state ($X^1\Sigma^+$) of the ion is observed, provided direct ionisation takes place.

III.3.1 Autoionisation Processes

At photon wavelengths shorter than 805Å, a low energy contribution to the photoelectron spectra was observed. This could not be attributed to transitions involved in direct ionization. Between 760Å and 805Å and between 665Å and 720Å, the photoelectron spectra showed a strong peak at about 0·5 e.v. which does not seem to vary in position with photon energy. Some of these spectra are shown in Figures III.20 and 21. This low energy peak, explained in Section III.2.1, is again not an instrumental effect.

This peak could not be explained on the basis of Franck-Condon principle as O_2 (chapters IV and V) and CO (section III.2.1). It is believed that the low energy peaks observed in some of the spectra are due to fluorescent autoionization. When the molecule is excited to a quasi-stable state, the state must be sufficiently long-lived for fluorescent autoionization to occur to a lower quasi-stable state and the transition to the ionization continuum is from this state. This process is illustrated schematically in Figure III.22. A cascade of fluorescent transitions with some probability of a transition to the ionization continuum from several of the quasi-stable states, occurs. This explains why the peak

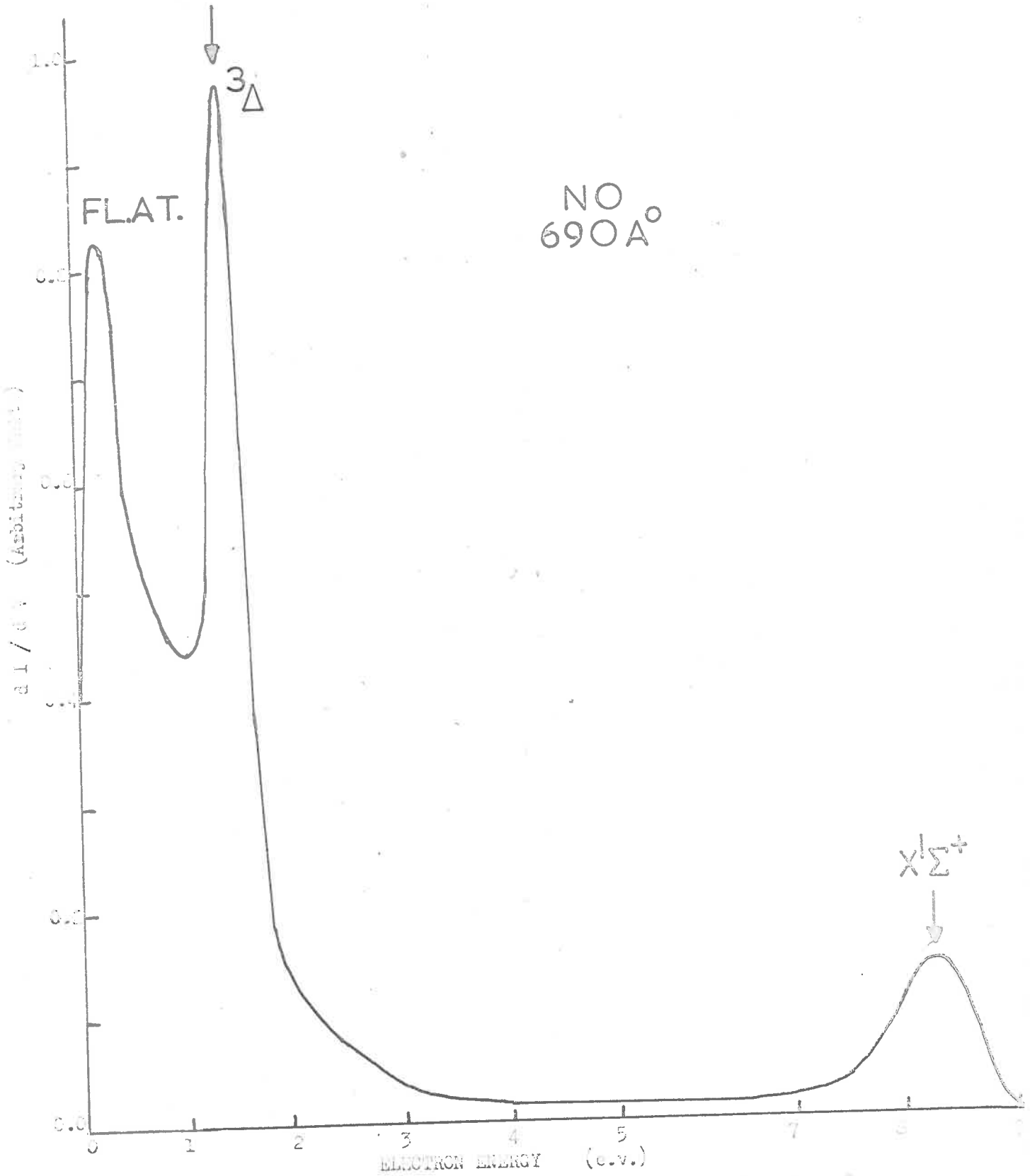

Fig. III.20. photoelectron energy spectra of NO at 690 A° -

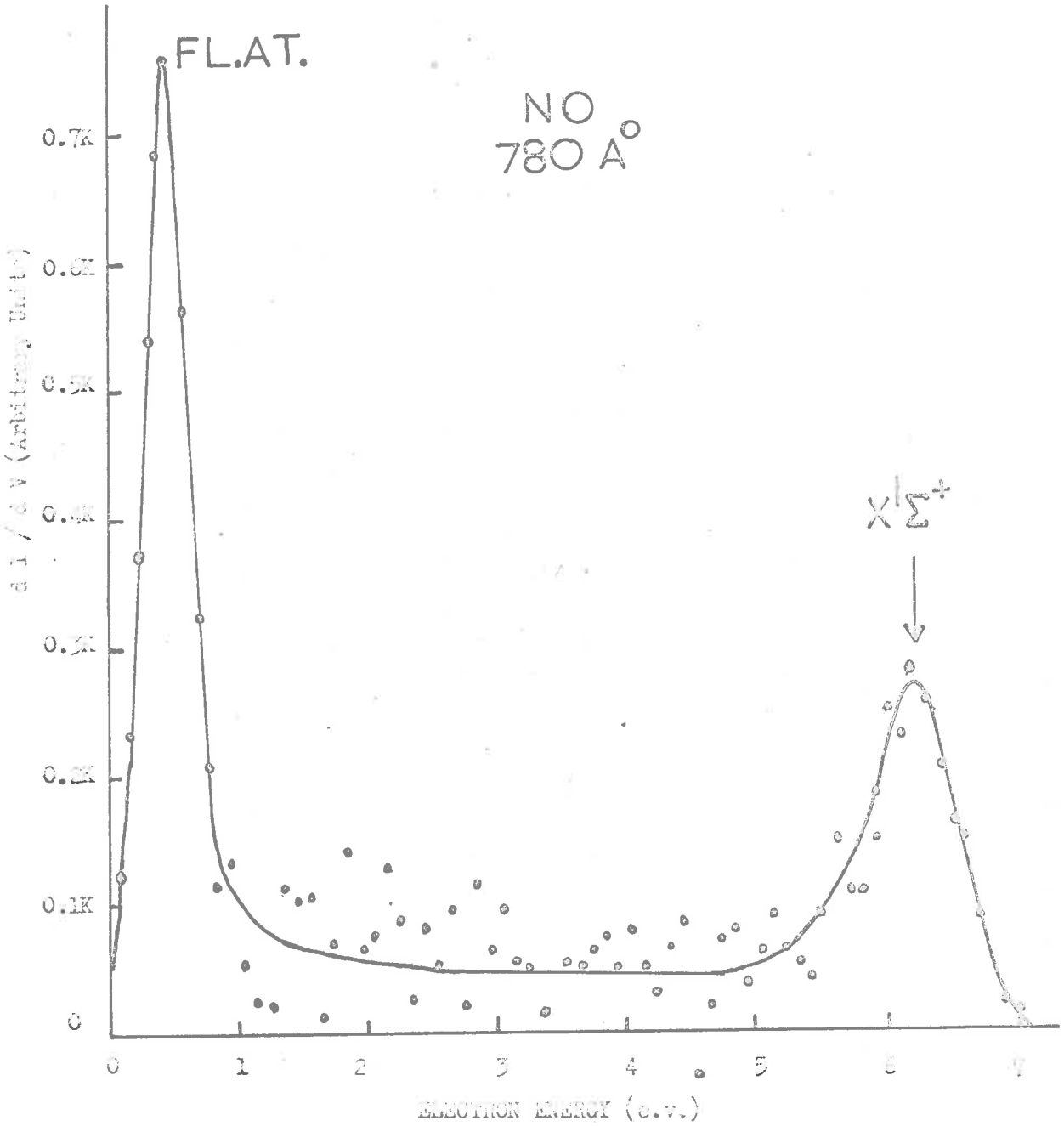

Fig. III.21. Photoelectron energy spectra of NO at 780 A°.

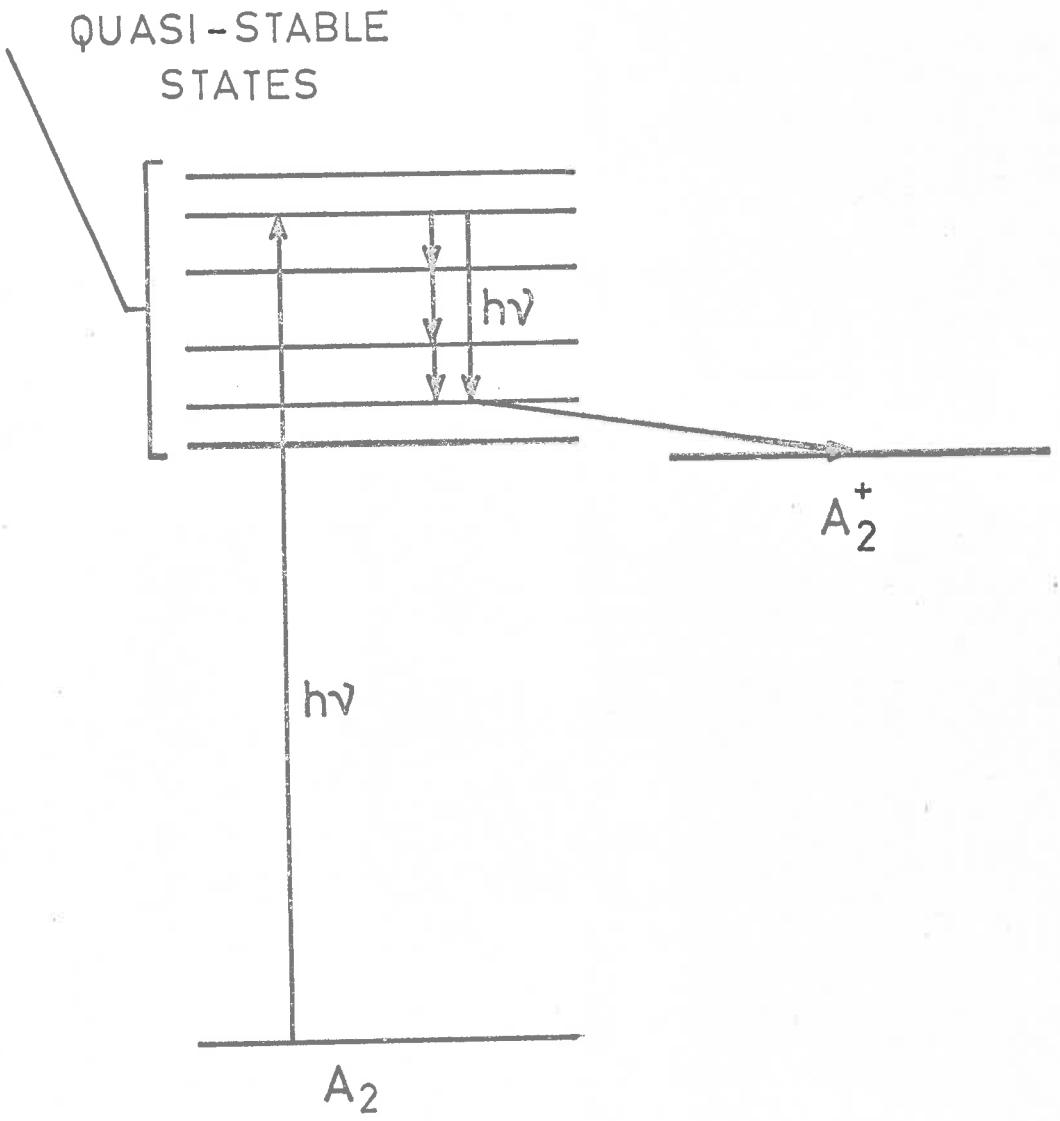

Fig. III.22. Energy level diagram of a hypothetical molecule A_2, illustrating a fluorescent autoionizing transition.

due to a fluorescent autoionization process does not vary in position with incident photon energy.

III.3.2 Partial Cross-Sections

The branching ratios for the $X^1\Sigma^+$, $^3\Delta$ and $A^1\Pi$ electronic states of the NO^+ ion have been measured in the same manner as for CO_2. For the low energy fluorescent autoionization peak, the branching ratios have also been calculated. Figure III.23 shows the plot of the branching ratios for different competing processes against wavelength. The only results with which the measurements of the present work may be compared are those of Vroom (1966) reported at only one photon wavelength, viz. 584Å. A comparison is shown in Table III.3. At this wavelength the branching ratios for $X^1\Sigma^+$, $^3\Delta$ and $A^1\Pi$ states as given by Vroom are in the ratio of 1 : 2·8 : 1·4 as against 1 : 2·9 : 2·8 for the present work, neglecting the contribution of $a^3\Sigma^+$ and other states.

TABLE III.3

Branching Ratios for Different States of NO^+ at 584Å

States	Branching Ratios	
	Vroom (1966)	Present Work
$X^1\Sigma^+$	0·36*	0·15
$a^3\Sigma^+$	0·06*	Not observed
$^3\Delta$	1·00*	0·43
$A^1\Pi$	0·51*	0·42

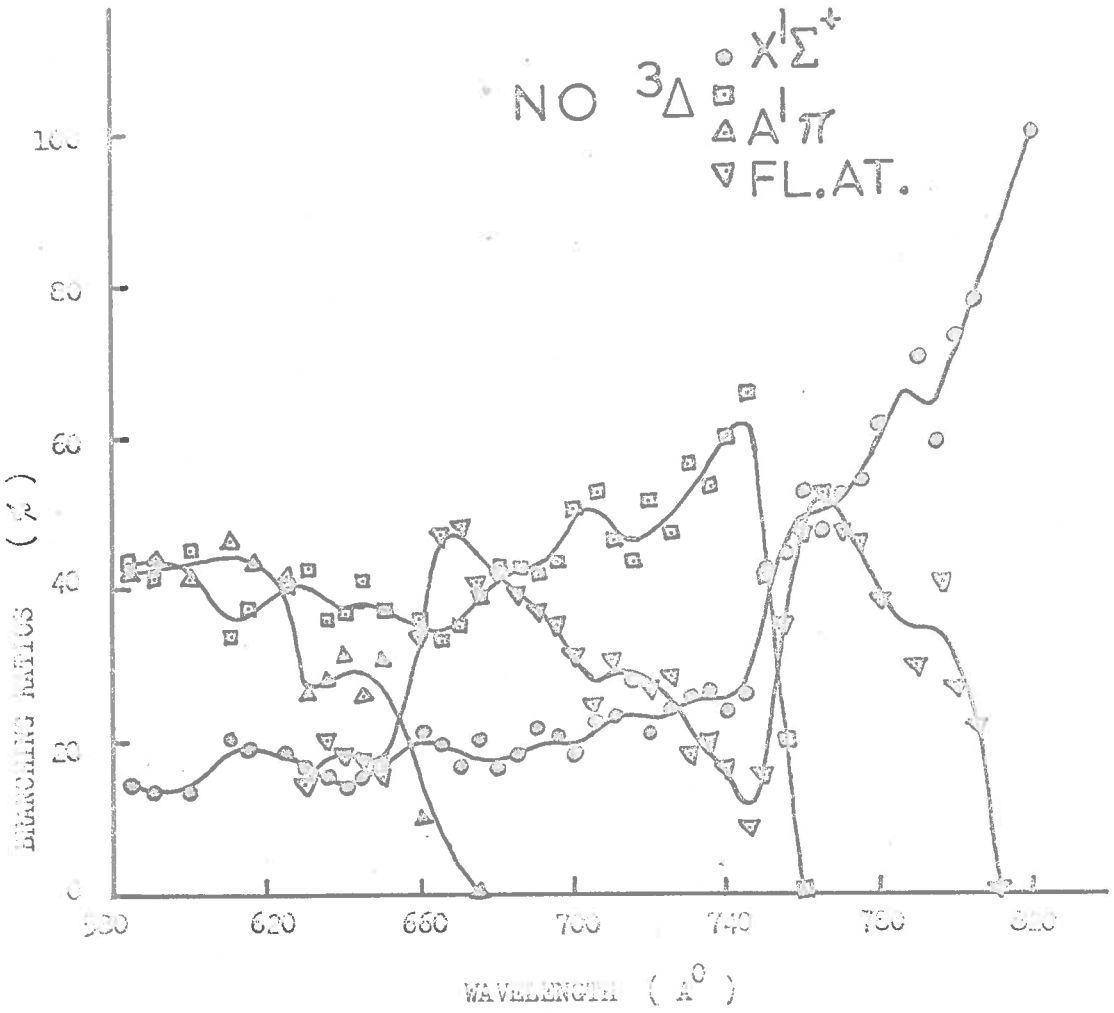

Fig. III.23. Branching ratios of different competing processes in nitric oxide as a function of wavelength .

*Relative values for several but not all the states.

There is a fair agreement in the two cases for the $X^1\Sigma^+$ and $^3\Delta$ electronic states but for $A^1\Pi$ state, the value reported in the present work is quite high.

For $X^1\Sigma^+$ state, there is a general trend towards increase in the branching ratios in the wavelength region of 584Å to 735 Å, the variation being between 10% and 25%. At wavelengths greater than 735Å the branching ratios increase quite rapidly, attaining a constant value of 100% at 810Å up to the threshold wavelength of the ground state. The $^3\Delta$ state has a wavelength threshold at 760Å. A rapid increase of branching ratios towards shorter wavelengths (< 760Å) is observed with a maximum (~60%) at 745Å, followed by a slow decrease at wavelengths shorter than 740Å down to 660Å. In the region 660Å to 584Å, the branching ratios of the $^3\Delta$ state vary between 35% and 45%. The $A^1\Pi$ state was observed at a few wavelengths between 584Å and the threshold wavelength, 665Å. The branching ratios for the fluorescent autoionisation process show two maxima at 670Å and 765Å.

Partial photoionization cross-sections for the various competing processes were calculated by combining

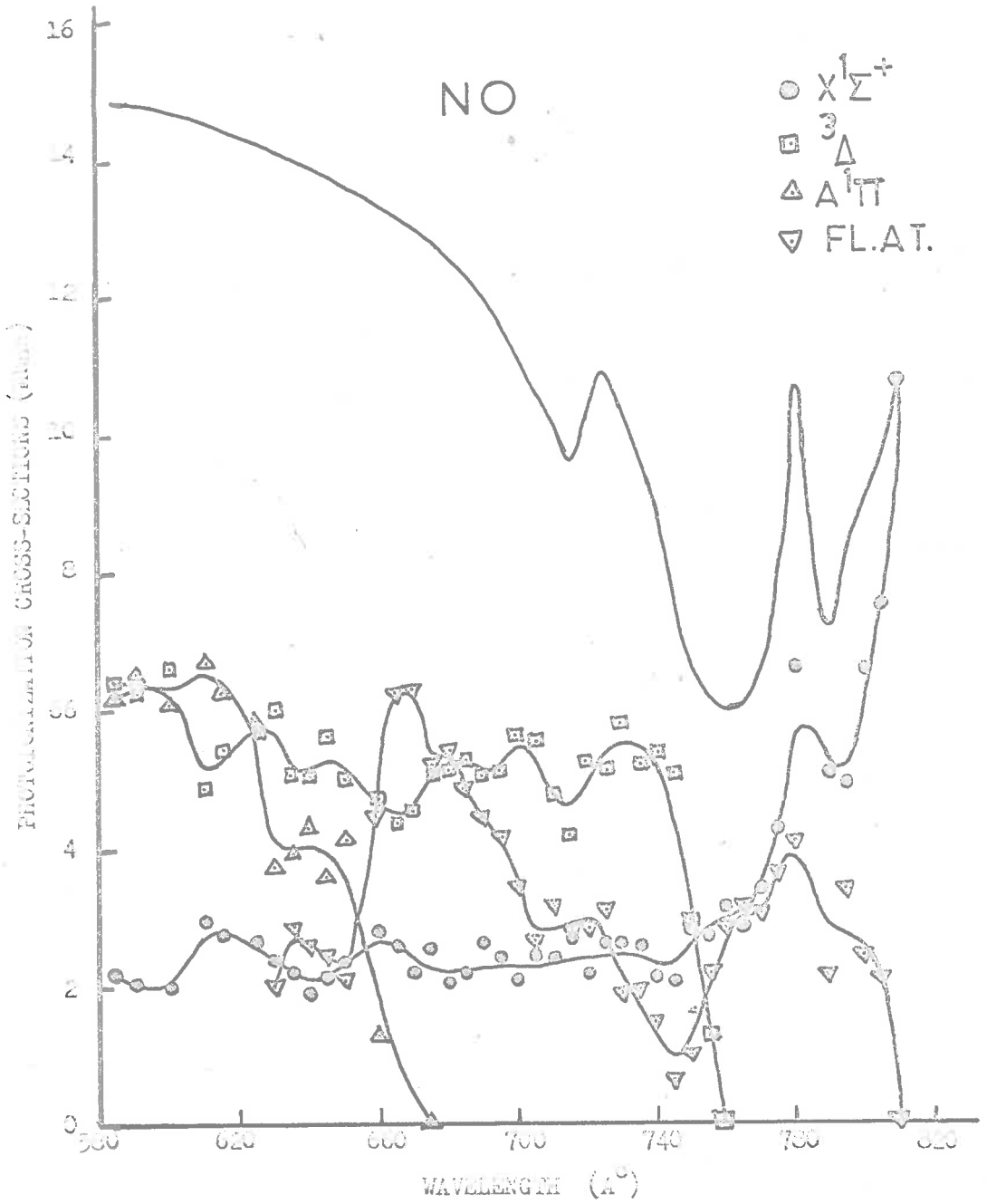

Fig. III.24 . Partial photoionization cross-sections for different competing processes in NO. The upper curve represents the total cross-sections of Metzger, Cook and Ogawa, 1967 averaged over 8 A° .

the branching ratios (Figure III.23) with total photoionization cross-sections. No measurements for absolute cross-sections were attempted with this apparatus. The values reported by Metzger, Cook and Ogawa (1967) were averaged over 8Å so as to match with the resolution used in the present work. The plot of partial photoionization cross-sections against wavelength is shown in Figure III.24.

III.4 Nitrous Oxide

Photoelectron spectra of nitrous oxide were recorded at 5Å intervals throughout the wavelength region between 600Å and 870Å. The different photodisintegration reactions which are accessible are listed in Table III.4

TABLE III.4

Nitrous Oxide Photodisintegration Reactions

Reaction	Threshold Energy (e.v.)	
	Turner and May (1967)**	Present Work***
N_2O(Ground State)+$h\nu$		
$\rightarrow N_2O^+(^2\Pi)+e^-$	12·90	12·9
$\rightarrow N_2O^+(^2\Sigma_u^+)+e^-$	16·40	16·4
$\rightarrow N_2O^+(A)^*+e^-$	17·66	18·3
$\rightarrow N_2O^+(B)^*+e^-$	20·08	20·1

*A and B are the arbitrary names of the third and fourth excited states of N_2O^+.
**Adiabatic excitation potentials.
***Vertical excitation potentials.

The $^2\Pi$, $^2\Sigma_u^+$ and B states of the N_2O^+ ionhave the same adiabatic and vertical excitation potentials but the A state of the ion with 17·66 e.v. as adiabatic potential has the vertical excitation potential of 18·14 e.v. (Turner and May, 1967) which is in fair agreement with that reported in the present work.

The photoelectron spectra of nitrous oxide at various different wavelengths are shown in Figure III.25, 26 and 27. At 600Å, as shown in Figure III.25, the photoelectron spectrum consisted of four bands corresponding to $^2\Pi$, $^2\Sigma_u^+$, A and B states of the N_2O^+ ion. The vibrational structure of the bands is not completely resolved because of the resolution used in the present work. The band corresponding to B state of the ion does not appear in the photoelectron spectra at photon wavelengths 620Å and upwards. The spectrum at 685Å comprising peaks of $^2\Pi$, $^2\Sigma_u^+$ and A states of the ion, is shown in Figure III.26. The photoelectron spectrum at incident photon wavelength of 745Å (Figure III.27) shows only $^2\Pi$ and $^2\Sigma_u^+$ bands. The 'A' state of the ion does not exist in the spectra at 700Å and beyond.

An anomalous peak not due to direct ionization occurs at an electron energy of 0·2 e.v. in the photoelectron spectra of N_2O in the wavelength region 620Å

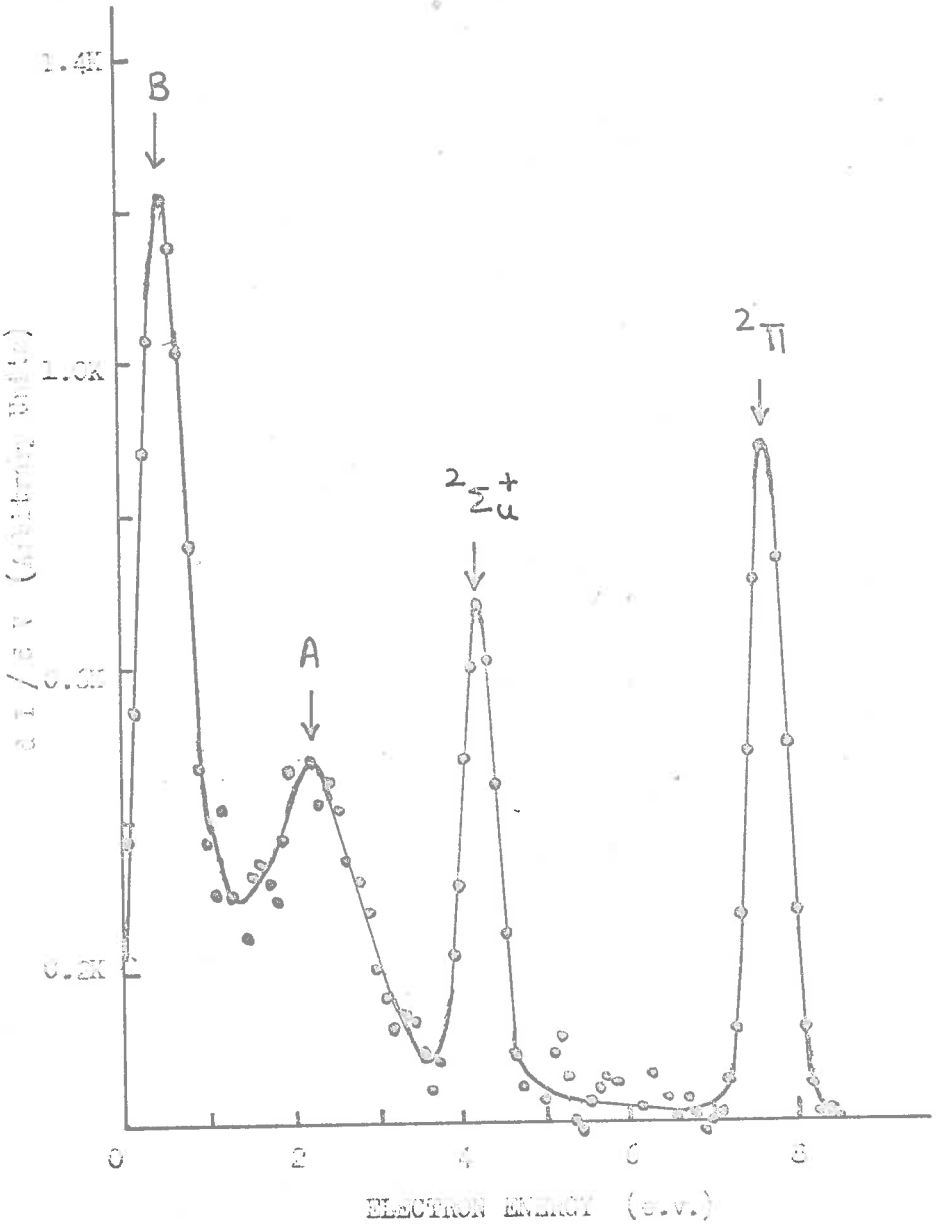

Fig. III.25 . Photoelectron energy spectra of N_2O at 600 A°.

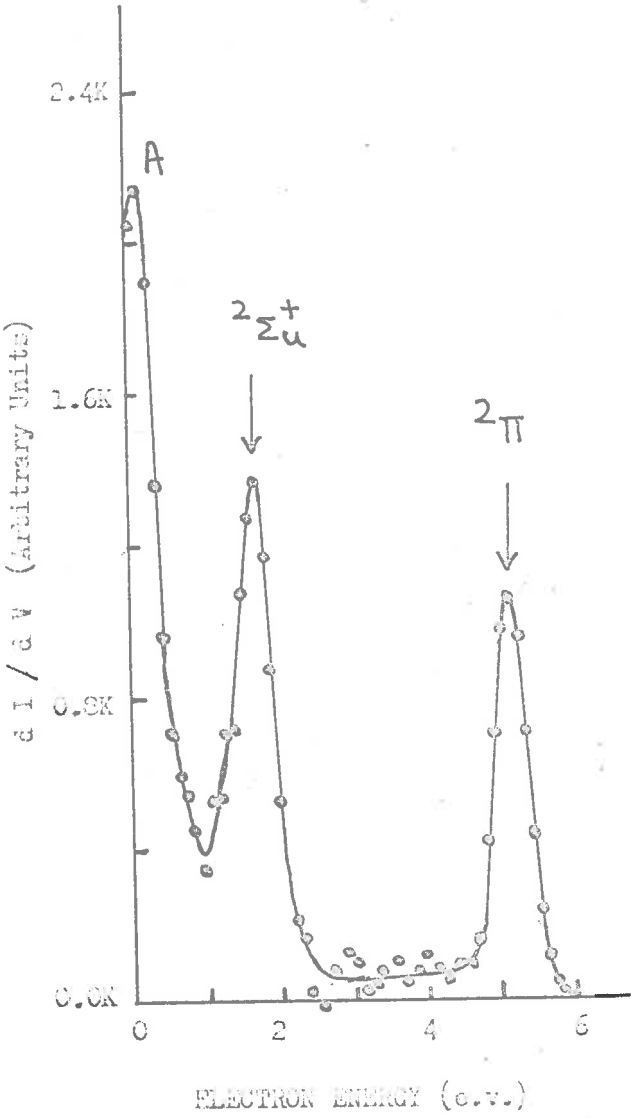

Fig. III.26. Photoelectron energy spectra of N_2O at 685 A^0 .

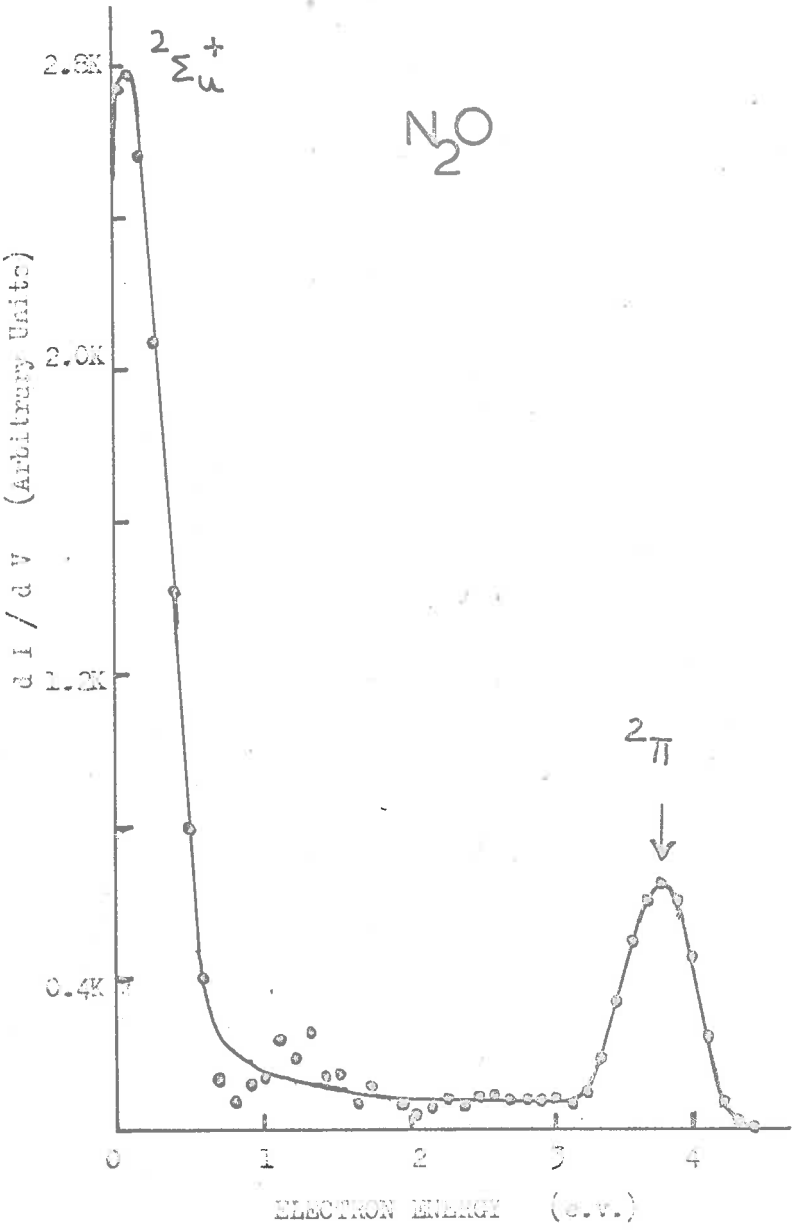

Fig. III.27. Photoelectron energy spectra at 745 Å.

to 665Å and also at photon wavelengths between 765Å up to the threshold wavelength of the electronic ground state of the ion at an electron energy of ~0·3 e.v. In Figure III.28 is shown the spectrum at 640Å. Three out of the four peaks shown correspond to $^2\Pi$, $^2\Sigma_u^+$ and A states of the ion but the fourth peak at 0·2 e.v. corresponds to the anomalous peak which does not change its position with the change in incident photon wavelength. At wavelengths greater than 660Å, no anomalous peak can be seen in the photoelectron spectra. Figure III.29 shows spectrum at 820Å with two peaks, one corresponding to to $^2\Pi$ state of the ion and the other is the anomalous peak at ~ 0·3 e.v. which also does not vary in position with photon wavelength.

This anomalous peak, observed in two wavelength regions in the photoelectron spectra of N_2O, is attributed to the process of fluorescent autoionisation. The process which occurs in NO also has been explained in Section III.3.1. One of the quasi-stable states of the molecule, to which the incident photon excites, emits a photon or cascade of photons with the subsequent emission of an electron to the $^2\Pi$ state of the ion. This explains the anomalous peak observed in the region of 765Å onwards. The other anomalous peak could be explained in the same way.

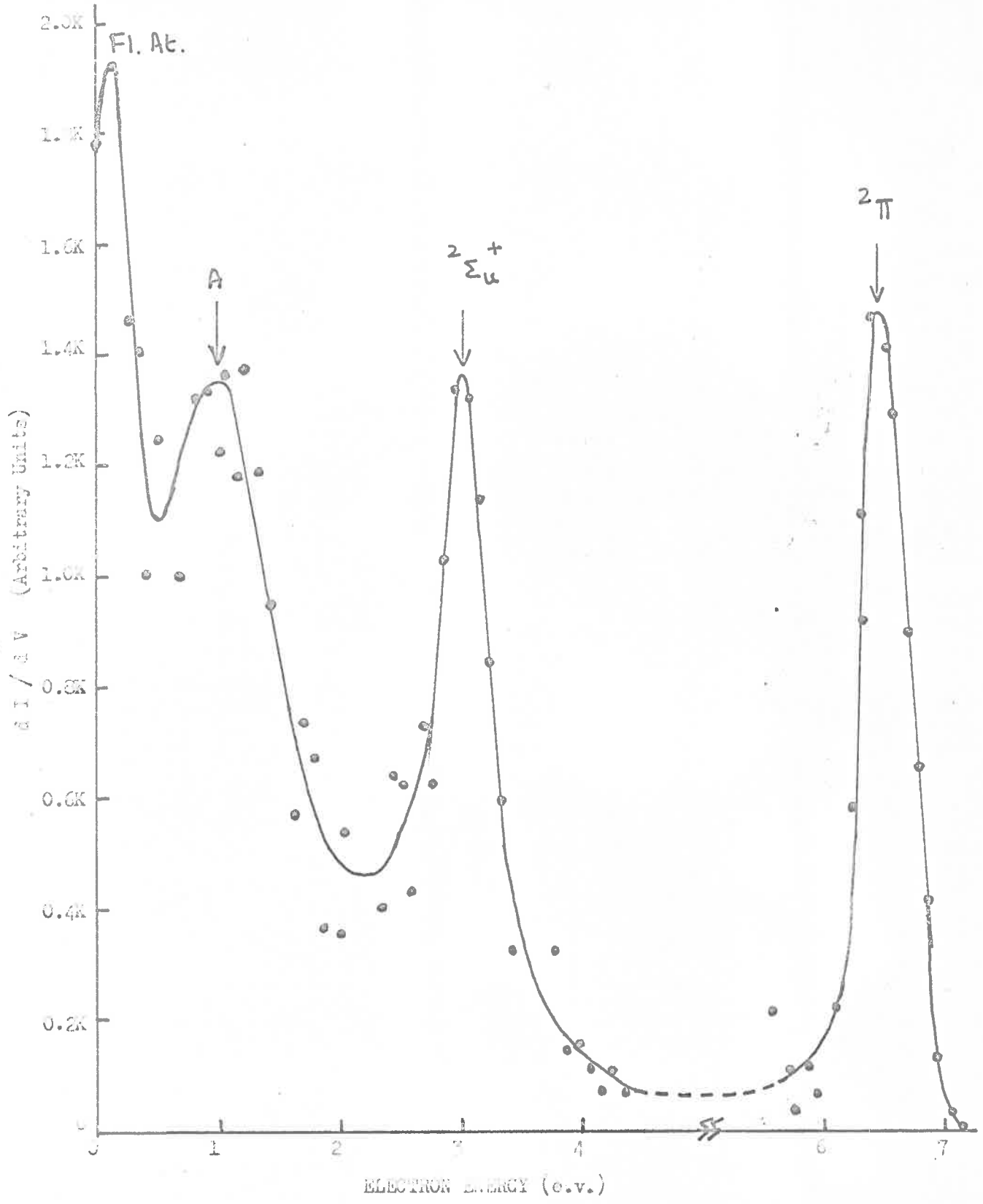

Fig. III.28. Photoelectron spectra of nitrous oxide at 640 A° .

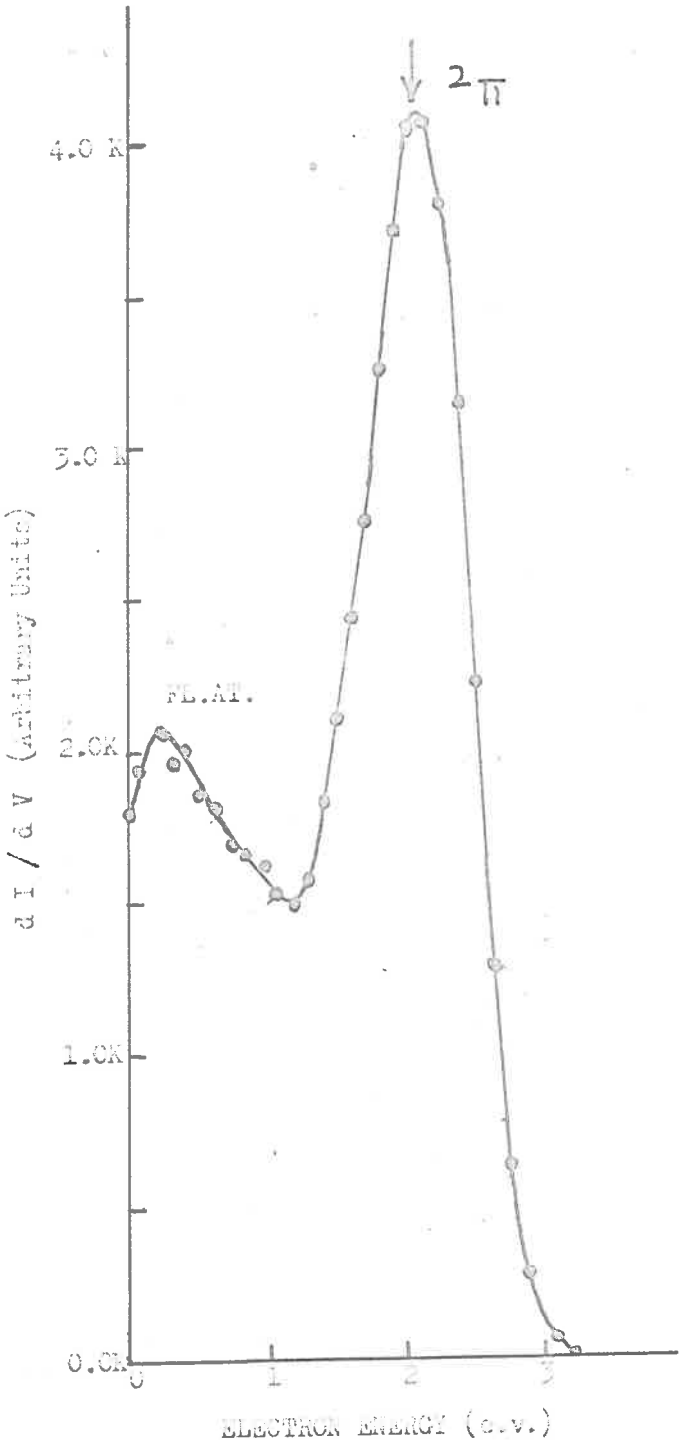

Fig. III.29. Photoelectron energy spectrum of N_2O at 820 A^0 .

At wavelengths between 875Å to the threshold of the electronic ground state of the ion, the photoelectron spectra show an unresolved broad band attributed to the direct ionization to the $^2\Pi$ state of the ion and the fluorescent autoionization.

III.4.1 Partial Cross-Sections

The branching ratios for the $^2\Pi$, $^2\Sigma_u^+$, A and B states of the ion have been measured throughout the wavelength region of 600Å to 870Å. The branching ratios for the fluorescent autoionization processes occurring in the wavelength regions 625Å to 660Å and 765Å and 870Å have also been calculated. In Figures III.30 and 31 are shown the plots of branching ratios for different competing processes against incident photon wavelength.

For $^2\Pi$ state of the ion, the branching ratios are fairly constant, varying from 26% to 28% between wavelengths 600Å and 620Å and start increasing with a maximum at 630Å. There is a trend toward increase of branching ratios thereafter with two broad maxima at 770Å (~ 76%) and 810Å (~ 87%). From 820Å to 870Å, the ratios are fairly constant, varying in the limits of 78 to 82%. For $^2\Sigma_u^+$ state, the branching ratios start increasing quite rapidly from 600Å onwards with two maxima at 720Å and

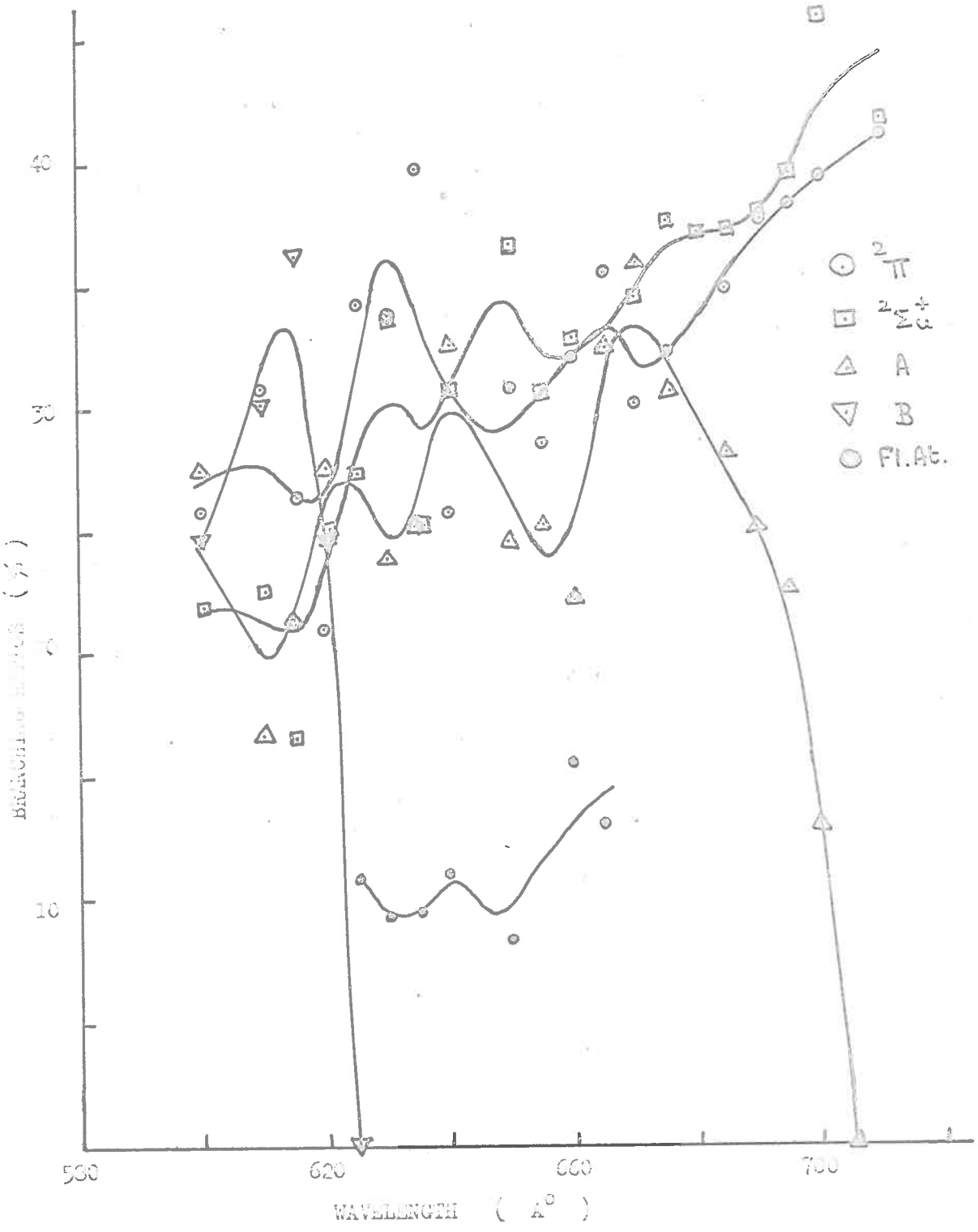

Fig. III.30 . Branching ratios for N_2O as a function of wavelength (500 to 700 A°)

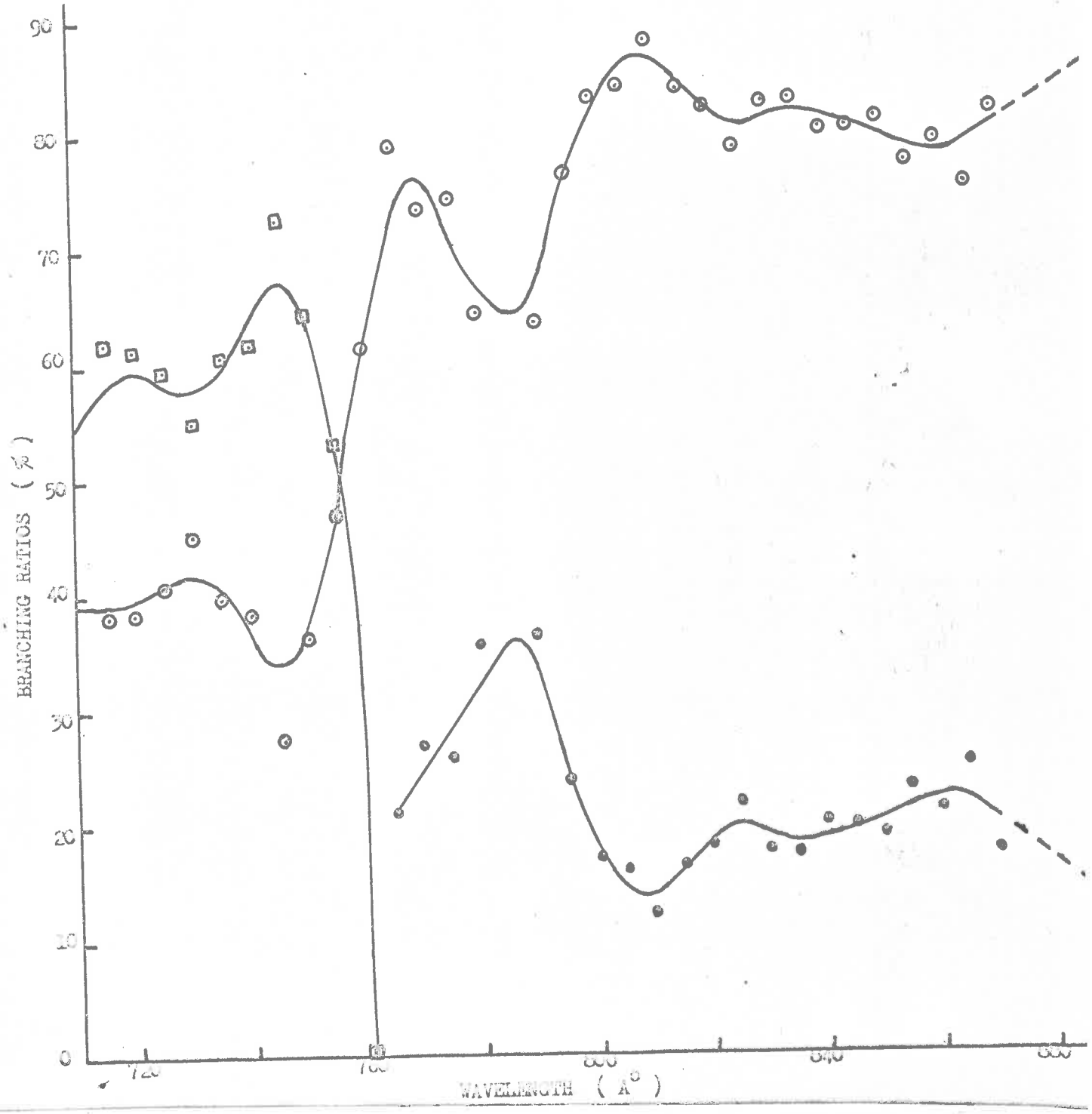

Fig. III.31. Branching ratios for different competing processes for N_2O as a function of wavelength (710 to 870 A°) .

745Å. The branching ratios versus wavelength curve for the A state of the ion shows three maxima at 625Å (~ 27%), 640Å (~ 30%) and 670Å (~ 33%) before reaching a minimum value (0%) at 705Å. The branching ratios for the B state start increasing at 600Å to a maximum value at 615Å (~ 33%) and show a rapid decrease. The B state ceases to exist at 625Å and onwards.

The branching ratios for the fluorescent autoionization process in the wavelength region of 625Å to 665Å vary from 9% to 15% but in the wavelength region of 765Å to 870Å, a broad maximum at 785Å (~ 36%) is reported followed by a trend of fairly constant branching ratios between 820Å to 875Å.

Partial photoionization cross-sections for all the competing processes against wavelength have been computed by combining the branching ratios of Figures III.30 and 31 with the total cross-sections reported by Cook et al. (1965) averaged over 8Å interval. The plot of partial cross-sections against wavelength is shown in Figures III.32 and 33.

III.5 Ammonia

Photoelectron spectra for ammonia excited by incident wavelengths of 625Å to 890Å were observed at 5Å intervals.

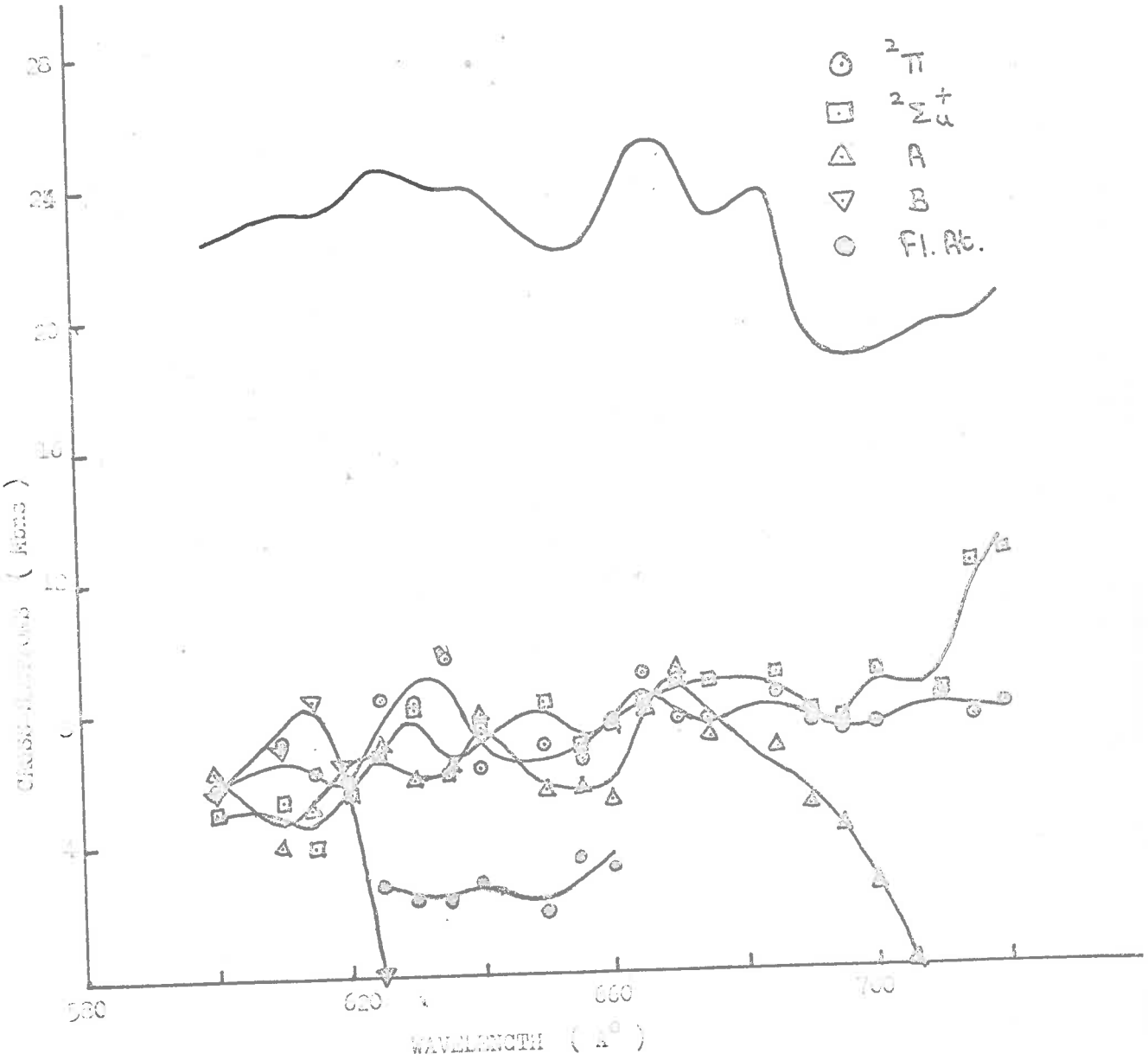

Fig. III.32 . Partial photoionization cross-sections for different ionic states processes for N_2O as a function of wavelength (600 to 720 A°). Total cross-sections (solid curve) of Cook et al, 1965 averaged over 8 A° are also shown in the figure .

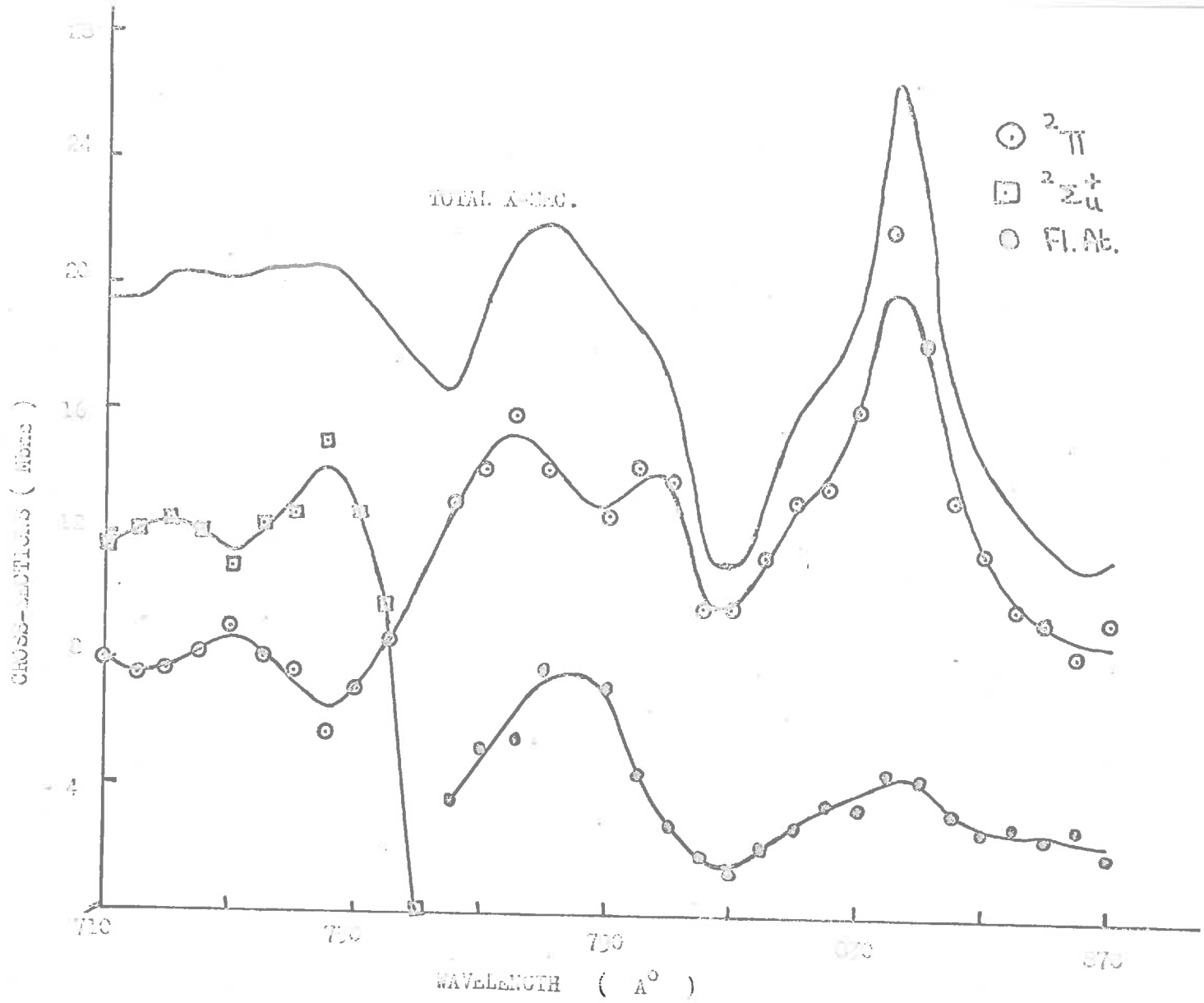

Fig. VII.33 . Partial photoionization cross-sections for different competing processes for H_2O as a function of wavelength (710 to 570 A^0) . Solid curve shows the total cross-sections averaged over 3 A^0 (Cook et al , 1965) .

Some typical examples of these spectra are illustrated in Figures III.34, 35 and 36. These spectra show several well-defined photoelectron peaks. The most energetic peak corresponds to a vertical ionization potential of 10·6 e.v. for the reaction $NH_3 + h\nu \rightarrow NH_3^+$ (ground state) $+ e^-$. Dibeler et al. (1966), in the mass spectrometric study of photoionization of ammonia, gave an adiabatic ionization potential of the ground state of the NH_3^+ ion as 10·16 e.v. Watanabe (1954) reported a difference of about 0·5 e.v. between the adiabatic and vertical ionization thresholds. The value of 10·6 e.v. obtained in the present work is thus in good agreement with Dibeler's results. The energy of the second peak corresponds to a vertical excitation potential of 15·4 e.v. and can probably be identified with transitions to the first excited state of NH_3^+ for which Lindholm (1954b) has determined a threshold of 15·2 e.v. and Cook and Samson (1959) of 14·9 e.v. (this latter measurement corresponds to the adiabatic threshold). The third peak at 16·0 e.v. is identified with the reaction $NH_3 + h\nu \rightarrow NH_2^+ + H + e^-$ for which Cook and Samson suggested a threshold of 15·8 e.v. and Dibeler et al. at 15·73 e.v. The discrepancy between these results is the difference between the vertical and adiabatic ionization potentials. This peak,

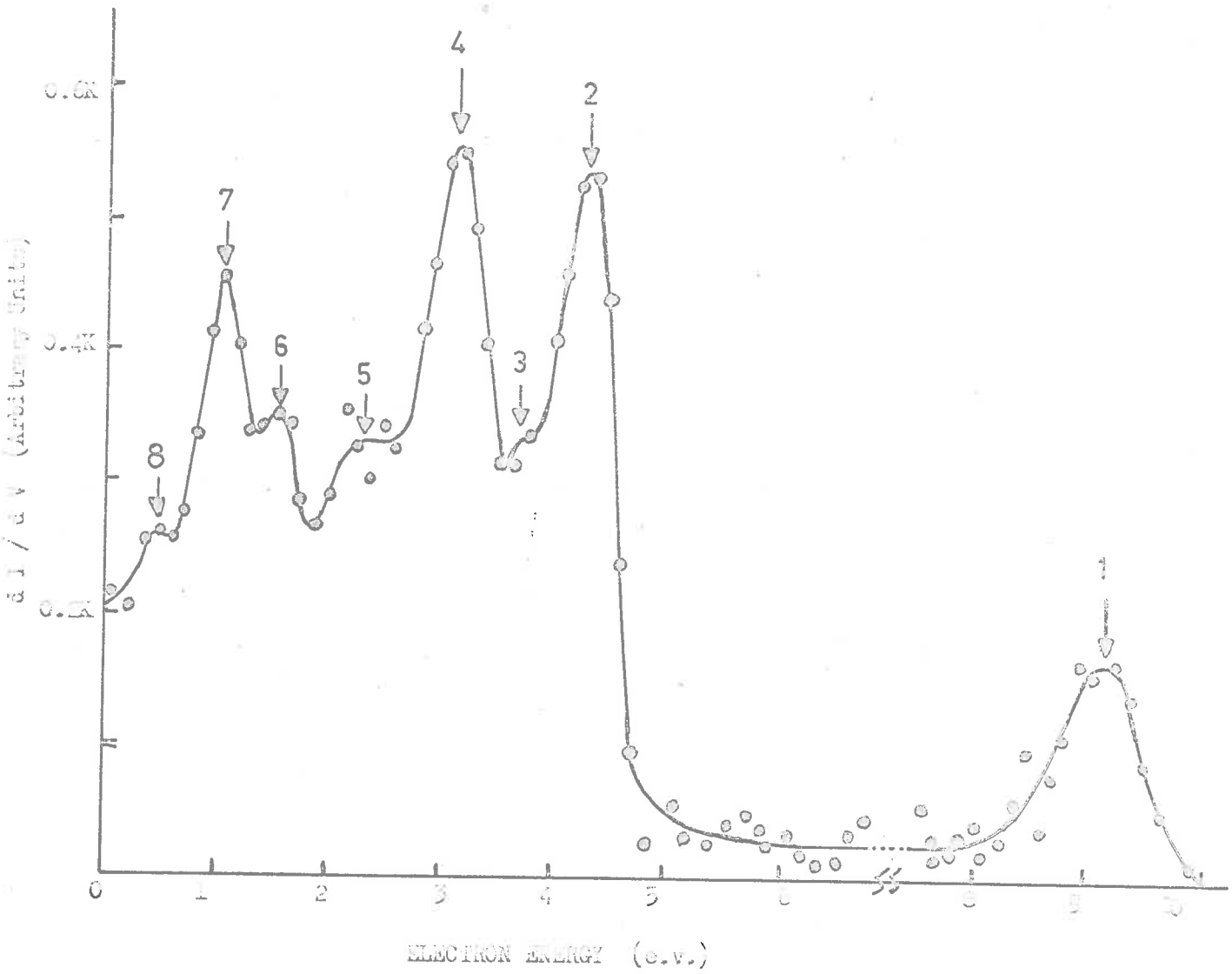

Fig. III.34 . Photoelectron energy spectra of ammonia at 630 A° .

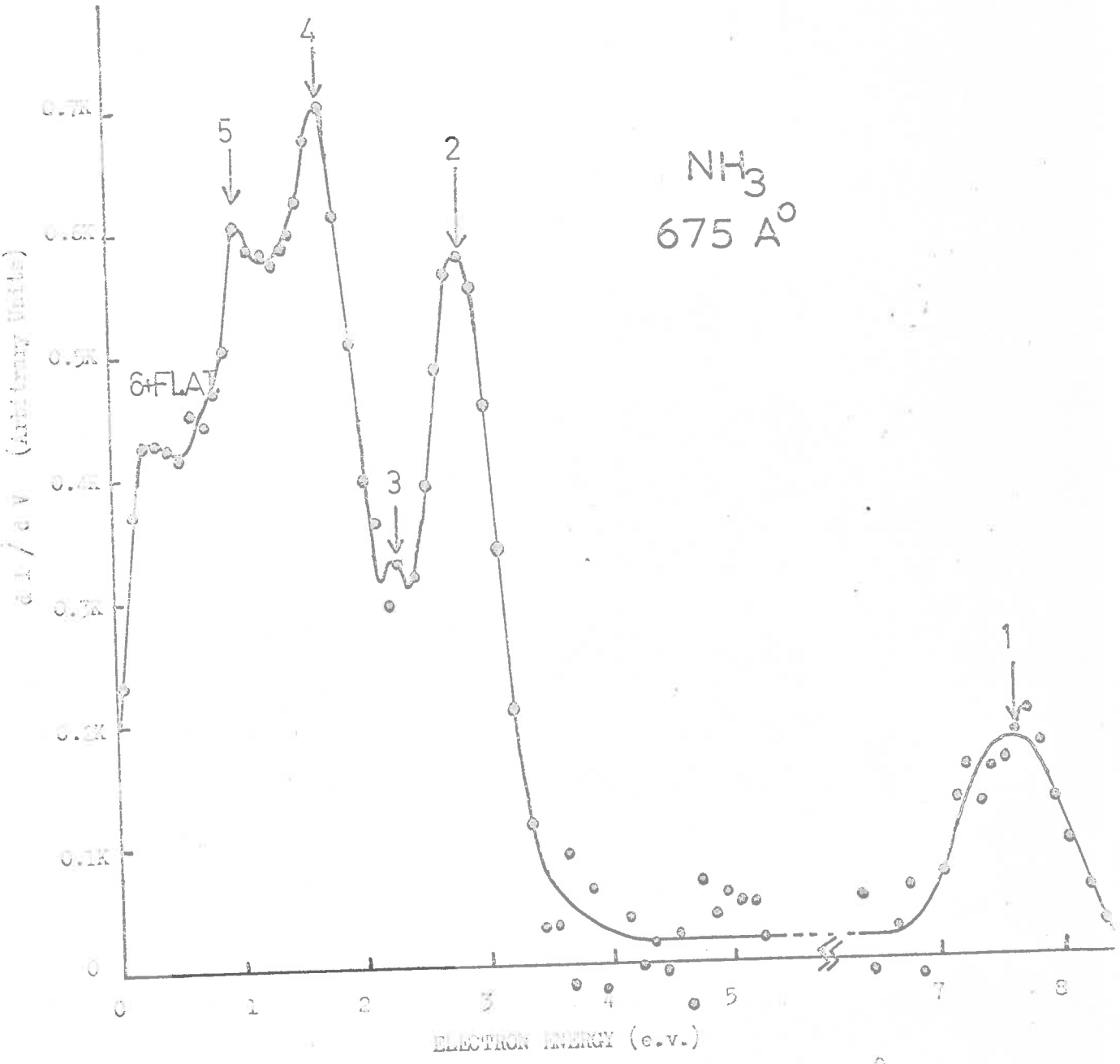

Fig. III.35. Photoelectron energy spectra of ammonia at 675 A°.

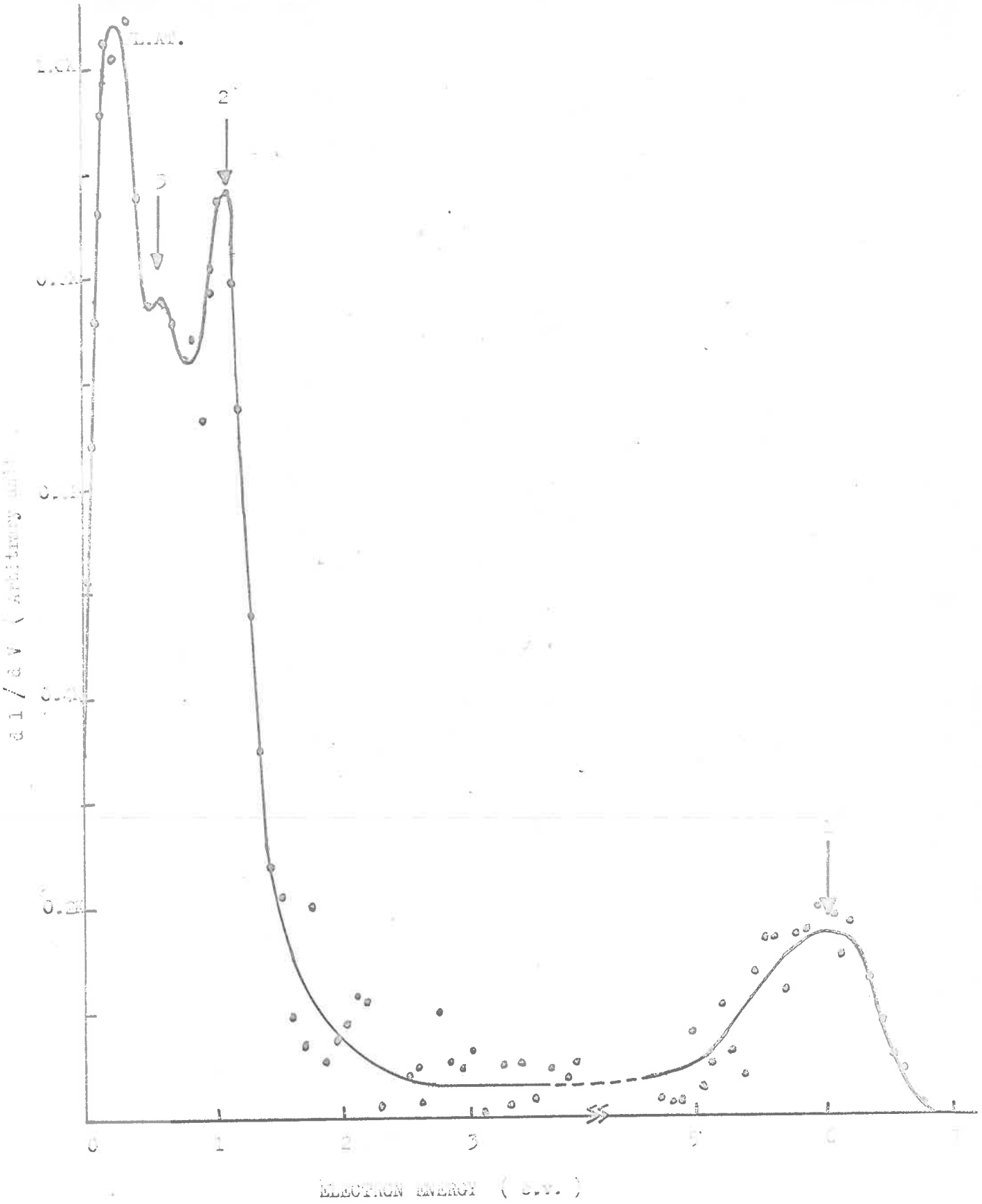

Fig. III.3C. Photoelectron energy spectra of ammonia at 745 A° .

corresponding to NH_3^+, is resolved only at a few wavelengths; at other wavelengths the peak is only partially resolved or unresolved. A peak corresponding to a threshold of 19·4 e.v. is clearly resolved in all spectra wherever it is energetically possible. The energy of this peak corresponds closely with estimates (Mann et al. 1940) of the threshold for the reaction $NH_3 + h\nu \rightarrow NH^+ + H_2 + e^-$. Other peaks are evident in the region 16·5 to 19 e.v. and probably correspond to other excited states of NH_3^+ and NH_2^+ but it is not possible from the present work to suggest any further indentifications. Table III.5 summarises the information obtained from the present measurements about the energies of the photoelectron groups from ammonia.

TABLE III.5

Photodisintegration of Ammonia

Photoelectron Group	Threshold		Suggested Identification
	Energy (e.v)	Wavelength (Å)	
1	10·6	1170	$NH_3+h\nu \rightarrow NH_3^+(G.S.)+ e^-$
2	15·4	805	$\rightarrow NH_3^+(Ex.S.)+ e^-$
3	16·0	775	$\rightarrow NH_2^+(G.S.)+H+e^-$
4	16·6	747	Uncertain
5	17·3	716	Uncertain
6	18·1	684	Uncertain
7	18·7	663	Uncertain
8	19·4	639	$\rightarrow NH^+ + H_2 + e^-$

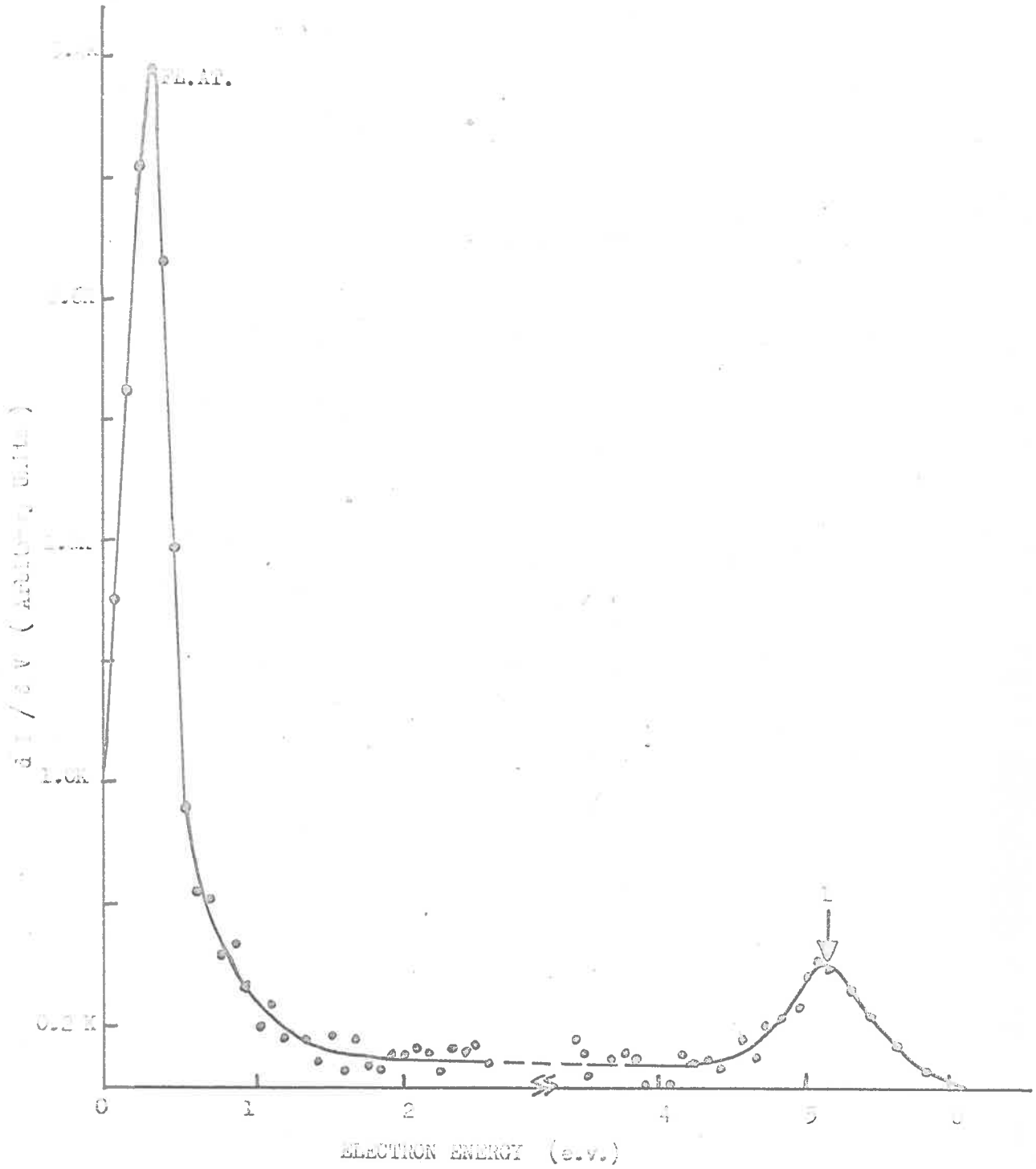

Fig. III.37. Photoelectron energy spectra for ammonia at 735 A^{o} .

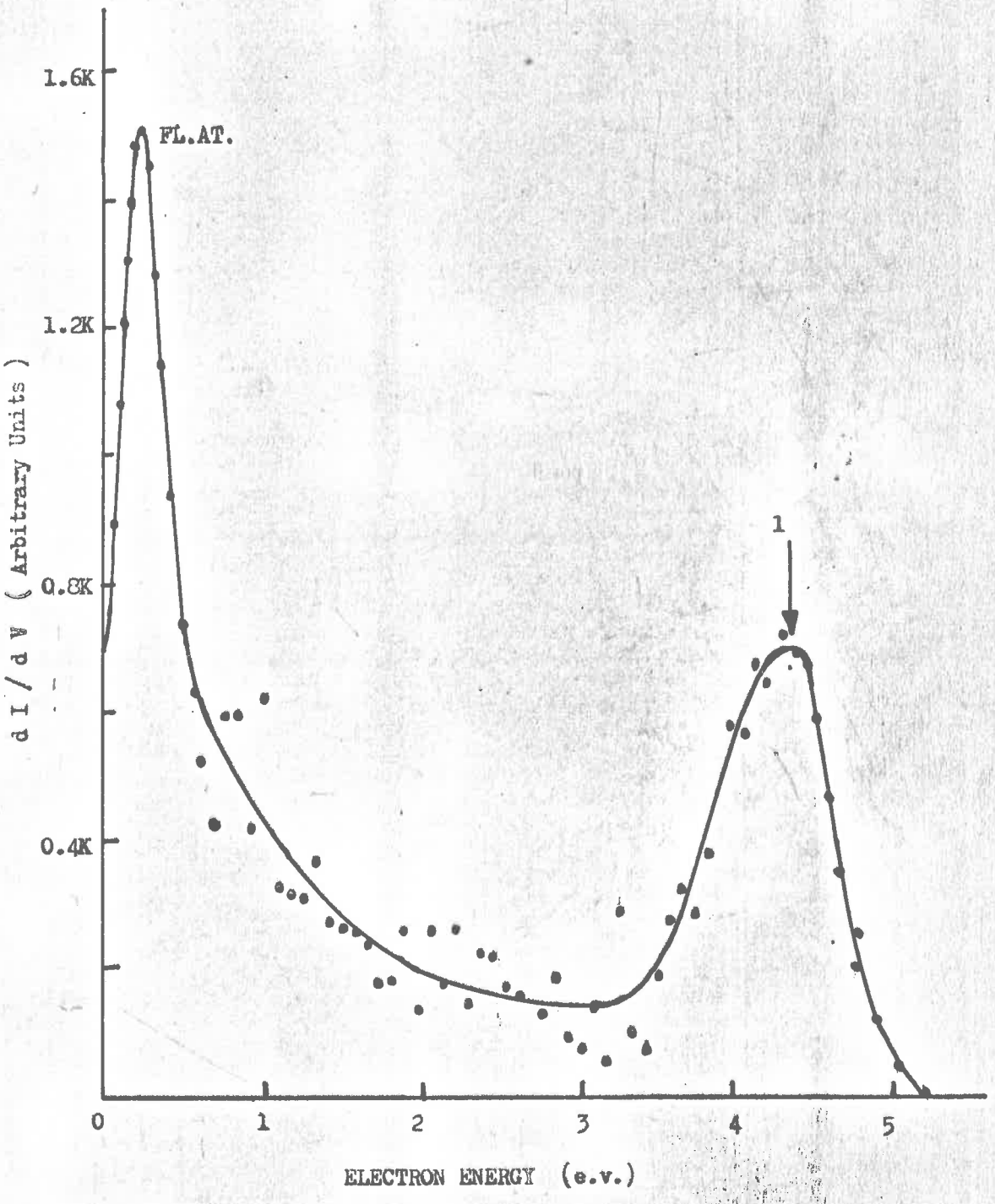

Fig. III.38 . Photoelectron energy spectra for ammonia at 820 A^{o} .

In the wavelength region of 660Å to 890Å, a low energy anomalous peak at about 0·5 e.v., the position of which did not change with photon energy, was observed. The behaviour of this peak is very similar to the fluorescent autoionization observed in nitric oxide (section III.3.1) and it appears that a similar process, involving radiative transitions in the neutral molecule, also occurs for ammonia. In figures III.37 and 38 are shown a few photoelectron spectra of ammonia with the low energy anomalous peak.

The measured branching ratios for various photodisintegration processes in ammonia are shown in Figures III.39 and 40. These measurements combined with the measured total photoionization cross-sections of Metzger and Cook (1964), which were averaged over 8Å intervals to obtain a resolution equivalent to that of the present work, give the partial photoionization cross-sections shown in Figures III.41 and 42.

III.6 Accuracy of Partial Cross-sections

The uncertainty involved in unfolding the spectra was one of the factors limiting the accuracy of the partial cross-sections. Ascertaining the area under low energy noise associated with each peak could not be very accurate. Moreover, the calibration curve (Figure II.19)

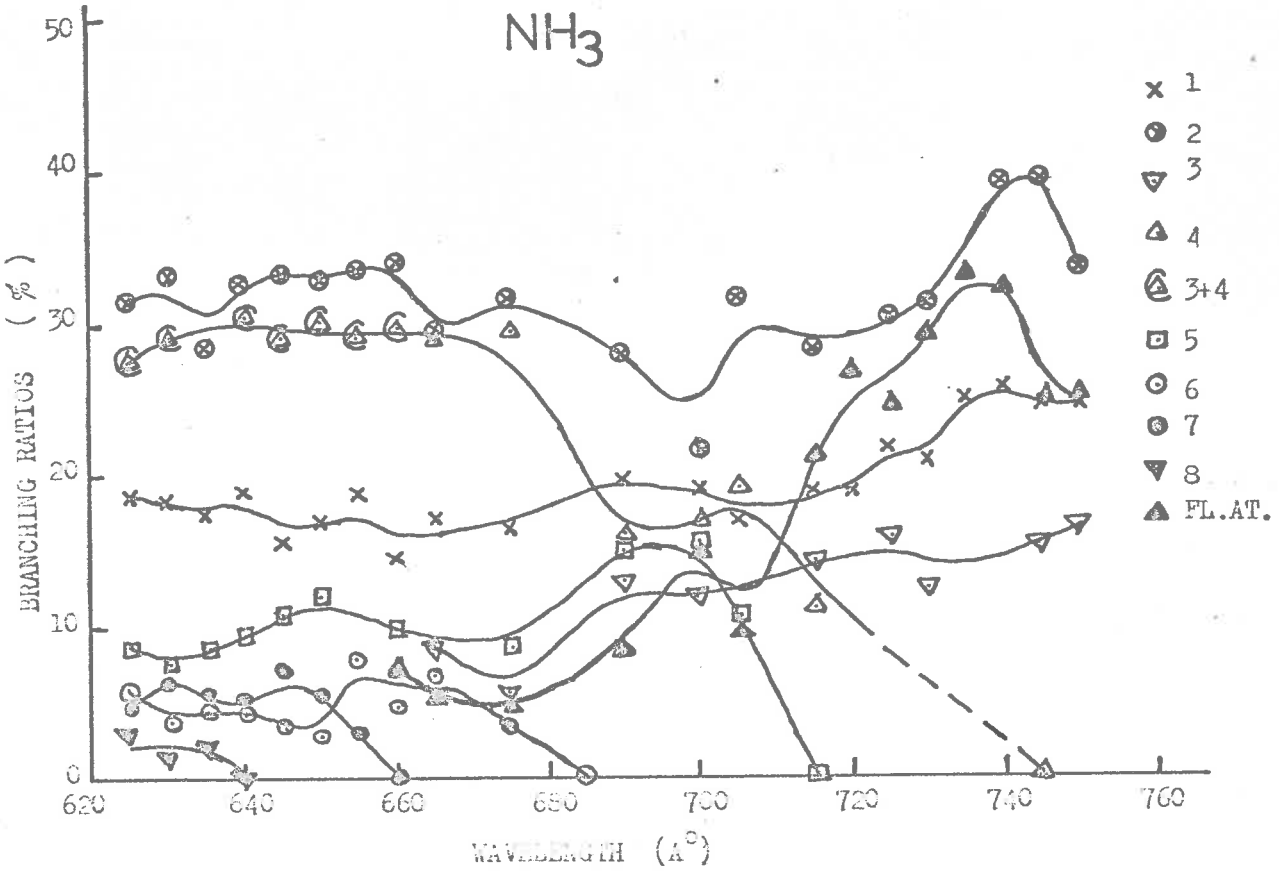

Fig. III.39. Branching ratios for different competing processes in ammonia from 620 A° to 760 A° .

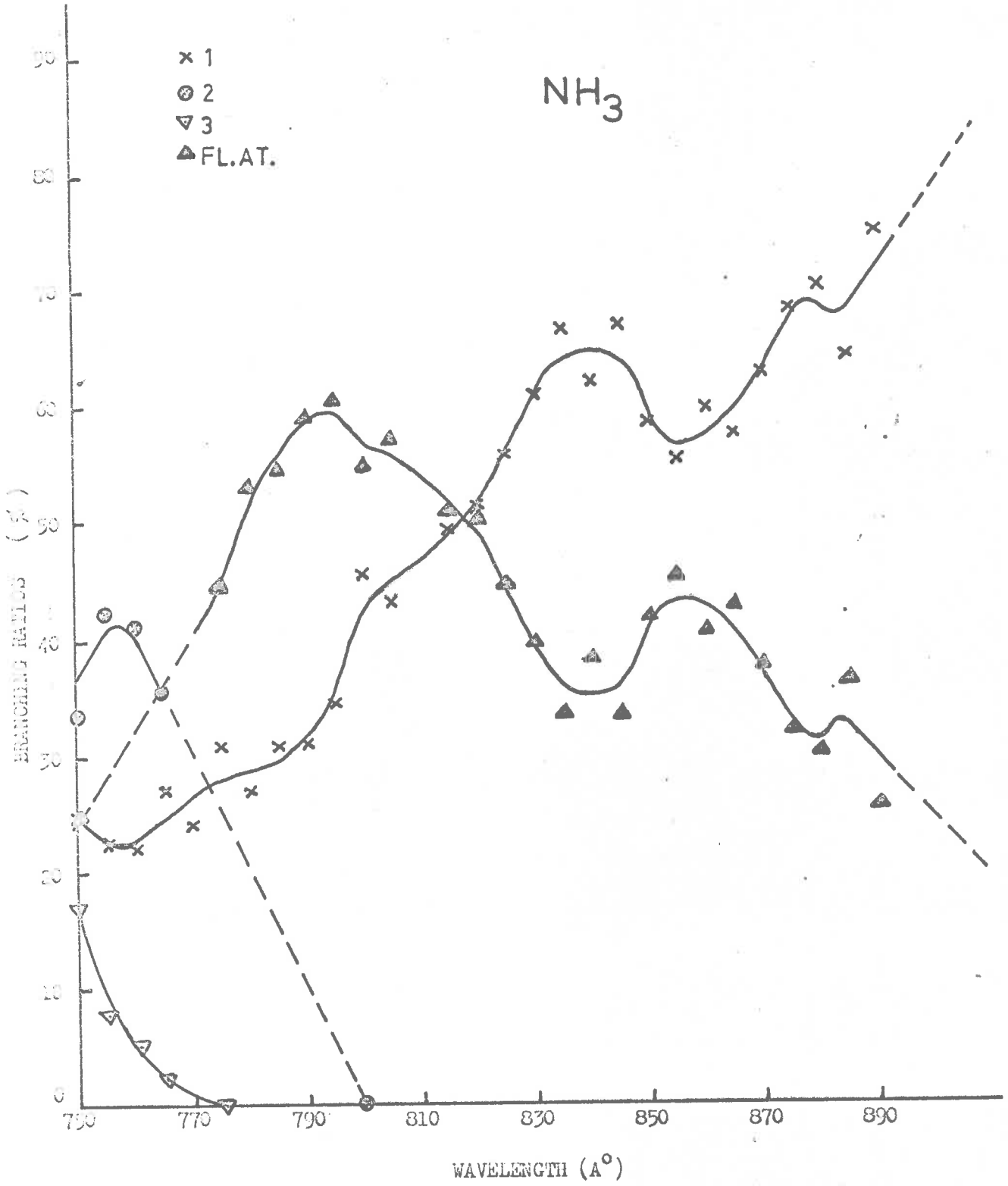

Fig. III.40. Branching ratios for different competing processes for ammonia from 750 to 890 A° .

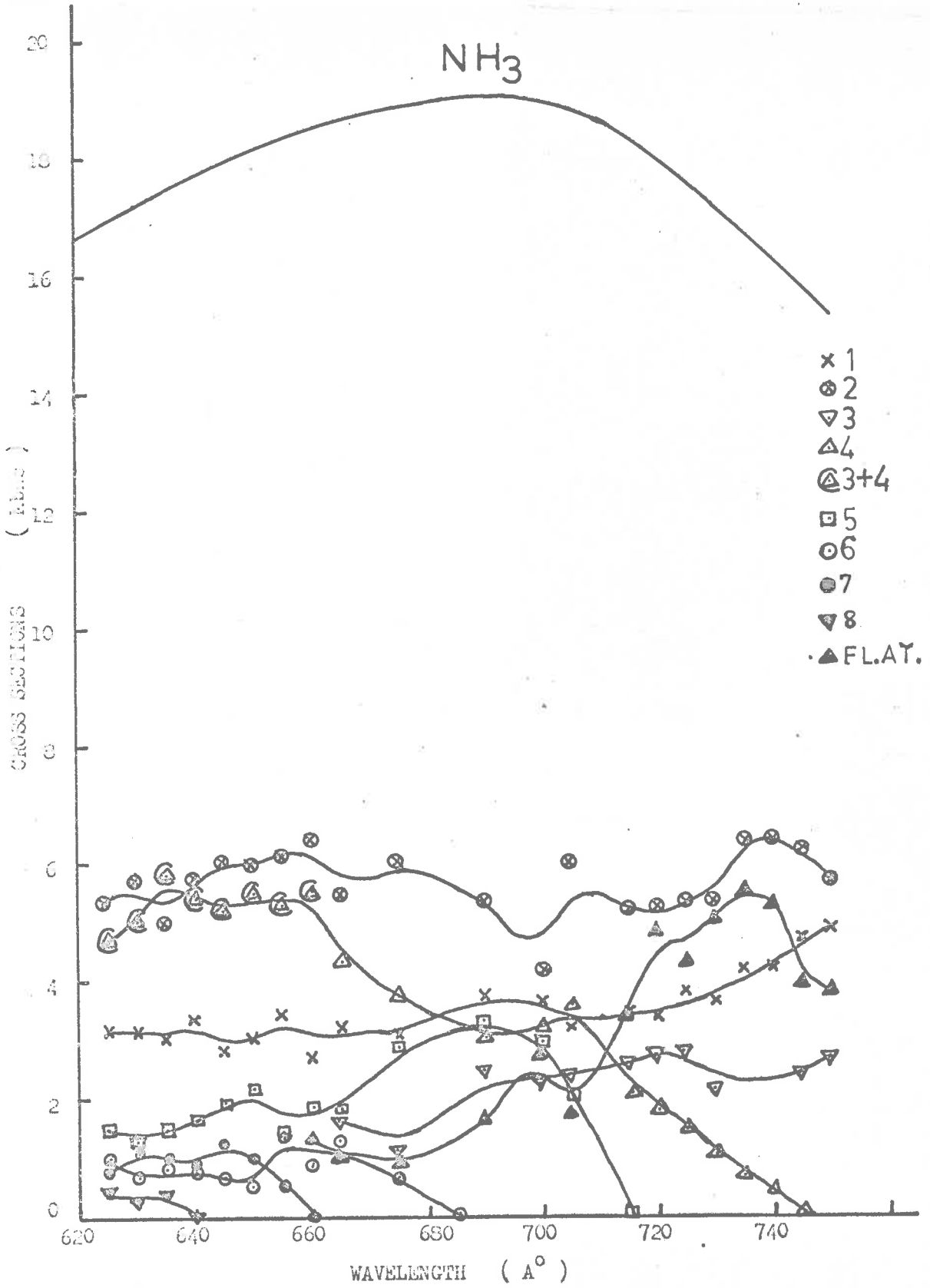

Fig. III.41. Partial photoionization cross-sections for different competing processes for ammonia from 620 to 750 A°. The upper curve shows the total cross-sections of Metzger and Cook, 1964 averaged over 8 A° interval.

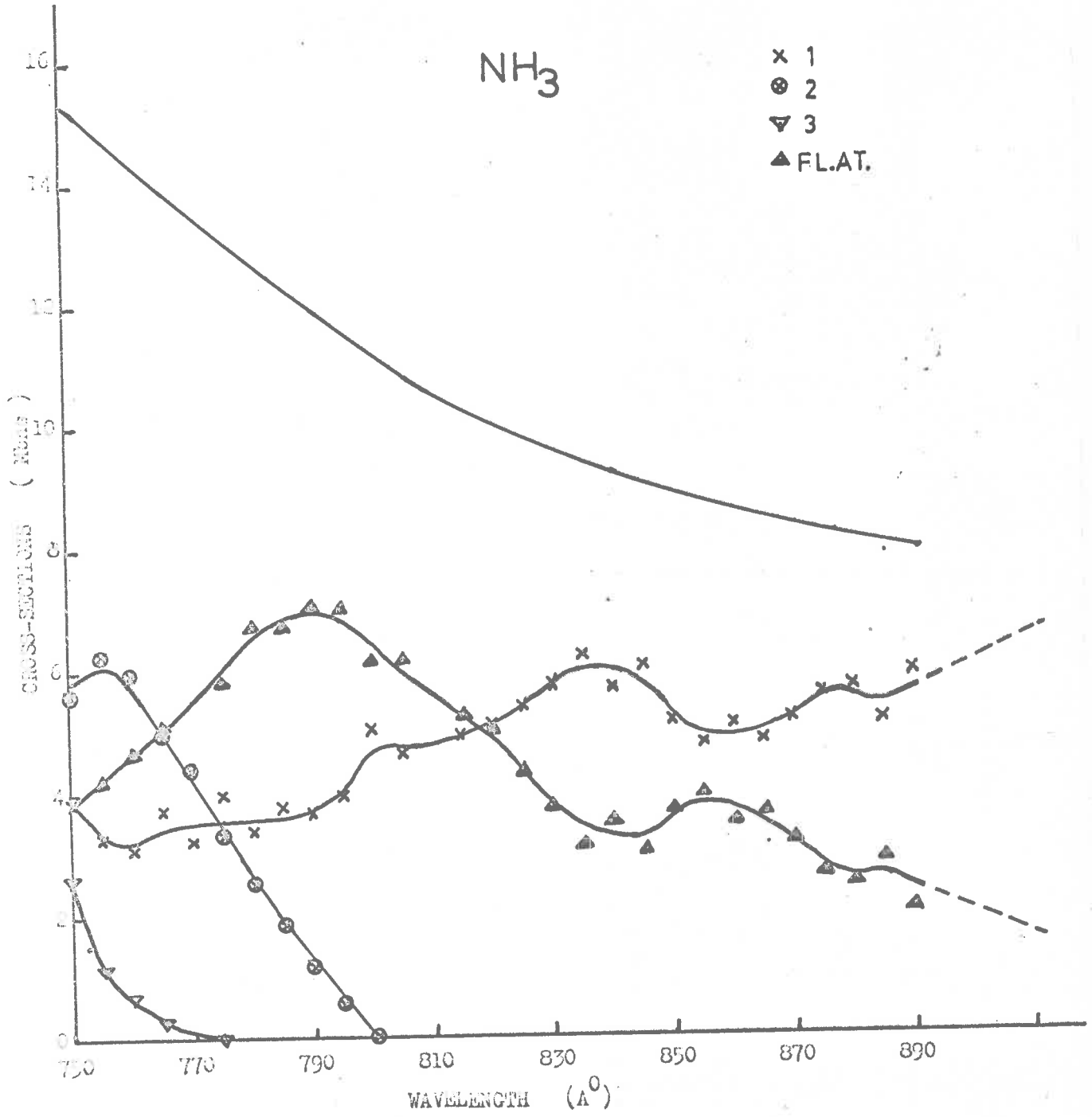

Fig. III.42. Partial photoionization cross-sections for different competing processes for ammonia from 750 to 890 A°. The upper curve is the total cross-sections of Metzger and Cook, 1964 averaged over 8 A° interval.

would not be of much help for finding low energy region associated with a peak of large electron energy, e.g. in case of ground state peak of nitrous oxide which occurs at 8·4 e.v. at an incident photon wavelength of 584Å.

In many of the spectra taken, a partial overlapping of the peaks due to low resolution used in the present work was observed. The total area under the envelope of the partially resolved peaks could be measured fairly accurately but it would be quite difficult to assign with accuracy the partial areas under individual peaks. For doing this, the shape and the peak width of the individual peaks has to be guessed from spectra at other wavelengths where the peaks are better resolved.

The estimated accuracy of the area under a given peak was found to be in the range of 8 to 10%, but the absolute error accumulated during the unfolding of the spectra. The error in case of peaks at lower energy was reduced by demanding that the unfolding should be self-consistent.

Near the threshold energy region of each electronic state, the peak was found to be small. The measurement of area under the peak in such a case would involve much

more error than elsewhere.

The accuracy of the partial photoionization cross-sections varied greatly, depending upon the position and size of the peak and the separation of different peaks. In most cases, the error in the cross-sections was probably between 15 to 20%.

CHAPTER IV

PHOTOELECTRON SPECTROSCOPY IN THE NEIGHBOURHOOD OF SOME AUTOIONIZING STATES OF MOLECULAR OXYGEN

IV.1 Introduction

In the measurement of the photoelectron spectra of molecular oxygen (Blake and Carver, 1967) and carbon monoxide and some other gases (chapter III of this thesis) a low energy anomalous peak has been observed in a few of the spectra. The transition probability of this peak has been found to vary effectively with incident photon energy. Such a structure is observed to be peculiar to those wavelength regions where the autoionized structure in the total photoionization cross-sections is strong. Doolittle and Schoen (1965) have studied the difference between on-resonance and off-resonance spectra in molecular hydrogen and have shown that autoionization can change the energy distribution of the emitted photoelectrons. This suggests the need of a detailed and comprehensive study of high resolution photoelectron spectra of some gases on the autoionized resonances and on the continuum on both sides of the resonances.

In the work described in this chapter, some of the autoionized resonances of molecular oxygen have been selected for experimental investigation. The resolution used for this work has made it possible to study the disintegration of oxygen molecule excited to an autoionized state by observing the variation, if any, in the photoelectron spectra between one autoionized resonance and another and between an autoionized resonance and the neighbouring off-resonance continuum.

IV.2 Experimental Method

The experimental arrangements are essentially the same in chapters II and III, except that the exit slit of the 1-metre monochromator has been adjsted to give a wavelength resolution of 1·6Å instead of 8Å used before. Improving the resolution in this way is accompanied by a corresponding reduction in beam intensity. In order to obtain satisfactory spectra, it has been necessary to make repeated scans of the electron retarding potential using the multichannel storage system described in chapter II. Typically, the time required under these conditions to accumulate a satisfactory photoelectron spectrum has been between one and two hours at each photon wavelength.

IV.3 Experimental Results

Total photoionization cross-section measurements

indicate the position of many sharp autoionized resonances for molecular oxygen (Cook and Metzger, 1964b; Matsunaga et al. 1967). In Figure IV.1 are shown the cross-sections as reported by Matsunaga et al. (1967). The I, J and K progressions have associated with them well defined resonance peaks. Two resonance peaks each from I and J progressions have been selected for investigations.

Measurements of O_2 photoelectron spectra at the following peaks have been made: 885·8Å and 878·1Å (J progression); 839·1Å and 832·5Å (I progression). The exact position of each peak was determined by adjusting the photon wavelength, in the neighbourhood of the value indicated in Figure IV.1, to obtain a maximum in the measured electron current. Photoelectron spectra were also measured at the following off-resonance wavelengths: 888Å (J progression); 841Å and 834Å (I progression). The resonance and off-resonance spectra are compared in Figure IV.2.

For wavelengths longer than 775Å, only the $X^2\Pi_g$ ground state of O_2^+ is accessible and the photoelectron spectra at these wavelengths might be expected to show but a single band close to the energy corresponding to the adiabatic ionsation potential. The off-resonance

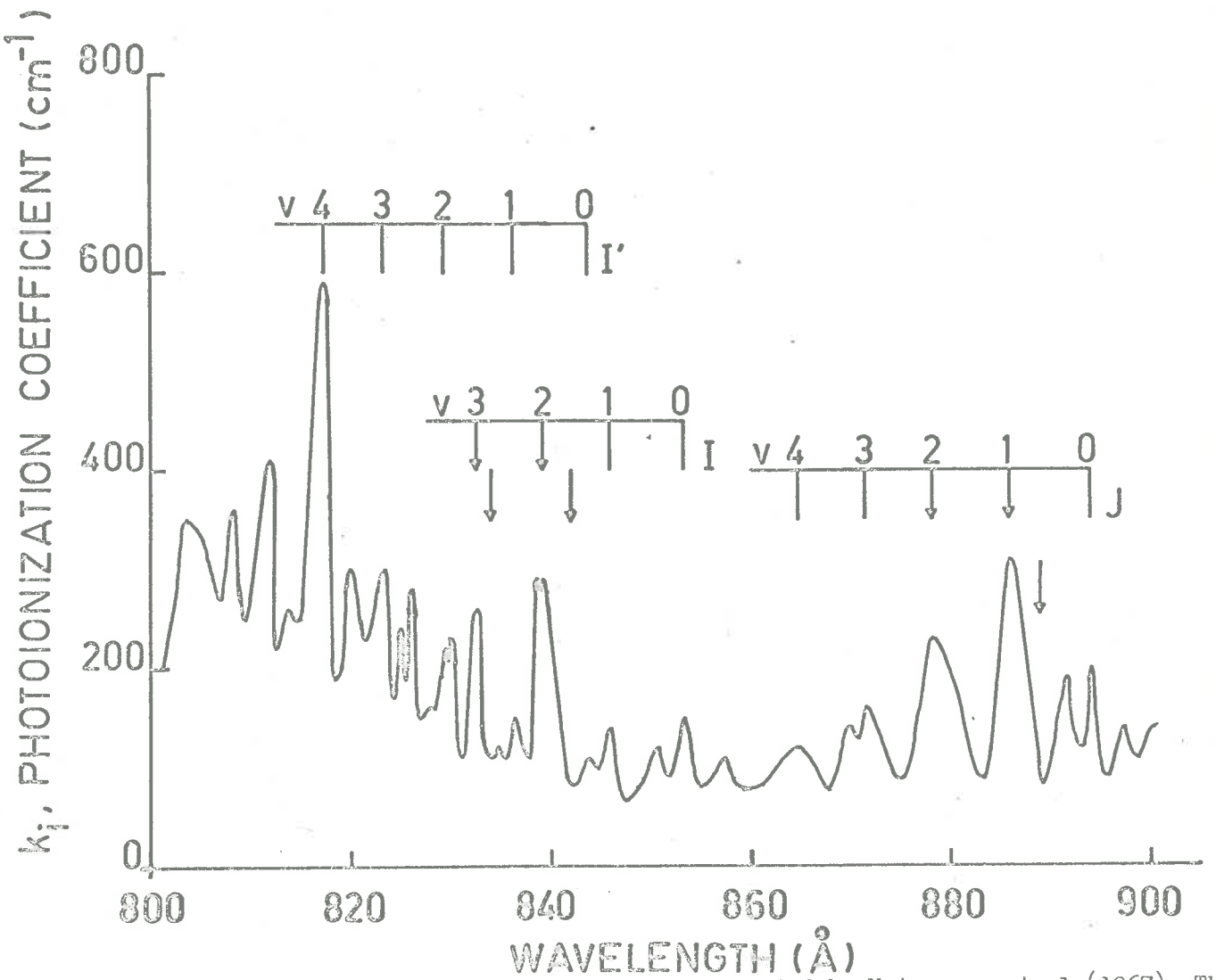

Fig. IV.1. Total photoionization cross-sections as reported by Matsunaga et al (1967). The arrows show where the on and off-resonace spectra were taken .

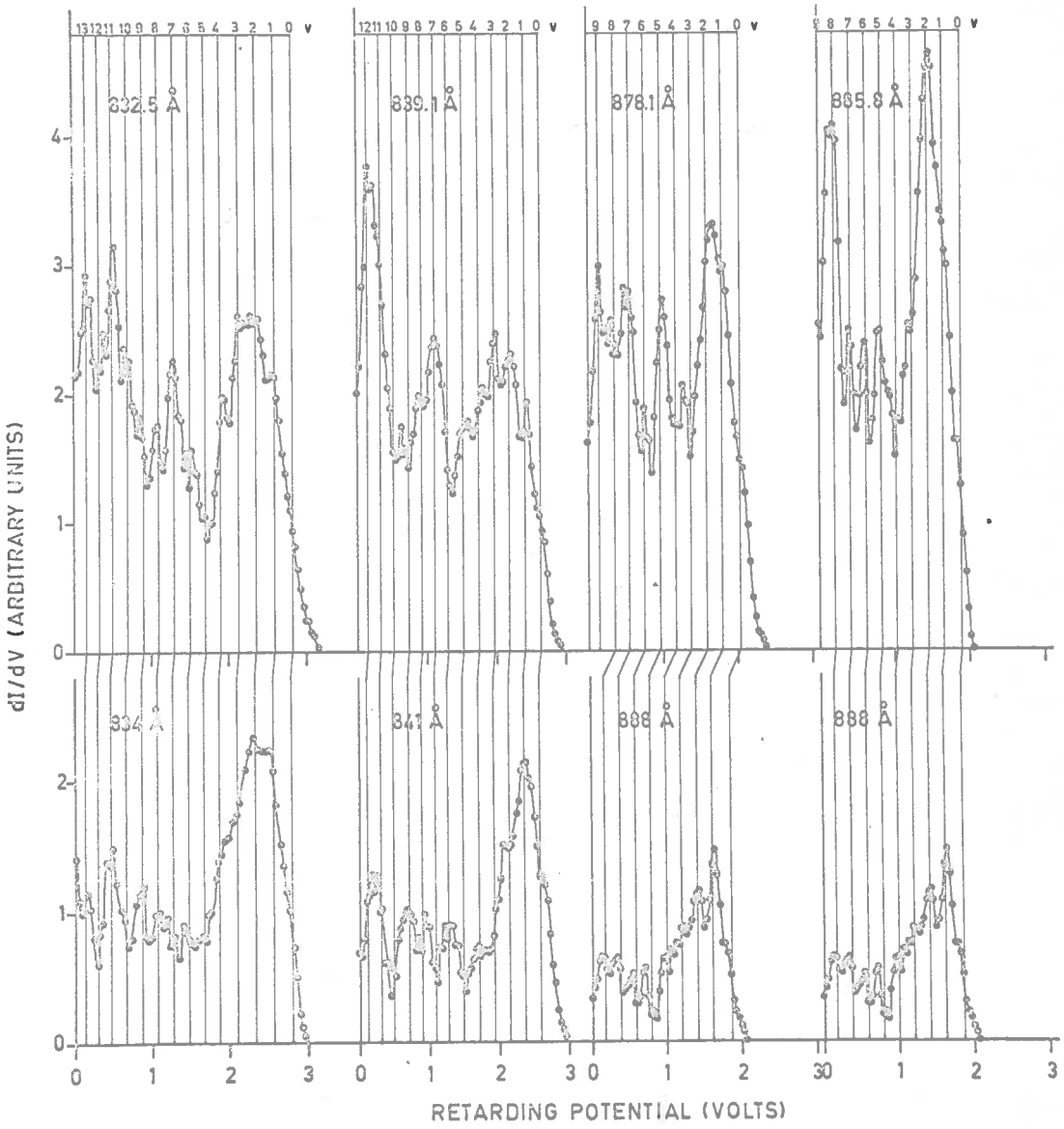

Fig. IV.2. A comparison of on-resonance (832.5 A^{o}, 839.1 A^{o}, 878.1 A^{o} and 885.8 A^{o}) and off-resonance spectra (834 A^{o}, 841 A^{o} and 888 A^{o}) as observed in the present work .

spectra shown in Figure IV.2 are of this form, but the resonance spectra are seen to have a more complicated form, similar to those reported by Blake and Carver (1967). These spectra have additional peaks at lower energies and the shape of the low energy component varies from one resonance to another in the range 885·5Å to 832Å. In addition to low energy peaks, partly resolved vibrational structure with spacing in good agreement with that of the $X^2\Pi_g$ state of O_2^+ can be traced through these spectra. The most significant difference between the photoelectron spectra (Figure IV.2) is that the low energy component is absent from (or at least very weak) the off-resonance spectra in this wavelength region. In each case of resonance spectra, it is noted that the total number of maxima in the distribution is equal to (v + 1) where v is the vibrational quantum number of the autoionizing level involved. The resonances at 885·8Å and 878·1Å are the v = 1 and 2 members of the J progression respectively and those of 839·1Å and 832·5Å the v = 2 and v = 3 members of the I progression respectively (Figure IV.1). The resonance spectra in Figure IV.2 show two maxima at 885·8Å, three maxima at 878·1Å and 839·1Å and four maxima at 832·5Å. This correlation between the shape of the photo-electron spectrum and the vibrational quantum number of

the autoionizing level suggests that the number of maxima in the resonance spectra may be explained with the help of Franck-Condon principle.

IV.4 Discussion

It was suggested previously (Blake and Carver, 1967) that such a feature could be explained by assuming that a fluorescent autoionizing process was occurring in which part of the excess energy was dissipated as a fluorescent photon, and that the transition to the continuum was from the second intermediate state, which was common to processes excited by different photon energies.

Judge et al. (1963) observed some weak fluorescence in oxygen excited by wavelengths longer than the threshold for the first excited state of the ion and this may or may not have been from such a process. But the intensity was too low to account for the strong anomalous peaks in the present spectra.

The fluorescent autoionization explanation would be necessary if there were no energy levels available in the ion which corresponded to the position of the anomalous low energy peaks. This however is not so because the potential curves of the autoionizing levels with a definite depth exist. On this account, the above explanation

seems to be unnecessary.

The form of these spectra can alternatively be explained on the basis of Franck-Condon principle by assuming an appropriate shape for the potential curve of the autoionizing state. Figure IV.3 shows the potential curves for the ground states of O_2 and O_2^+ as given by Gilmore (1965). A hypothetical curve for the autoionizing state (I progression) is drawn such that the part to the left of the minimum is of the same shape as the corresponding part of the O_2^+ $X^2\Pi_g$ curve but displaced about 1·5 volts above it, and similarly on the right hand side, where the vertical displacement is about 0·5 volts. (The shape of the autoionizing curve is only arbitrary to explain the spectra qualitatively. The exact shape has been computed and is shown in chapter V).

It is clear that for transitions from any vibrational level of the autoionizing state, maxima occur in the Franck-Condon distribution 0·5 volts and 1·5 volts below the initial level, thus producing a spectrum of the form observed on the resonance (Figure IV.3) which belongs to v = 2 vibrational member of the I progression. For 839Å resonance spectra, the (v + 1) empirical rule for

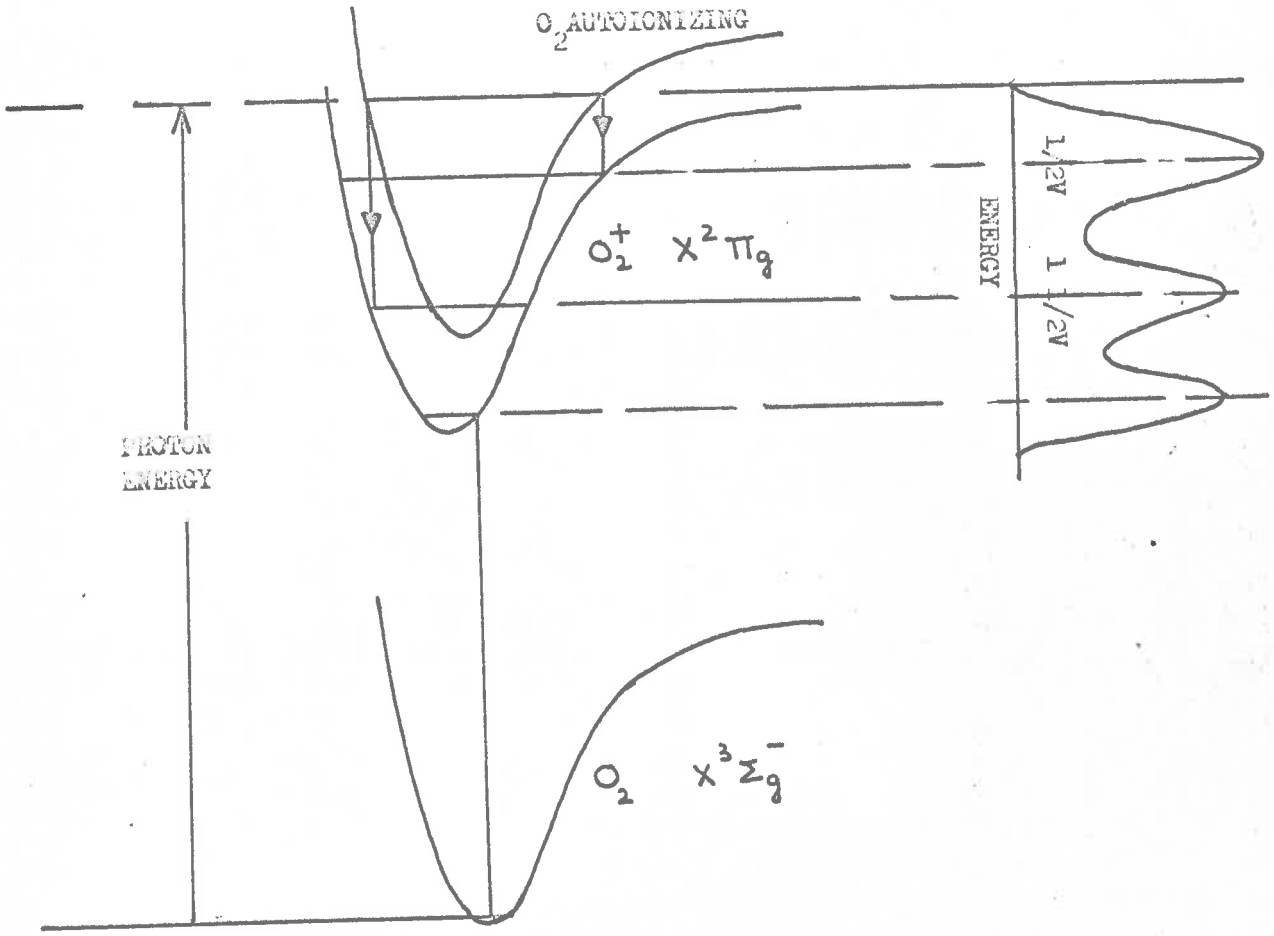

Fig. IV.3. Figure explaining 839 A^o spectra by Franck-Condon principle. The ground states of O_2 molecule and ion are shown as reported by Gilmore (1965) but the autoionizing state is taken to be arbitrary.

the number of peaks holds good but the explanation given for Figure IV.3 does not account for the number of peaks for v = 3,4 etc. vibrational members of the I-progression. To explain this, the vibrational wavefunctions for v = 0, 1, 2 -- members of the autoionization state have to be computed. The total number of broad maxima in the photoelectron spectra is equal to the number of maxima in the vibrational wavefunction of the autoionising state (see Figure V.1 of chapter V).

This qualitative explanation seems to agree fairly well with the experimental results. In order to test this conclusion, the Franck-Condon factors for the autoionization from the levels that have been observed, should be computed. In chapter V, the Franck-Condon factors have been calculated and the general form of the spectra has been reproduced.

CHAPTER V

FRANCK-CONDON FACTORS FOR AUTOIONIZING TRANSITIONS IN MOLECULAR OXYGEN

V.1 Introduction

The photoelectron spectra obtained at resonance and off-resonance wavelengths (chapter IV) have been discussed qualitatively with the help of Franck-Condon principle. This analysis explained only the number of maxima in the resonance photoelectron spectra but would not ascertain the distribution of maxima with respect to electron energy. Thus a complete theoretical basis to replace this qualitative analysis is required. The shape of the photoelectron spectra and its relation to the vibrational quantum number of the autoionizing level (see chapter IV) suggests that the form of the spectrum may be reproduced by the distribution of Franck-Condon factors for the autoionization transitions.

An arbitrary assumption about the shape of the potential curve of the autoionizing state was made (chapter IV). A choice of the potential function would give a definite idea about the potential curve and would help in calculating the Franck-Condon factors. For the present work, Morse potential function was used.

V.2 Method for Franck-Condon Calculations and Results

The radial part of the wave equation for the nuclear motion of a diatomic molecule as given by Morse (1929) is

$$\frac{d^2R}{dr^2} + \frac{8\pi^2\mu}{h^2}\left[E - U(r)\right]R = 0 \qquad (V.1)$$

where E is the vibrational energy, μ the reduced mass of the molecule and U(r) is a complicated potential function of internuclear distance r and of the electronic quantum numbers. The most suitable form of U(r) as reported by Morse is

$$U(r) = E_{e\phi} + D_e\left[1-e^{-\beta(r-r_e)}\right]^2 \qquad (V.2)$$

where $E_{e\phi}$ is the energy of the electronic excitation, D_e the dissociation energy measured from the bottom of the potential curve and r_e is the equilibrium internuclear distance. The expressions for β and D_e as derived by Herzberg (1950) are the following:

$$\beta = \sqrt{\frac{2\pi^2 C\mu}{D_e h}} \cdot \omega_e$$

$$D_e = \omega_e^2/4\omega_e x_e$$

Another useful transformation can be made by letting

$y = e^{-\beta(r-r_e)}$. Then

$$\frac{d^2R}{dy^2} + \frac{1}{y}\frac{dR}{dy} + \frac{8\Pi^2\mu}{\beta^2h^2}\left[\frac{W}{y^2} + \frac{2D_e}{y} - D_e\right]R = 0$$

where $W = E - E_{e\ell} - D_e$.

W is the energy measured from dissociation limit. To transform the above expression into a differential equation, let the radial wavefunction R have the form

$$R = e^{-2ay}\cdot(2ay)^{b/2}\cdot F(y)$$

and put $z = 2ay$.

Then if

$$a = \frac{2\Pi(2\mu D_e)^{\frac{1}{2}}}{\beta h}$$

$$W = -\frac{\beta^2h^2b^2}{32\Pi^2\mu}$$

the wave equation reduces to

$$z\frac{d^2F}{dz^2} + (b+1-z)\frac{dF}{dz} + \left[\frac{-8\Pi^2\mu D_e}{\beta^2ah^2} - \frac{b+1}{2}\right]F = 0 \qquad (V.3)$$

$v = \frac{8\Pi^2\mu D_e}{\beta^2ah^2} - \frac{b+1}{2}$ is known as the vibrational quantum number. Equation V.3 is soluble if the coefficient of F is a positive integer. Thus

$$R = Ne^{-z/2} \cdot z^{b/2} \cdot F(-v, b+1, z)$$

where N is the normalization constant and F (-v, b+4, z), the confluent hypergeometric function is a form of the generalized Laguerre polynomial. Pekeris (1934) gave a solution for N and if the rotational effects are neglected, it assumes the form

$$N = \left[\frac{\beta}{\Gamma(b)} \binom{v+b}{v} \right]^{\frac{1}{2}}$$

where $\Gamma(b)$ is a gamma function.

The Franck-Condon factor is the square of the overlap integral of the states participating in the transition and is given by

$$q_{v',v''} = \left| \int R_{v'} R_{v''} \, dr \right|^2$$

in which $R_{v'}$ is the vibrational wavefunction of the vibrational level v' of the upper electronic state and $R_{v''}$ is the vibrational wavefunction of level v" of the lower electronic state.

Lack of knowledge of the molecular constants especially the equilibrium internuclear distance, r_e for the autoionizing state has restricted greatly in the past the computations of Franck-Condon factors. In the

present calculations, r_e for the autoionizing state has been introduced as a parameter and the other molecular constants, ω_e, $\omega_e x_e$ for each electronic state and the reduced mass μ of the molecule have been taken from Herzberg (1950). For the members of the J progression no constants are available. The molecular constants ω_e, $\omega_e x_e$ the harmonic vibrational frequency and the anharmonicity constant for this autoionized state can be obtained by substituting the experimental energies of the lines in the progression into the energy equation of the anharmonic oscillator. This gives a series of simultaneous equations for ω_e, $\omega_e x_e$.

The value of r_e for the autoionized state was varied until an optimum r_e value gave the distribution of Franck-Condon factors which was in best agreement with the resonance photoelectron spectrum observed experimentally. In Table V.1 are listed the values used for the molecular constants, together with the optimum values obtained for r_e of the autoionizing states. With the known values of r_e and other constants for I and J autoionizing states, the form of the potential curves for the two states could be obtained, using the equation V.2.

TABLE V.1

Molecular constants for O_2 and O_2^+ states used in the Franck-Condon calculations, and the optimum values of r_e obtained for the autoionized states of O_2 (Herzberg, 1950).

	$\omega_e(cm^{-1})$	$\omega_e x_e(cm^{-1})$	μ_α(a.m.u.)	$r_e(\mathring{A})$
$O_2 X^3\Sigma_g^-$	1580·361	12·073	8·00000	1·20739
I	1050	15	8·00000	1·35
J	1097	19·5	8·00000	1·30
$O_2^+ X^2\Pi_g$	1876·4	16·53	7·99986	1·1227

Figure V.1 shows the potential curve for the ground electronic state of O_2^+ ion as given by Gilmore (1965). The form of the potential curve, for the I autoionizing state is also shown in the figure. The vibrational wavefunctions for v' = 3 member of the I progression and v" = 2, 6, 10 and 13 of the ground electronic state of O_2^+ ion have been computed and are shown in Figure V.1. The v' = 3 wavefunctions (I state) show four maxima as expected (observed at the 832·5$\mathring{A}$) in the photoelectron spectrum. The vibrational quantum numbers at which these maxima occur (i.e. the values of v" for which the overlap integral has its maximum value) can be seen to depend

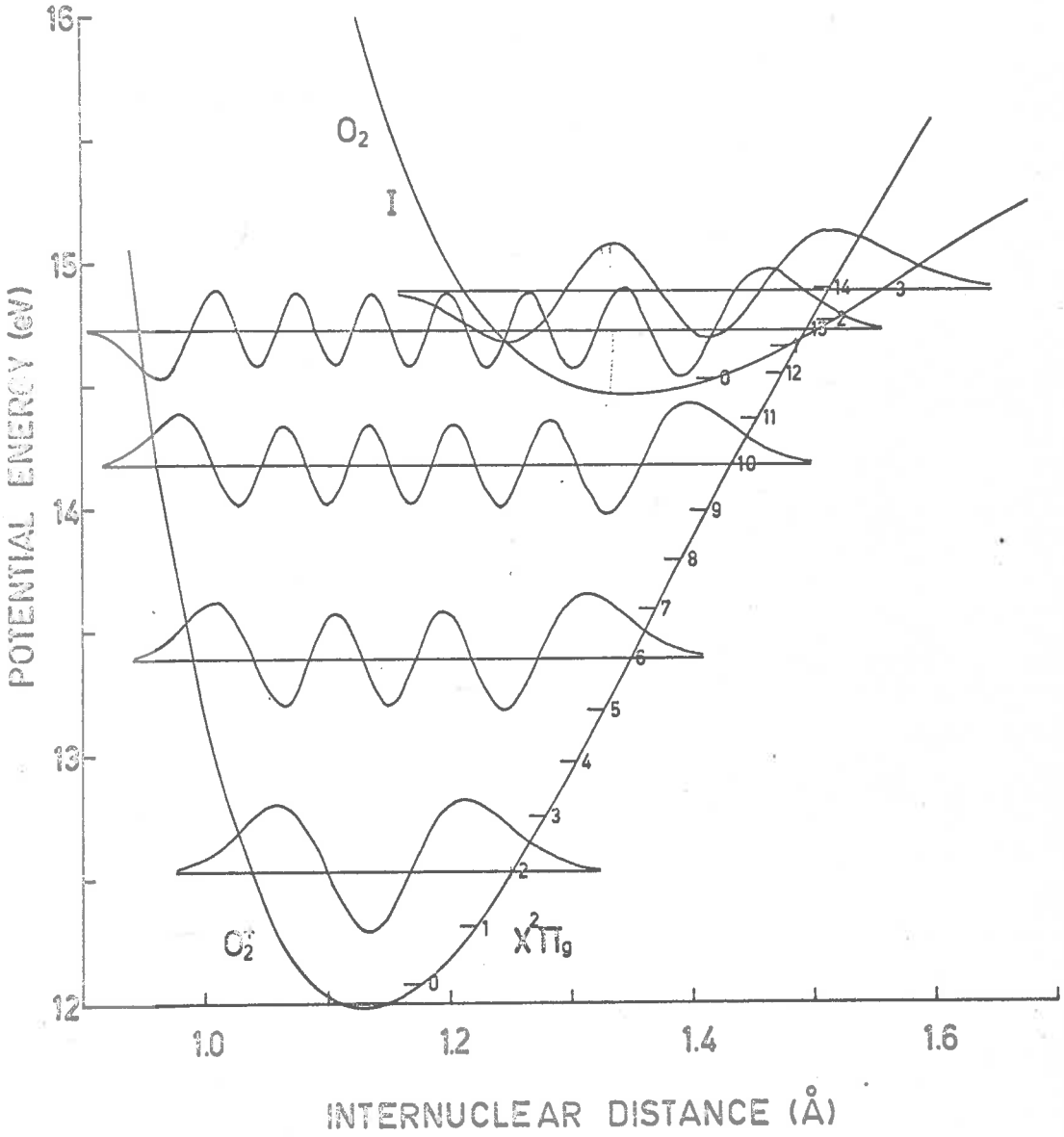

Fig. V.1. Potential energy diagram illustrating the overlap between the vibrational wavefunctions of the $X^2\Pi_g$ state of O_2^+ and the v'=3 level of the I autoionization state of O_2.

sensitively on the difference between the equilibrium radii for the autoionized state of the molecule and the final state of the ion.

Franck-Condon computations were performed on a CDC 6400 computer. Franck- Condon factors so computed for direct ionization from the $X^3\Sigma_g^-$ ($v = 0$) ground state of the O_2 molecule to the ground state of the O_2^+ ion are given in Table V.2 along with the results reported by Wacks (1964) and Halmann et al. (1968). A comparison shows a reasonably good agreement between the three results. Franck-Condon factors for autoionization from members of the I and J progressions of O_2 to the $X^2\Pi_g$ state of O_2^+ are given in Table V.3.

V.3 Discussion

The photoelectron spectra obtained at resonance wavelengths correspond to the sum of the contributions of 'continuum' and 'autoionized' components while the off-resonance spectra contain the 'continuum' component with a very small autoionized contribution. The differences between the respective on and off-resonance spectra represent the autoionization transitions only. These differences are shown in Figure V.2, together with the corresponding Franck-Condon factors. From the figure, it

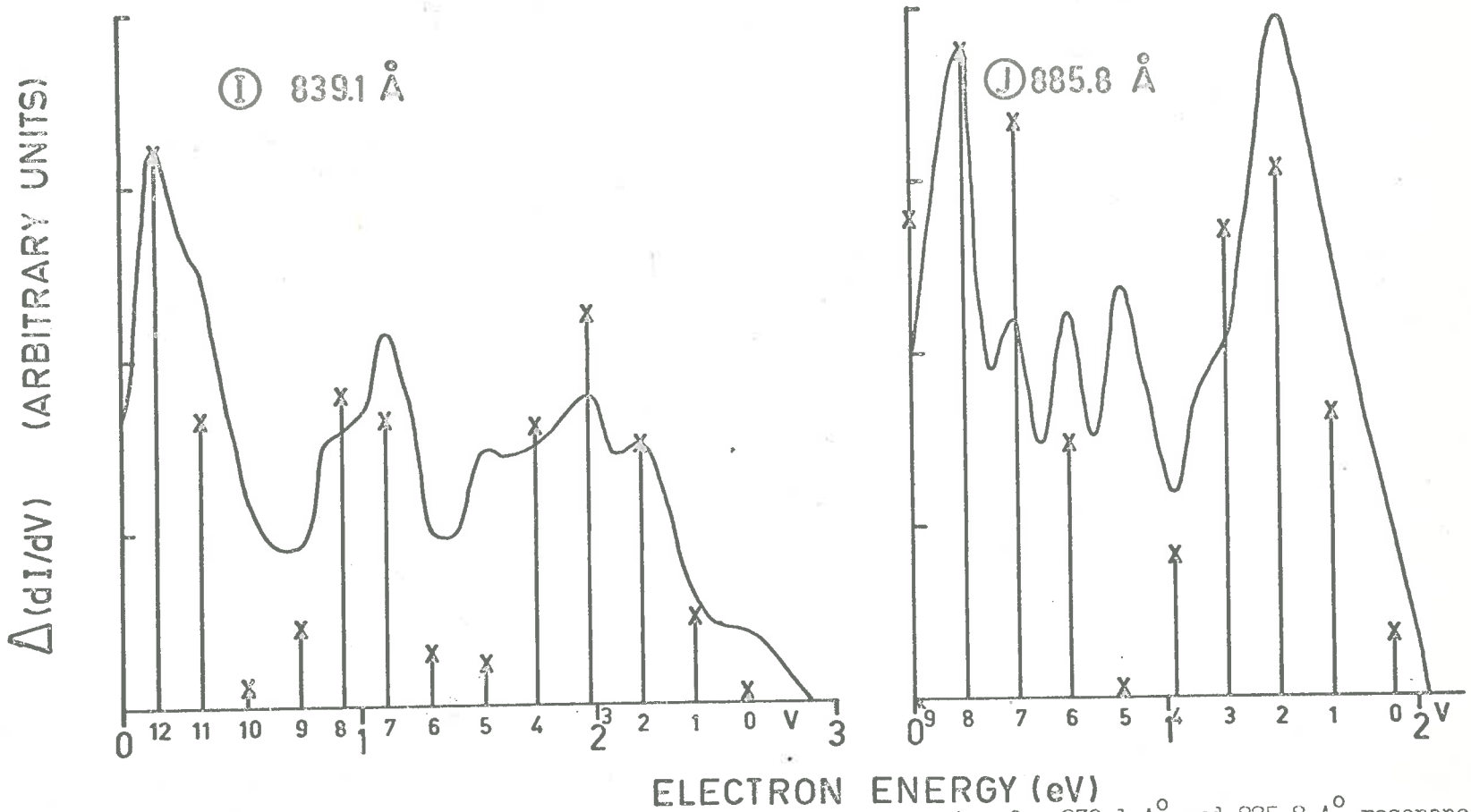

Fig. V.2. The difference between resonance and off-resonance spectra for 839.1 A° and 885.8 A° resonances of molecular oxygen, compared with the calculated Franck-Condon factors .

TABLE V.2

Franck-Condon factors for direct ionization in molecular oxygen.

$$O_2 X^3\Sigma_g^-(v'') \rightarrow O_2^+ X^2\Pi_g(v')$$

$q_{v'v''}$

v'←v''	WACKS[9]	HALMANN et al.[6]	Present Work
0 - 0	•23545	•23535	•23544
1 - 0	•39021	•29016	•39021
2 - 0	•26277	•26283	•26279
3 - 0	•09197	•09202	•09199
4 - 0	•01771	•01773	•01772
5 - 0	•00182	•00182	•00182
6 - 0	•00008	•00009	•00009
7 - 0	-	-	-

TABLE V.3

Franck-Condon factors for autoionization in molecular oxygen

$$O_2 I(v') \rightarrow O_2^+ X^2\Pi_g(v'')$$

v'' \ v'	0	1	2	3	4
0	•00017	•00098	•00311	•00709	•01301
1	•00193	•00903	•02259	•04019	•05690
2	•01046	•03679	•06766	•08545	•08166
3	•03510	•08598	•10274	•07441	•03097
4	•08193	•12314	•07281	•01257	•00230
5	•14119	•10308	•01021	•01266	•05041
6	•18621	•03696	•01369	•06578	•04296

...cont'd.,

Table V.3 Continued:

v' / v''	0	1	2	3	4
7	•19229	•00001	•07485	•04702	•00006
8	•15776	•04107	•08103	•00035	•04049
9	•10375	•11952	•02092	•03954	•05589
10	•05496	•16056	•00560	•02113	•00436
11	•02347	•13882	•07494	•03569	•02838
12	•00807	•08583	•14512	•00096	•07868
13	•00222	•03965	•14589	•06312	•03547
14	•00048	•01400	•09529	•14161	•00167
15	•00007	•00392	•04319	•14741	•06978
SUM	1•00006	0•99944	1•07964	0•85598	0•59299

$O_2 J(v') \rightarrow O_2^+ X^2\Pi_g(v'')$					
0	•00407	•01599	•03482	•05577	•07361
1	•02710	•07369	•10710	•10897	•08505
2	•08385	•13735	•10393	•03966	•00322
3	•16014	•12150	•01878	•00573	•04313
4	•21180	•03681	•01559	•07195	•05483
5	•20631	•00165	•08881	•04880	•00009
6	•15366	•06604	•07848	•00022	•04965
7	•08967	•14957	•00891	•05809	•05354
8	•04168	•16821	•02174	•08312	•00030
9	•01560	•12427	•10915	•01856	•04795
10	•00474	•06659	•15918	•01144	•07987
11	•00117	•02713	•13307	•09440	•01873
12	•00024	•00862	•07582	•15296	•01165
13	•00004	•00218	•03159	•13232	•09536
14	•00000	•00046	•00989	•07579	•15060
15	•00000	•00015	•00200	•03264	•12303
SUM	1•00007	1•00021	0•99886	0•99042	0•89061

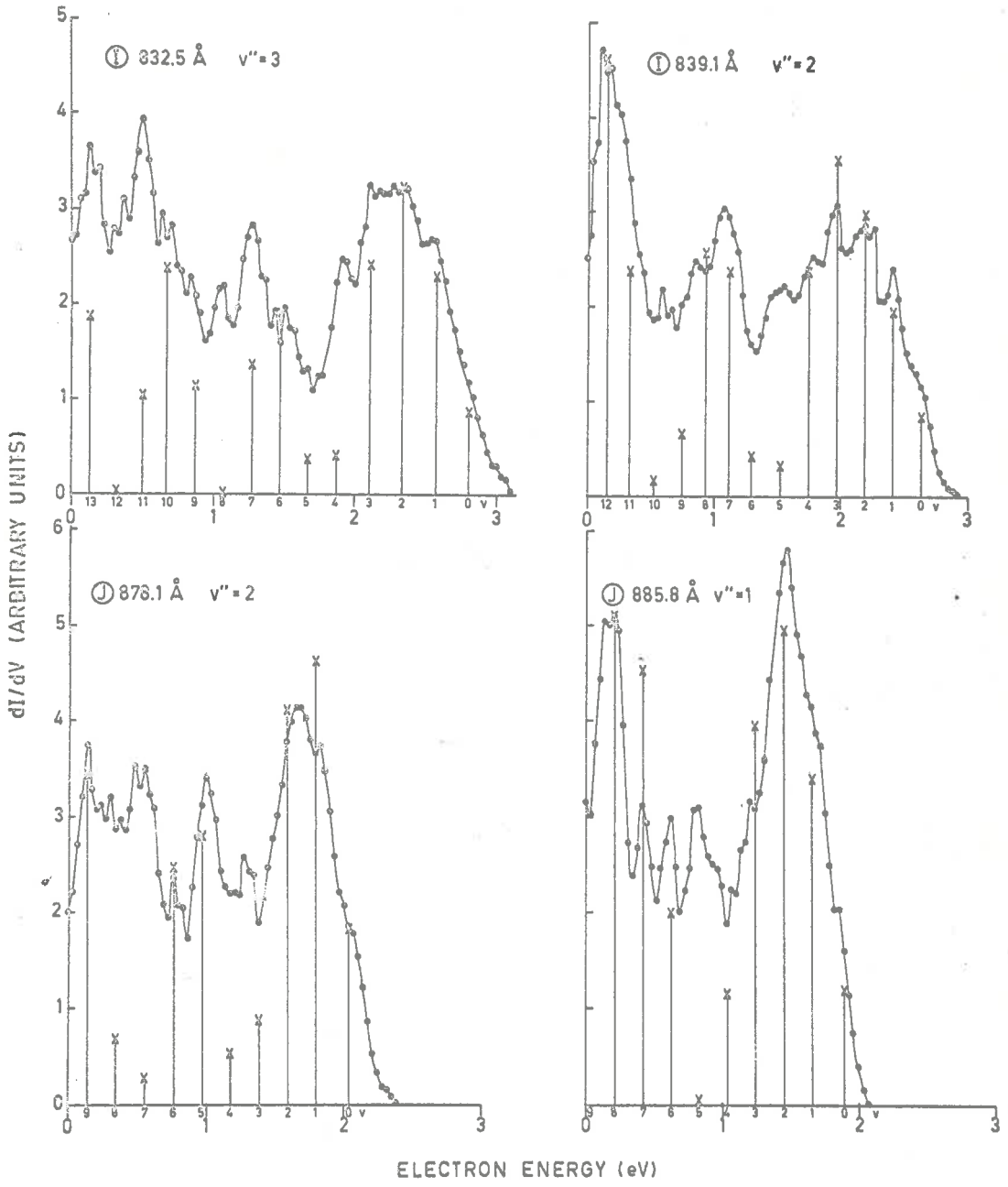

Fig. V.3. A comparison of the resonance spectra with the optimum combination ofF-C factors for direct and autoionizing transitions to the $X^2\Pi_g$ state of O_2^+.

is quite clear that the general form of the spectrum in each case has been reproduced through these calculations. For the I state of the molecular oxygen, the optimum value of the equilibrium internuclear distance, r_e was found to be 1·35Å. The value gave maxima at the correct energies for both the 839·1Å and 832·5Å resonances. The optimum value of r_e for the J state was found to be 1·30Å which gave maxima correctly at 885·8Å and 878·1Å. The sensitivity of the determination of r_e to the position of the maxima in the photoelectron spectra is 0·11Å/volt.

The Franck-Condon factors for autoionisation have been combined with the continuum Franck-Condon factors in the proportion which gives the best fit to the resonance spectra. This is shown in Figure V.3. The relative strengths which have to be assumed for the continuum and the resonance cross-section are in the ratio of 1 : 10. This indicates that the continuum cross-section underlying the autoionised structure is very weak.

CHAPTER VI

SCOPE FOR FURTHER STUDY OF PHOTOELECTRON SPECTROSCOPY

VI.1 Partial Photoionization Cross-Sections

The measurement of partial photoionization cross-sections as a function of photon wavelength for several atmospheric gases has been made using a retarding potential type electron spectrometer with a spherical grid geometry. The spectrometer had a high resolution with an efficient detecting system. The low energy area in the spectra which was one of the limiting factors for determining the accuracy of the partial cross-sections, was reduced but not to a minimum possible value. The possibility of further reduction of low energy area needs to be investigated.

A parallel plate electrostatic analyser (Harrower, 1955) and magnetic focussing spectrometer (Turner and May, 1966) could be considered for use in obtaining higher resolution. This would allow a more accurate unfolding of the spectra. The single photoelectrons produced could be detected by a chain of channel electron multipliers.

For the purpose of calculating the energy distribution

of the primary photoelectrons in the ionosphere, Blake (1966) assumed that the removal of an inner electron makes only a small contribution to the total photoionization cross-sections. But to obtain accurate energy distribution at different altitudes of the atmosphere, the measurement of partial cross-sections at shorter wavelengths is essential. Thus, partial cross-sections need to be extended to wavelengths shorter than 584Å, exciting emission lines. Emission lines could be excited using a rotating spark gap instead of the fixed one as described in Section II.4.4. This would give a shorter spark and higher current density (Samson, private communication).

The measurement of partial photoionization cross-sections for some of the gases presented in this thesis could be useful for finding the partial photoionization rates in the upper atmospheres of other planets such as Venus, Mars and Jupiter. For example, following the standard Cytherean atmosphere for the planet Venus, an estimate about the abundance of CO_2 and N_2 in the atmosphere above the top of the cloud could be formed. Also the dissociation and recombination processes imply the presence of CO and O_2 (see footnote). A detailed

---

Footnote: This work has been reviewed by Shimizu (1966).

experimental and theoretical investigation is needed to find the number density of these gases at different altitudes above the top of the cloud. These investigations, combined with the results reported in this thesis, would be useful in the interpretation of some of the aeronomical phenomena occurring in these planets.

The measurement of partial photoionization cross-sections for atomic oxygen should be the next step. Because of many technical difficulties in the design and construction of the apparatus and also in the analysis of the combined data for atomic and molecular oxygen, little thought has been given to the experimental investigation of this gas. A need for such a study is warranted for its usefulness in many fields.

VI.2 Autoionization Processes

In chapters IV and V are shown the spectra of O_2 at 1.6Å beam resolution observed on and off a few of the autoionization resonances. These spectra have been reproduced in shape by Franck-Condon factors calculated for autoionization. It is suggested that the spectra on and off the resonances should be measured for CO and H_2 and Franck-Condon factors should be calculated to reproduce the shape of the spectra.

The photoelectron spectra of NO and N_2O shows a low energy anomalous peak which has been attributed to the fluorescent autoionization process (chapter III). To confirm this theory, it is suggested that the fluorescence yield should be measured on and off the autoionization resonances of NO and N_2O.

VI.3 Angular Distribution of Photoelectrons

The partial photoionisation cross-sections for some gases reported in this thesis were measured from a sample of electrons emitted from a point source of electrons and emanating to the grid system in a cone of 60°. It was assumed that this is the representative sample for all transitions. But if the angular distribution for various transitions at various photon energies is different, the partial cross-sections in the present work are slightly in error and thus would require correction. This suggests the need for theoretical and experimental study of angular distribution of different transitions.

Berkowitz et al. (1967) investigated this problem experimentally for various gases using the 584Å helium resonance line. It is unlikely that the angular distribution for different transitions at 584Å would be the same as at other wavelengths. This suggests that measurement of such distribution at all wavelengths upto threshold

of the ground state of the gas would be essential. Also, the angular distribution depends upon the angular momentum of the photoelectron; thus it contains the information about the nature of transitions of the photoelectrons. It is suggested that the angular distribution of photoelectrons emitted by processes of autoionization may be entirely different from that of other transitions, depending on whether the quasi-stable states are sufficiently long-lived. For this reason also, the study of angular distribution of photoelectrons throughout the wavelength region from 300Å to the threshold energy of the ground state of the molecule, is desirable.

The apparatus suggested for the experiment is shown in Figure VI.1. The photon beam, dispersed from a one-metre monochromator, enters from one side of the interaction chamber and the gas under investigation, from the other side. The photoelectrons emitted at the center of the chamber can be detected by the two spectrometers A and B of similar design as described in chapter II but with dimensions to suit the interaction chamber. The two spectrometers A and B are exactly identical except for the fact that A can be moved from 30° to 150° to measure the angular distribution and B is fixed at right angles to the photon beam and may be used to monitor the spectra.

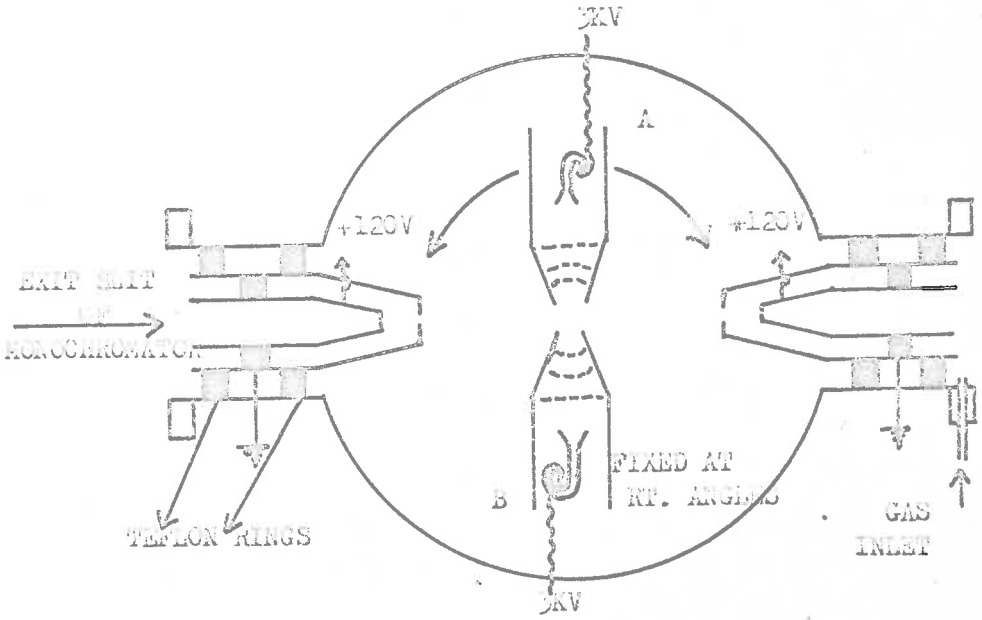

Fig. VI.1. The suggested apparatus for measurement of angular distribution of photoelectrons .

The photoelectrons emitted could be prevented from going to the monochromator by using some metal surfaces at a high positive potential as shown in Figure VI.1. The chamber should be maintained at a pressure of about 10^{-4} m.m.

APPENDIX

Publications

The following papers have been written on the work described in this thesis:

1. Photoelectron spectra and partial photoionization cross-section for carbon dioxide.
   To be published in J.Q.S.R.T.

2. Franck-Condon factors and autoionization in the photoelectron spectra of diatomic molecules.
   To be published in Proc. Roy. Soc.

3. Partial photoionization cross-sections of NO, CO, N_2O and NH_3.
   To be sent for publication in J.Q.S.R.T.

BIBLIOGRAPHY

Adams, J. and Manley, B.W., 1965, Electronic Engineering.

Al-Joboury, M.I. and Turner, D.W., 1963, J. Chem. Soc. p. 5141. 1964, J. Chem. Soc. p.4434.

Al-Joboury, M.I., May, D.P. and Turner, D.W., 1965, J. Chem. Soc., p. 616; 6350.

Allison, R., Burns, J. and Tuzzolino, A.J., 1964, J. Opt. Soc. Am., 54, 747.

Astoin, N. and Granier, J., 1955, C.R. Acad. Sci. (Paris), 241, 1736.

Auger, P., 1925, J. Phys. Radium, 6, 205.
1926, Ann. Phys. (Paris), 6, 183.

Axelrod, N. and Givens, M.P., 1959, Phys. Rev., 115, 97.

Bates, D.R., 1946, Monthly Notices Roy. Astron. Soc., 106, 423.

Bates, D.R. and Massey, H.S.W., 1943, Phil. Trans. Roy. Soc. (Lond), 239A, 269.

Bates, D.R. and Seaton, M.J., 1949, Monthly Notices Roy. Astron. Soc., 109, 698.

Bates, D.R., Opic, U. and Poots, G., 1953, Proc. Roy. Soc. (Lond), A66, 1113.

Berkowitz, J., Ehrhardt, H. and Tekaat, T., 1967, Z. Physik, 200, 69.

Beutler, H., 1935, Z. Physik, 93, 177.

Beutler, H. and Jungen, H.O., 1936, Z. Physik, 98, 181.

Beynon, J.D.E. and Cairns, R.B., 1965, Proc. Phys. Soc. (Lond), 86, 1343.

Blake, A.J., 1966, "Photoionization of Gases", Thesis submitted to University of Adelaide, S. Australia.

Blake, A.J. and Carver, J.H., 1967, J. Chem. Phys., 47,1038.

Cairns, R.B. and Samson, J.A.R., 1965, Phys. Rev., 139,A1403.

Chalonge, D., 1934, Ann. Phys. (Paris), 1, 123.

Chandraskhar, S., 1945, Astrophys. J., 102, 223 and 395.

Clark, K.C., 1952, Phys. Rev., 87, 271.

Clarke, E.M., 1954, Can. J. Phys., 32, 764.

Codling, K. and Madden, R.P., 1964, Phys. Rev. Letters, 12, 106.

Codling, K. and Madden, R.P., 1965, J. Chem. Phys. 42, 3935.

Condon, E.U. and Shortley, G.H., 1935, The Theory of Atomic Spectra, Cambridge Univ. Press, London and New York.

Cook, G.R. and Samson, J.A.R., 1959, Bull. Am. Phys. Soc., 4, 454.

Cook, G.R. and Metzger, PH., 1965a, J. Opt. Soc. Am., 54, 968.

Cook, G.R. and Metzger, P.H., 1965b, J. Chem. Phys., 41, 321.

Cook, G.R., Metzger, P.H. and Ogawa, M., 1965, Can. J. Phys., 43, 1706.

Cook, G.R., Metzger, P.H., Ogawa, M., Becker, R.A. and Ching, B.K., 1965, Aerospace Corporations Cont. No. AF04(695)-469.

Cook, G.R., Metzger, P.H. and Ogawa, M., 1966, J. Chem. Phys., 44, 2935.

Cooper, J.W., 1962, Phys. Rev., 128, 681.

Dalgarno, A., 1952, Proc. Phys. Soc. (Lond). A65, 663.

Dalgarno, A. and Parkinson, D., 1960, J. Atmos. Terr. Phys., 18, 335.

Dalgarno, A., Henry, R.J.W. and Stewart, A.L., 1964, Planet. and Space Sci., 12, 235.

Dibeler, V.H., Walker, J.A. and Rosenstock, H.M., 1966, J.R. NBS, 70A, 459.

Ditchburn, R.W., 1955, Proc. Roy. Soc. (Lond) A229, 44.

Ditchburn, R.W., 1960, Proc. Phys. Soc. (Lond), A75, 461.

Ditchburn, R.W., Jutsum, P.J. and Marr, G.V., 1953, Proc. Roy. Soc. (Lond) 219A, 89.

Ditchburn, R.W. and Young, P.A., 1962, J. Atmos. Terr. Phys., 24, 127.

Doolittle, P.H. and Schoen, R.L., Unpublished.

Doolittle, P.H. and Schoen, R.L., 1965, Phys. Rev. Letters, 14, 348.

Farnsworth, 1930, U.S. Patent 1 969 399.

Fano, U, 1935, Nuovo Cimento, 12, 156.
1961, Phys. Rev., 124, 1866.

Fano, U. and Cooper, J.W., 1965, Phys. Rev., 137, A1364.

Flannery, M.R. and Opic, U., 1965, Proc. Phys. Soc. (Lond), 86, 491.

Fox, R.E., Hickam, W.M., Kjeldaas, T. and Grove, D.J., 1951, Phys. Rev., 84, 859.

Fox, R.E. and Hickam, W.M., 1954, J. Chem. Phys., 22, 2059.

Frost, D.C. and McDowell, C.A., 1955, Proc. Roy. Soc. A, 232, 227. 1958, Can. J. Phys., 36, 39.

Frost, D.C., McDowell, C.A. and Vroom, D.A., 1965, Phys. Rev. Letters, 15, 612.

Frost, D.C., McDowell, C.A. and Vroom, D.A.S., 1967, Proc. Roy. Soc. (Lond), 196, 566.

Gaunt, J.A., 1930, Phil. Trans. Roy. Soc. (Lond) 229A, 163.

Gilmore, F.R., 1965, J. Quant. Spectros. Radiative Transfer 5, 369.

Goodrich, G.W. and Wiley, W.C., 1961, Rev. Sci. Instr., 32, 846.

Goodrich, G.W. and Wiley, W.C., 1962, Rev. Sci. Instr., 33, 761.

Halmann, M. and Laulicht, I.J., 1968, J. Chem. Phys., 43, 438.

Harrower, G.A., 1955, Rev. Sci. Instr., 26, 850.

Hartree, D.R., 1957, The Calculation of Atomic Structure, Wiley, New York.

Henning, H.J., 1932, An. Phys. (N.Y.), 13, 599.

Herzberg, G., 1950, Molecular Spectra and Molecular Structure, Vol. 1, Spectra of Diatomic Molecules, Van Nostrand, N.Y.

Herzberg, G., 1966, Molecular Spectra and Molecular Structure, Vol. III, Electronic Spectra and Electron Structure of Polyatomic Molecules, Van Nostrand, N.Y.

Hopfield, J.J., 1930, Astrophys. J., 72, 133.

Hopfield, J.J., 1930, Nature, 125, 927.
1935, Phys. Rev., 47, 788.

Hudson, R.D., 1964, Phys. Rev., 135, A1212.

Huffman, R.E., Tanaka, Y. and Larrabee, J.C. 1963, J. Chem. Phys., 38, 1920.

Huffman, R.E., Tanaka, Y. and Larrabee, J.C., 1963a, J. Chem. Phys., 39, 902.

Huffman, R.E., Larrabee, J.C. and Tanaka, Y., 1964, J. Chem. Phys., 40, 356.

Huffman, R.E., Larrabee, J.C. and Tanaka, Y., 1965, Appl. Opt., 4, 1581.

Hughes, A.L., 1910, Proc. Cambridge Phil. Soc., 15, 483.

Hurzeler, H., Inghram, M.G. and Morrison, J.D., 1957, J. Chem. Phys., 27, 313.

Jarmain, W. and Nicholls, R.W., 1964, Proc. Phys. Soc. (Lond) 84, 417.

Johnson, F.S., Watanabe, K. and Tonsey, R., 1951, J. Opt. Soc. Am., 41, 702.

Judge, D.L., Morse, A.L. and Weissler, G.L., 1963, Sixth International Conference on Ionisation Phenomenon in Gases (Paris), Vol. 3, p.373.

Judge, D.L. and Weissler, G.L., 1968, J. Chem. Phys., 48, 4590.

Klemperer, O., Electron Optics (Cambridge Univ. Press, N.Y., 1953), Sec. Ed. p. 337; 368.

Kramers, H.A., 1923, Phil. Mag., 46, 836.

Kunz, J., and Williams, F.H., 1920, Phys. Rev., 15, 550.
1923, Phys. Rev., 22, 456.

Kurbatov, B.L., Vilesov, F.I. and Terenin, A.N., 1961, Soviet Phys.-Dokl., 6, 490.

Ladenberg, R. and Van Voorhis, C.C., 1933, Phys. Rev., 43, 315.

Lee, P., 1955, J. Opt. Soc. Am., 45, 703.

Lee, P. and Weissler, G.L., 1952, Astrophys. J., 115, 570.

Lee, P. and Weissler, G.L., 1955, Phys. Rev., 99, 540.

Leffel, jr., C.S., 1964, Rev. Sci. Instr., 35, 1614.

Lenard, P., 1900, Ann. Phys. 1, 486.
3, 298.

Lenard, P. and Ramsauer, C., 1910-11, Sitzgsber. Heidelberg. Akad. Wiss.

Lindholm, E., 1954a, Arkiv. Fysik, 8, 433.

Lindholm, E., 1954b, Z. Naturforsch, 9a, 535.

Lossing, F.P. and Tanaka, Y., 1956, J. Chem. Phys., 25, 1031.

Madden, R.P. and Codling, K., 1963, Phys. Rev. Letters, 10, 516.

Madden, R.P. and Codling, K., 1965, J. Appl. Phys., 36, 380.

Mann, M.M. Illustralid, A. and Tate, J.T., 1940, Phys. Rev., 58, 340.

Matsunaga, F.M., Jackson, R.S. and Watanabe, K., 1965, J. Quant. Spectros. Radiat. Transfer, 5, 329.

Matsunaga, F.M. and Watanabe, K., 1967, Science of Light, 16, 31.

McGuire, E.J., 1965, Tech. Rep. No. 6 ARO(D), Proj. No. 2810, Cornell Univ., Phys. Dept.

Menzel, H. and Pekeris, C.L., 1935, Monthly Notices Roy. Astron. Soc., 96, 77.

Metzger, P.H., and Cook, G.R., 1964, J. Chem. Phys., 41, 642.

Metzger, P.H., Cook, G.R. and Ogawa, M., 1967, Can. J. Phys., 45, 203.

Mohler, F.L., Foote, F.D. and Chenault, R.L., 1926, Phys. Rev., 27, 37.

Mohler, F.L. and Boeckner, C., 1929, J. Res. Nat. Bur. Stand., 3, 303.

Mrozowski, S., 1941, Phys. Rev., 60, 730.
1942, Rev. Mod. Phys., 14, 216.
1942, Phys. Rev., 62, 270.
1947, Phys. Rev., 72, 782.

Mulliken, R.S., 1942, Rev. Mod. Phys., 14, 204.

Nicholson, A.J.C., 1963, J. Chem. Phys., 39, 954.

Nottingham, W.B., 1939, Phys. Rev., 55, 203.

Oschepkov, G., 1960, Pribory i Tekhnika Eskperimenta, 4, 89.

Page, T.L., 1938, Nature, 142, 615.

Pekeris, C.C., 1934, Phys. Rev., 45, 98.

Perry-Thorne, A. and Garton, W.R.S., 1960, Proc. Phys. Soc. (Lond), 76, 833.

Rustgi, O.P., 1964, J. Opt. Soc. Am., 54, 464.

Samson, J.A.R., 1964, J. Opt. Soc. Am., 54, 6.

Samson, J.A.R., 1966, J. Opt. Soc. Am., 56, 552.

Samson, J.A.R. and Kelly, F.L., 1964, G.C.A. Tech. Rep. No. 64-3-N.

Schneider, E.G., 1937, J. Chem. Phys., 5, 106.
1940, J. Opt. Soc. Am., 30, 128.

Schoen, R.I., 1964, J. Chem. Phys., 40, 1830.

Schoen, R.I., Judge, D.L. and Weissler, G.L., 1961, Fifth International Conference on Ionization Phenomenon in Gases (Munich), p.25.

Seaton, M.J., 1951, Proc. Roy. Soc. (Lond), 208A, 418.

Shimizu, M., 1960, J. Phys. Soc. Japan, 15, 1440.

Shimizu, M., 1966, Rep. Ion. Sp. Res. Japan, 20, 271.

Smith, L.G., 1951, Rev. Sci. Instr., 22, 166.

Sommerfeld, A., 1930, Wave Mechanics (London: Methuen), p.181.

Spohr, R. and Puttkamer, E. van, 1967, Z. Naturfersch, 22a, 705.

Stewart, A.L. and Webb, T.G., 1963, Proc. Phys . Soc. (Lond), 82, 532.

Suguira, Y., 1927, J. Phys. Radium, 8, 113.
1929, Bull. Inst. Phys. Chem. Res. Tokyo Sci. Papers, 11, 1.

Sun, H. and Weissler, G.L., 1955, J. Chem. Phys., 23, 1160; 1372; 1625.

Takamine, T., Tanaka, Y. and Iwata, M., 1943, Sci. Papers Inst. Phys. Chem. Res. (Tokyo), 40, 371.

Tanaka, Y., 1942, Sci. Papers Inst. Phys. Chem. Res. (Tokyo), 39, 447.

Tanaka, Y., 1944, Inst. Phys. Chem. Res. Tokyo Sci. Papers, 42, 49.

Tanaka, Y., Jursa, A.S. and LeBlanc, F.J., 1958, J. Opt. Soc. Am., 48, 304.

Tanaka, Y., Jursa, A.S. and LeBlanc, F.J., 1960, J. Chem. Phys., 32, 1199; 1205.

Tanaka, Y., Huffman, R.E. and Larrabee, J.C., 1962, J. Quant. Spectros. Radiat. Transfer, 2, 451.

Trumpy, B., 1928, Z. Physik, 47, 805.

Tuckwell, H., Private Communication.

Turner, D.W. and May, D.P., 1966, J. Chem. Phys., 45, 471.
1967, J. Chem. Phys., 46, 1156.

Vilesov, F.I., Kurbatov, B.L. and Terenin, A.N., 1961, Soviet Physics-Doklady, 6, 490.

Viselov, F.I. and Terenin, A.N., 1957, Dokl. ANSSSR, 115, 744.

Vroom, D.A.S., 1966, Thesis (unpublished), University of British Columbia.

Wacks, M.E., 1964, J. Chem. Phys., 41, 930.

Wainfan, N., Walker, W.C. and Weissler, G.L., 1955, Phys. Rev., 99, 542.

Wannier, G.H., 1956, Phys. Rev., 100, 1180.

Watanabe, K., 1954, J. Chem. Phys., 22, 1564.
1957, J. Chem. Phys., 26, 542.

Watanabe, K. and Marmo, F.F., 1956, J. Chem. Phys., 25, 965.

Weinbaum, S., 1933, J. Chem. Phys., 1, 593.

Weissler, G.L., 1956, Handbuch der Physik, 21, 304.

Weissler, G.L., Lee, P. and Mohr, E.I., 1952, J. Opt. Soc. Am., 42, 200.

Weissler, G.L., Samson, J.A.R., Ogawa, M. and Cook, G.R., 1959, J. Opt. Soc. Am., 49, 338.

Wigner, E.P., 1948, Phys. Rev., 73, 1002.

Wilkinson, P.G. and Byram, E.T., 1965, Appl. Opt., 4, 581.

Wilson, C.T.R., 1899, Phil. Trans. Roy. Soc. (Lond), 192A, 403.

Yarnold, G.D. and Bolton, H.C., 1948, J. Sci. Instr., 26, 38.